Techniques for evaluating one-loop feynman diagrams and their application

Miller, David J.

Techniques for Evaluating One-Loop Feynman Diagrams and their Application

A thesis submitted for the degree of
Doctor of Philosophy
by

David J. Miller

University of Durham
Department of Physics
December 1996

Abstract

For a full understanding of QCD and a precise comparison of the theory with experiment, QCD observables must be calculated to next-to-leading order in the strong coupling constant. This thesis will discuss some of the techniques used for calculating the one-loop Feynman diagrams which are required for such calculations, and their associated tensor integrals. In particular, conventional methods introduce Gram determinants. This can lead to unnecessarily complicated expressions and numerical instabilities in the limit of vanishing Gram determinant. An alternative method is presented which removes these problems by gathering together scalar integrals in combinations which are finite as the Gram determinant vanishes. These combinations are related to the corresponding scalar integrals in higher dimensions.

This method is applied to the evaluation of the one-loop QCD corrections for the decay of an off-shell vector boson with vector couplings into two pairs of quarks of equal or unequal flavours. These matrix elements are required for the next-to-leading order corrections to four jet production in electron-positron annihilation, the production of a gauge boson and two jets in hadron-hadron collisions, and three jet production in lepton-nucleon scattering.

Acknowledgements

I would especially like to thank my supervisor, Nigel Glover, for his guidance and support throughout my three years in Durham. I am very grateful for the privilege and opportunity of working and collaborating with him. He has taught me all I know about particle physics and has shared with me some of his physical intuition.

A special thanks goes to John Campbell, for his collaboration and friendship. Much of the work presented here was done with John's help. Thank you, John, for being there for me during the writing of this thesis, and for helping me save the world so many times.

To Elena Boglione, thank you for your kind words and encouragement when times were difficult. Sharing an office with you has been a pleasure — thank you for putting up with me.

I am grateful to all my friends and fellow students for their encouragement, support and friendship during the last three years, and for making the physics department such a pleasant place to work. Thank you, Adnan, Andy, Anna, Aude, Ayse, Charlie, Claire, Darrell, Ghadir, Jacques, Matthew, Matthias, Sabine and Thomas.

My gratitude goes to all the staff in the particle physics group here in Durham. To Valya and Valery Khoze, Chris Maxwell, Alan Martin, Mike Pennington, James Stirling, and Mike Whalley, thank you all for giving me the opportunity to be part of the group, and for giving me a future in particle physics.

Most importantly, I would like to thank my family, for always being there for me, and for their support and encouragement over the years. Thank you, Mum, Dad and Andrew, for having faith in me.

My love and thanks go to Kirsten Büttner, who has made me happy in the last three years. Thank you for being my motivation and my inspiration, and for keeping me going during the harder moments. Most of all, thank you for loving me and looking after me.

This thesis is dedicated to my family,
To Mum and Dad
and Kirsten
with all my love.

Declaration

I declare that no material presented in this thesis has previously been submitted for a degree at this or any other university.

The research described in this thesis has been carried out in collaboration with Dr. E.W.N. Glover and J.M. Campbell and has been published as follows:

- The One-Loop QCD Corrections for $\gamma^\star \to Q\bar{Q}q\bar{q}$
  E.W.N. Glover and D.J. Miller, Durham Preprint DTP/96/66, hep-ph/9609474.
- One-Loop Tensor Integrals in Dimensional Regularization
  J.M. Campbell, E.W.N. Glover and D.J. Miller, Durham Preprint DTP/96/96.

Contents

Chapter 1

Introduction

Particle physics is the study of the interactions of the fundamental particles of nature at very small distance scales (usually $10^{-15}m$–$10^{-17}m$). At these distances, all matter is observed to interact via four fundamental forces of nature: the strong and weak nuclear forces, the electromagnetic force, and gravity. Excluding gravity, these forces, and the fundamental particles which are influenced by them, are well described by *Quantum Field Theories.* The force of gravity is not understood at small distance scales, but it is so weak that it is usually ignored in the study of particle physics.

The combination of these Quantum field theories, providing a model for all (non-gravitational) particle interactions at a quantum scale, is known as the **Standard Model** of Particle Physics. Within this, the electromagnetic force is described by the theory of *Quantum Electro-Dynamics* (QED). This is a gauge theory based on the Abelian symmetry group $U(1)$, and describes the interactions of particles carrying electromagnetic charge. This theory and the weak nuclear force have been partially unified to form the *Electro-Weak* Theory, embodying the symmetry group $U(1) \otimes SU(2)$. This symmetry is not manifest in the physical world but is broken into the smaller group of QED by the *Higgs Mechanism.*

The final pillar of the Standard Model is **Quantum Chromo-Dynamics** (QCD), and it is this theory, and its manifestation in experiment, which will be the main focus of this thesis. QCD is based on the non-Abelian gauge symmetry group $SU(3)$ and

describes the interactions of particles carrying the quantum numbers of *colour*, namely *quarks* and *gluons*. The strong nuclear force which binds together protons and neutrons to form atomic nuclei, can be explained through the residual interactions of these coloured particles. Chapter 2 will provide a brief theoretical overview of QCD, describing some of the concepts which are essential to an understanding of the subsequent chapters. This will include discussions of the symmetry group $SU(3)$, the Lagrangian of QCD, and the renormalization of the strong coupling constant.

Any useful theory must be able to make predictions which can be experimentally tested. QCD makes such predictions and Chapter 3 will describe how these can be tested in experiment. In particular, the high energy collisions of electrons and positrons in particle accelerators result in the production of jets of strongly interacting particles. These jets are instrumental in forming a link between the theory and experiment of QCD and the theoretical calculation of jet quantities provides good experimental tests of the interactions of quarks and gluons.

In order to provide precise theoretical predictions it is necessary to perform QCD calculations to next-to-leading order in the strong coupling constant. These calculations are notoriously difficult, in part because of the appearance of integrations over the unconstrained momentum flowing around closed particle loops. Some of the more conventional methods for performing these integrals are discussed in Chapter 4. These conventional methods are plagued by the introduction of *Gram determinants*, which appear in the denominators of the expressions for the integrals. This often leads to unnecessarily complicated results. Furthermore, the next-to-leading order matrix elements calculated using these methods display fake singularities in the regions of phase space where these Gram determinants vanish. This can lead to instabilities in the numerical programs which must be constructed before the theoretical predictions can be compared with experiment.

However, since divergences in these limits are unphysical, it must be possible either to remove the Gram determinants from the denominator of the integral expressions, or to combine terms together in such a way as to construct functions which are finite as the Gram determinant vanishes. In addition to removing any problems with numerical

stability, this procedure combines together dilogarithms and logarithms in a natural, but non-trivial way, resulting in more compact expressions for QCD matrix elements. The construction of these finite functions will be described in Chapter 5.

Finally, these methods are applied to the calculation of the one-loop virtual corrections to $\gamma^* \to q\bar{q}Q\bar{Q}$ in Chapter 6. This is the first step towards the calculation of the next-to-leading order corrections for $e^+e^- \to 4$ jets. This correction is needed in order to make a more precise measurement of the QCD colour factors, and will also lead to a better understanding of the backgrounds to W pair production near threshold at LEP 2. Furthermore, its use is not restricted to e^+e^- collisions, but it is also needed for the next-to-leading order corrections for $p\bar{p} \to W/Z + 2$ jets and $e^{\pm}p \to e^{\pm} + 3$ jets.

Chapter 2

A Theoretical Overview of QCD

2.1 Introduction

By the 1960s a large number of strongly interacting particles, called *hadrons*, had been observed in high energy scattering experiments. In 1964, Gell-Mann [1] and Zweig [2] attempted to explain this proliferation in the number of hadrons by advocating that they are not fundamental but are composed of point-like spin-$\frac{1}{2}$ particles called *quarks*. They demonstrated that all hadrons could be explained as bound states of either three quarks (*baryons*) or a quark-antiquark pair (*mesons*).

Then, in 1968, deep inelastic scattering experiments of high energy electrons off a liquid hydrogen target began at the Stanford Linear Accelerator Center (SLAC) [3]. These experiments showed that protons are not fundamental but are indeed composed of three charged, point-like constituents. It did not take long to identify these constituents with the quarks of Gell-Mann and Zweig.

However, the quark model had several problems. Firstly, the wavefunction of the Δ^{++} baryon appeared to be totally symmetric under the exchange of two of its quark constituents. This contradicts the usual anti-symmetry expected from the exchange of two fermions, and was known as the *spin-statistics* problem. Furthermore, the quark model could not explain why quarks are never seen individually in experiment, nor indeed in exotic combinations such as qq or $qq\bar{q}$.

These problems were solved by the introduction of an extra degree of freedom called *colour*[1]. Quarks exist in three different colour states — red, green or blue. Making the colour part of the Δ^{++} wavefunction antisymmetric to quark exchange solves the *spin-statistics* problem. In addition, only *colourless* hadrons (ie. with equal amounts of red, green and blue) are observed in experiment. Individual quarks cannot be colourless, and are *confined* within protons.

The dynamics of these quarks are described by the theory of **Quantum Chromo-Dynamics** (QCD). This describes the interactions of the fermionic quarks via the exchange of bosonic force mediators, called *gluons*. Quarks and gluons are collectively termed *partons*. It is QCD which binds quarks together to form protons and neutrons and, in turn, binds these nucleons together to form the atomic nucleus[2].

This chapter will briefly discuss the theory of QCD. The property of colour and its link to the QCD gauge group $SU(3)$ will be discussed in section (2.2), and the QCD Lagrange density will be presented in section (2.3). Section (2.4) will discuss the renormalization of QCD and, in particular, the running of the strong coupling constant. A convenient method for simplifying the colour algebra of QCD Feynman diagrams will be given in section (2.5), and finally, in section (2.6), the basics of spinor helicity methods will be outlined.

2.2 Colour and $SU(3)$

Quantum Chromo-Dynamics is a gauge theory based upon the non-Abelian group $SU(3)_C$, where the subscript C denotes colour. Formally, quarks are fundamental representations of $SU(3)_C$. They are vectors in a three dimensional *colour space*,

$$\psi = \begin{pmatrix} \psi_R \\ \psi_G \\ \psi_B \end{pmatrix}. \tag{2.1}$$

[1]This has nothing to do with colour in its more usual sense.

[2]The lower energy effect of QCD, binding nucleons together, is known as the *strong nuclear force* and is mediated by the exchange of pions.

As with all vectors, ψ is coordinate independent — the above labeling is an arbitrary coordinate choice. It must be possible to make a rotation of the coordinates in this colour space, ie. intermix the definitions of red, green and blue, without changing the physics. This *global symmetry* can be described by the group $SU(3)$.

$SU(N)$ is the group of symmetry transformations,

$$\psi \longrightarrow U\psi, \tag{2.2}$$

where U are *unitary* $N \times N$ matrices with determinant one.

$$U^{\dagger}U = 1, \qquad \det|U| = 1. \tag{2.3}$$

U has $N^2 - 1$ parameters (since it is an $N \times N$ matrix with one constraint) and can be written,

$$U = e^{i\Theta_a T^a}, \tag{2.4}$$

where the repeated index implies summation over $a = 1 \ldots (N^2-1)$. The $N \times N$ hermitian matrices T^a are the *generators* of $SU(N)$, and Θ_a are the parameters of the transformation. In the case of $SU(3)$, T^a are known as the *colour matrices*. They obey the commutation relation,

$$\left[T^a, T^b\right] = if^{abc}T^c, \tag{2.5}$$

where f^{abc} are the *structure constants* of QCD. Also, since,

$$\det|U| = \det\left|e^{i\Theta_a T^a}\right| = e^{i\Theta_a Tr(T^a)}, \tag{2.6}$$

it follows that T^a are traceless. They are usually normalised so that,

$$Tr(T^a T^b) = \frac{\delta^{ab}}{2}. \tag{2.7}$$

Any description of quark interactions must be invariant under an $SU(3)$ symmetry transformation. A stronger restriction can be made by requiring that this $SU(3)$ symmetry be *local*. That is, a colour space rotation, U, can be performed which varies with the space-time point,

$$U(x) = e^{i\Theta_a(x)T^a}, \tag{2.8}$$

This requirement is reasonable since the rotation parameters cannot be propagated from one point in space to another arbitrarily quickly. Enforcing the theory of quarks and their interactions to be *locally* $SU(3)$ invariant naturally leads to the theory of Quantum Chromo-Dynamics.

2.3 The QCD Lagrange Density

The theory is completely described by the QCD Lagrange density, given by,

$$\mathcal{L}_{QCD}\left[\bar{\psi}_f, \psi_f, \bar{\omega}, \omega, A\right] = \mathcal{L}_{SU(3)} + \mathcal{L}_{gauge-fixing} + \mathcal{L}_{ghost}. \tag{2.9}$$

This is dependent on the quark fields, ψ_f, of flavour f, the gluon field, A, and the ghost field, ω.

The QCD Dynamics: $\mathcal{L}_{SU(3)}$

$\mathcal{L}_{SU(3)}$ describes the dynamics of QCD and is the most interesting part of the QCD Lagrange density. It is given by,

$$\mathcal{L}_{SU(3)} = \sum_f \bar{\psi}_f \left(i\mathcal{D}^\mu \gamma_\mu - m_f\right) \psi_f - \frac{1}{4} F^a_{\mu\nu} F^{\mu\nu}_a. \tag{2.10}$$

Here the sum is over n_f quark flavours and m_f is the quark mass. $\mathcal{D}$ is the covariant derivative, defined by,

$$\mathcal{D}^\mu = \partial^\mu - i g_s A^\mu_a T^a, \tag{2.11}$$

where g_s is the coupling strength of quarks to gluons and T^a, $i = 1 \ldots 8$, are the $SU(3)_C$ generators.

Finally, the field strength tensor, $F^{\mu\nu}_a$ is given by,

$$F^{\mu\nu}_a = \partial^\mu A^\nu_a - \partial^\nu A^\mu_a + g_s f_{abc} A^\mu_b A^\nu_c. \tag{2.12}$$

Some properties of this Lagrange density are immediately apparent:

- As required, $\mathcal{L}_{SU(3)}$ is invariant under local $SU(3)_C$ gauge transformations, eq. (2.8). Under this transformation the quark fields transform as the fundamental representation, and gluon fields transform as the adjoint representation of $SU(3)_C$,

$$\begin{aligned} \psi_f(x) &\longrightarrow U(x)\psi_f(x), \\ A^\mu_a(x)T^a &\longrightarrow U(x)A^\mu_a(x)T^aU^\dagger(x) + \frac{i}{g_s}U(x)\partial^\mu U^\dagger(x), \end{aligned} \tag{2.13}$$

  where summation over a is assumed.

- The non-Abelian structure of $SU(3)$ leads to glue-glue interactions. This is caused by the term quadratic in the gluon field in eq. (2.12), which gives three and four gluon vertices in the term $-\frac{1}{4}F^{\mu\nu}_a F^a_{\mu\nu}$ of the Lagrange density. In other words, the *gluon carries a colour charge.* It is this property which is thought to lead to the confinement of quarks.

Gauge Fixing

Since $\mathcal{L}_{SU(3)}$ is invariant under $SU(3)_C$ transformations, field configurations which can be transformed onto one another are equivalent. In order to prevent over-counting of these gauge equivalent field configurations, a gauge-fixing term must be added. An arbitrary choice can be made as to how the gauge should be fixed, and all physical quantities should be independent of this choice. Throughout this thesis the *Feynman Gauge* will be used. This is a covariant gauge with the gauge parameter ξ set to unity,

$$\mathcal{L}_{gauge-fixing} = -\frac{\xi}{2}\left(\partial_\mu A^\mu_a\right)^2 = -\frac{1}{2}\left(\partial_\mu A^\mu_a\right)^2. \tag{2.14}$$

Ghost Fields

In a covariant gauge ghost fields are also required to remove unphysical longitudinal polarizations of the gluon field. The ghost field dynamics are determined by $\mathcal{L}_{ghost}$,

$$\mathcal{L}_{ghost} = \left(\partial_\mu \bar{\omega}_a\right)\left(\partial^\mu \delta_{ac} - g_s f_{abc} A^\mu_b\right)\omega_c. \tag{2.15}$$

The Perturbative Expansion and The Feynman Rules

The probability of quantum transitions from initial to final states is given by the S matrix. This S matrix can be formally linked to the Lagrange density using Feynman's *Path Integral* formalism (see for example [4]). Furthermore, when the strong coupling constant is small, a perturbative expansion of the S matrix can be made and the usual QCD Feynman rules derived. These allow matrix elements, ie. the probability of transition from one set of particles with definite momenta to another, to be calculated by drawing all topologically distinct Feynman diagrams (of the appropriate order) linking initial and final states — these diagrams can then be translated into mathematical formulae using the Feynman rules. A derivation of the Feynman rules can be found in [5] and will not be reproduced here. The Feynman rules, in the Feynman gauge, can be found in Appendix D.

2.4 The Renormalization of QCD

Next-to-leading order matrix elements often include Feynman diagrams containing closed particle loops. Momentum conservation is insufficient to constrain the momentum flowing around these loops, and the unconstrained momentum must be integrated over. Unfortunately this integral is frequently divergent.

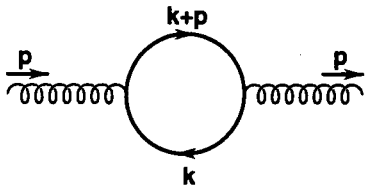

Figure 2.1: The inclusion of a fermion loop in the gluon propagator.

For example, consider the inclusion of a fermion loop in the gluon propagator, fig. (2.1). Using the Feynman rules of Appendix D, this diagram contains an integral over the loop momentum, k. Naïve power counting shows that this integral diverges due to the

behaviour of the integrand for large k^2.

$$\int d^4k \frac{\not{k}(\not{k}+\not{p})}{k^2(k+p)^2} \sim \int d^4k \frac{1}{k^2} \sim \infty. \tag{2.16}$$

Clearly these divergences must be removed from all physical quantities. They are classified into two types:

- **Ultra-Violet Divergences**: These are caused by the divergent behaviour of the integrand as the loop momenta becomes large. The example given above is of this type. They are removed by a redefinition of the quark-gluon coupling to absorb the infinity. This process is know as *renormalization* and will be the explained more completely below.
- **Infra-Red Divergences**: These are caused by the divergent behaviour of the integrand as the loop momenta becomes small. Such divergences have been shown to cancel at all orders in perturbation theory for all physical quantities [6, 7], and will be discussed in Chapter 3.

The Effective Quark-Gluon Coupling

Beyond leading order the quark-gluon coupling, g_s, is modified by higher order Feynman diagrams. Fig. (2.2) shows the Feynman diagrams contributing at next-to-leading order.

Most of these diagrams contain ultra-violet divergences which can be regulated by imposing an upper limit on the momentum. This ultra-violet cut-off, κ, will be taken to infinity at the end of the calculation. The cut-off method is used here only for illustrative purposes, and other, better methods for regulating these divergences will be discussed in section (3.5).

The Feynman diagrams of fig. (2.2) give the effective quark-gluon coupling to one loop,

$$\tilde{g_s} = g_s - \beta_0 \frac{g_s^3}{32\pi^2} \left(\log\left(\frac{Q^2}{\kappa^2}\right) + c \right) + \mathcal{O}(g_s^5), \tag{2.17}$$

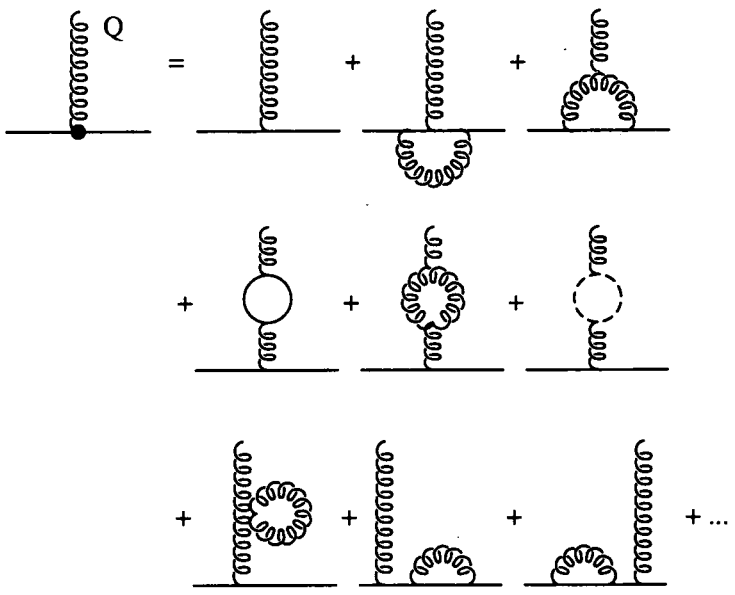

Figure 2.2: The effective coupling truncated at next-to-leading order.

where c is a constant, and the first term of the β-function is given by,

$$\beta_0 = \frac{11N_c - 2n_f}{3}. \tag{2.18}$$

N_c is the number of colours (ie. $N_c = 3$ for QCD) and n_f is the number of active flavours. Notice that the coupling now depends on the gluon momentum, Q.

This equation requires some interpretation. The coupling $\tilde{g}_s$ (to all orders) is a measurable quantity and therefore must be finite. However, the bare coupling g_s is unmeasurable and can be interpreted as being infinite. The ultra-violet divergence (when $\kappa \to \infty$) conspires with g_s to give a finite result for $\tilde{g}_s$. The divergence has been absorbed into the definition of the coupling. This process is known as *renormalization.*

The appearance of these divergences is not surprising. They are caused by the behaviour of the Feynman diagrams when the loop-momentum approaches infinity — at these high energies, one would expect that some more fundamental theory, of which QCD is an effective lower energy approximation, would control particle dynamics. The ability to remove ultra-violet divergences consistently via renormalization implies that the dy-

namics of particles at energy scales appropriate to QCD are little affected by the details of this fundamental theory at higher energies.

The Running of the Strong Coupling Constant

Eq. (2.17) is more usually written in terms of the strong coupling constant,

$$\alpha_s(Q) = \frac{\tilde{g_s}^2}{4\pi}. \tag{2.19}$$

The equation then becomes,

$$\alpha_s(Q) = \alpha_s - \frac{\beta_0}{4\pi}\alpha_s^2\left(\log\left(\frac{Q^2}{\kappa^2}\right) + c\right) + \mathcal{O}(\alpha_s^3), \tag{2.20}$$

where α_s without an argument is the bare tree-level coupling constant. Of course, this is true for any arbitrary (perturbative) scale μ and $\alpha_s(\mu)$ is given by,

$$\alpha_s(\mu) = \alpha_s - \frac{\beta_0}{4\pi}\alpha_s^2\left(\log\left(\frac{\mu^2}{\kappa^2}\right) + c\right) + \mathcal{O}(\alpha_s^3). \tag{2.21}$$

Subtracting these two equations, κ can be eliminated and $\alpha_s(Q)$ related to the strong coupling constant at the scale μ,

$$\alpha_s(Q) = \alpha_s(\mu) - \frac{\beta_0}{4\pi}\alpha_s^2(\mu)\log\left(\frac{Q^2}{\mu^2}\right) + \mathcal{O}(\alpha_s^3). \tag{2.22}$$

Since κ and α_s (bare) have been eliminated from the equation, the cut-off can now be returned to infinity, $\kappa \to \infty$. This expression can then be resummed to give,

$$\alpha_s(Q) = \frac{\alpha_s(\mu)}{1 + \frac{\beta_0}{4\pi}\alpha_s(\mu)\log\left(\frac{Q^2}{\mu^2}\right)}. \tag{2.23}$$

This expression allows the strong coupling constant to be written independently of μ. Rearranging gives,

$$\frac{1}{\alpha_s(Q)} - \frac{\beta_0}{4\pi}\log Q^2 = \frac{1}{\alpha_s(\mu)} - \frac{\beta_0}{4\pi}\log\mu^2. \tag{2.24}$$

The left and right hand sides of the above are of identical form and therefore must be independent of both Q and μ. It is usual to define,

$$\frac{1}{\alpha_s(Q)} - \frac{\beta_0}{4\pi}\log Q^2 \equiv -\frac{\beta_0}{4\pi}\log\Lambda^2, \tag{2.25}$$

where Λ is a fundamental QCD parameter. Rearranging gives,

$$\alpha_s(Q) = \frac{4\pi}{\beta_0 \log\left(\frac{Q^2}{\Lambda^2}\right)}. \tag{2.26}$$

The strong coupling "constant" *runs* with energy scale as seen in fig. (2.3).

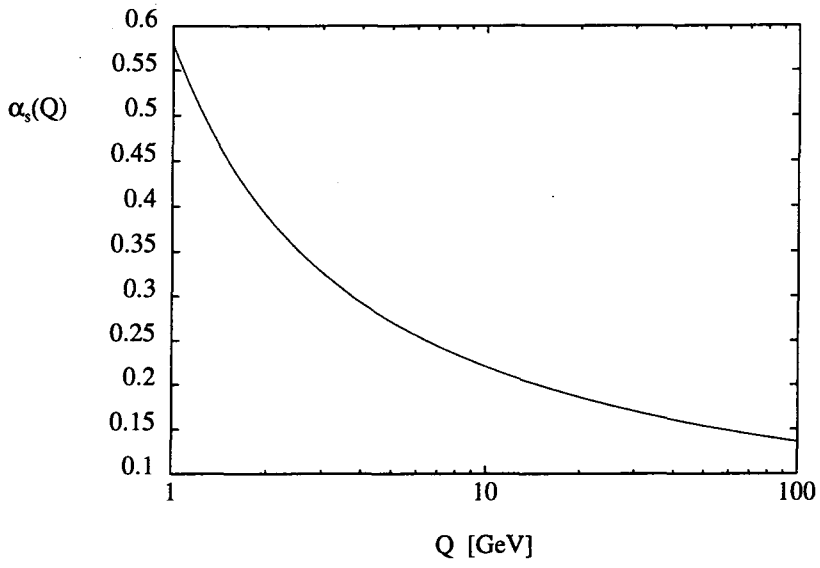

Figure 2.3: The running of the strong coupling constant with energy scale, in the perturbative region.

Measuring $\alpha_s(M_Z)$

Since theoretical predictions of QCD quantities are dependent on the value of α_s at the scale of the hard scattering, it is important to know precisely the value of α_s over a broad range of energies. In principle, this can be done by making experimental measurements of the QCD parameter Λ which, in turn, gives $\alpha_s(Q)$ via eq. (2.26). Beyond leading order, the value of Λ is dependent on the *renormalization scheme* used, and it is usual to choose the modified minimal subtraction scheme ($\overline{MS}$) [8].

In practise, due to the large statistics obtained from e^+e^- collisions at the Z peak (ie. $Q = M_Z \sim 91.2\ GeV$), it is better to measure $\alpha_s(M_Z)$. This can then be used to give α_s

at any perturbative scale by use of eq. (2.23). Measurements of α_s have been performed in e^+e^- collisions, hadron-hadron collisions, and deep-inelastic lepton-nucleon scattering, over a broad range of energies ($Q^2 \sim 1$–$10^5\ GeV^2$). Recent results for these measurements can be seen in fig. (2.4), together with the world average [9],

$$\alpha_s(M_z) = 0.118 \pm 0.005. \tag{2.27}$$

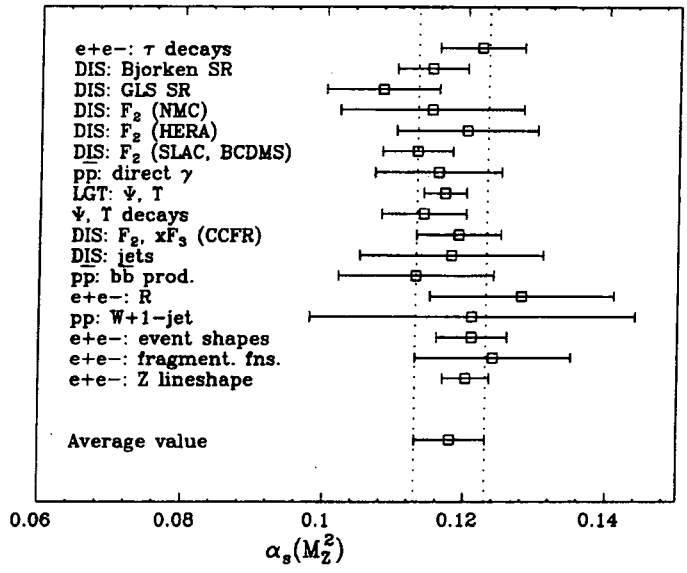

Figure 2.4: Average values of $\alpha_s(M_Z)$ evolved from measurements of $\alpha_s(Q)$, where Q is scale of the appropriate hard interaction. The results are ordered vertically in Q. This figure is reproduced from [9].

Confinement, Asymptotic Freedom, and the Gluon Self Interaction

The running of the strong coupling constant demonstrates the properties of *asymptotic freedom* and *confinement.*

- **Confinement**: At small energies ($Q^2 \sim \Lambda^2$) the strong coupling constant becomes large and confines quarks within baryons and mesons. In this region $\alpha_s(Q) > 1$ and

perturbation theory can no longer be applied.

- **Asymptotic Freedom**: At high energies ($Q^2 \gg \Lambda^2$) $\alpha_s(Q)$ is small and the quarks behave increasingly as if they were free. Perturbation theory can be applied with increasing confidence as Q^2 increases.

Notice that these properties are dependent on $\beta_0 > 0$ (which is true for $n_f < 16$). This is to be compared with QED where $\beta_0 = -\frac{4}{3}$, resulting in a behaviour exactly contrary to QCD: at low energies the electromagnetic coupling is small, and it becomes larger as energy increases.

This difference in behaviour is entirely due to the different group structures of the two theories. QCD is a *non-Abelian* theory. The field strength tensor, eq. (2.12), contains a term which is quadratic in the gluon field. When inserted into the Lagrange density this leads to three and four gluon interactions. It is these three and four gluon interactions in the diagrams of fig. (2.2) which force the β function to be positive. QED, however, is an *Abelian* theory based on the symmetry group $U(1)$. Its field strength tensor lacks a term quadratic in the photon field, and the photon has no self interaction.

2.5 Colour Algebra

Due to the non-Abelian structure of QCD, its Feynman rules contain colour matrices T^a_{ij}. Consequently, QCD Feynman diagrams consist of products of colour matrices, multiplying a kinematical part.

The colour part can be simplified using the following *Fierz identity*:

$$T^a_{ij}T^a_{kl} = \frac{1}{2}\left(\delta_{il}\delta_{jk} - \frac{1}{N_c}\delta_{ij}\delta_{kl}\right). \tag{2.28}$$

Eq. (2.28) holds generally for the generators of $SU(N)$ and is easily proven.

Proof of the Fierz identity:

Consider an arbitrary vector A given by,

$$A = \alpha_0 \mathbf{1} + \alpha_a T^a, \tag{2.29}$$

where summation over a is assumed. Taking the trace of A gives an expression for α_0:

$$Tr(A) = \alpha_0 N. \tag{2.30}$$

Similarly, to find α_a, A is first multiplied by T^a before the trace is taken,

$$Tr(AT^a) = \alpha_b Tr(T^b T^a) = \alpha_b \frac{\delta^{ab}}{2} = \frac{\alpha_a}{2}. \tag{2.31}$$

Then A is given by,

$$A = \frac{Tr(A)}{N}\mathbf{1} + 2Tr(AT^a)T^a. \tag{2.32}$$

Rearranging this, and making the colour indices explicit gives,

$$T^a_{ij}T^a_{kl}A_{ji} = \frac{1}{2}\left(\delta_{il}\delta_{jk} - \frac{1}{N_c}\delta_{ij}\delta_{kl}\right)A_{ji}. \tag{2.33}$$

However, since A_{ji} is arbitrary it can be removed and eq. (2.28) follows.

The Diagrammatic Form of the Fierz Identity

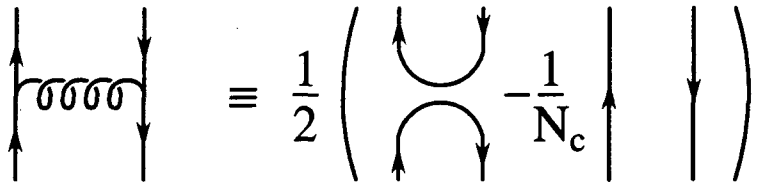

Figure 2.5: A diagrammatic representation of eq. (2.28).

Eq. (2.28) can be represented in the diagrammatic form of fig. (2.5). It should be stressed that the diagrams of fig. (2.5) are not Feynman diagrams but represent only the

colour part of the Feynman diagram. This diagrammatic method can be used to systematically remove all repeated colour indices, ie. internal gluon lines, writing the colour parts of each Feynman diagram as a sum over standard *colour factors.* The kinematical parts of the Feynman diagrams can then be grouped with regard to these colour factors. Each of these groupings is a gauge invariant set called a *partial amplitude.*

Note that Feynman diagrams containing the three gluon vertex can also be simplified in this manner by making the replacement,

$$if^{abc} = 2Tr\left(\left[T^a, T^b\right] T^c\right). \tag{2.34}$$

2.6 Spinor Helicity Methods

QCD matrix element calculations are often simplified by the use of *spinor helicity methods.* This involves decomposing the matrix elements into different configurations, where the external particles have fixed helicities. The helicity of a particle is defined by,

$$h \equiv \frac{\vec{p}\cdot\vec{S}}{|\vec{p}|}, \tag{2.35}$$

where $\vec{p}$ is the three-momentum of the particle and $\vec{S}$ is its spin.

Clearly this is only a good quantum number if the particle is massless. If a Lorentz boost is made to an inertial frame moving faster than the particle, then the particle three-momentum $\vec{p}$, and hence its helicity, will change sign. For a massless particle, travelling at the speed of light, no such frame exists and helicity is a good quantum number. For many QCD calculations, the quark mass is small compared to the energy scale of the interaction and it can be neglected. This will be assumed, and the quark mass neglected, throughout this thesis.

For most processes the spin of initial and final states is unknown. Traditionally, the matrix element is calculated without specifying these spins and this general amplitude is squared. A sum over the different spin states is then made.

However, if the matrix elements are particularly complicated, it is sometimes better

to calculate them for specific helicities of the external particles. These helicity amplitudes are individually simpler than the general expression with unspecified helicities. Furthermore, since they do not interfere with one another, the helicity amplitudes can be added *incoherently*, ie. they can be squared before adding them together. This is usually done numerically.

Many alternative approaches have been suggested for calculating these helicity amplitudes [10]. Here the spinor helicity methods of [11] will be discussed.

Let $u(p)$ be a four dimensional spinor of momentum p ($p^2 = 0$) satisfying the massless Dirac equation.

$$\not{p}u(p) = 0. \tag{2.36}$$

By projecting this spinor with the helicity projection operator, $\omega_\pm$, a spinor, $u_\pm(p)$, with definite helicity $\pm\frac{1}{2}$ can be defined,

$$u_\pm(p) = \omega_\pm u(p), \qquad \omega_\pm = \frac{1}{2}\left(1 \pm \gamma_5\right). \tag{2.37}$$

Notice that $\omega_\pm$ has the usual properties of a projection operator:

$$\begin{aligned} \omega_+ + \omega_- &= 1, \\ \omega_\pm^2 &= \omega_\pm, \\ \omega_+\omega_- &= 0. \end{aligned} \tag{2.38}$$

The original spinor can be regained by adding its different helicity projections,

$$u(p) = u_-(p) + u_+(p). \tag{2.39}$$

A notation choice for the conjugate spinor must be made[3]. Here $\bar{u}_\pm$ is given by,

$$\bar{u}_\pm(p) = \bar{u}(p)\omega_\mp. \tag{2.40}$$

[3]For massless particles there is no need to distinguish between particles and antiparticles. The spinor of an anti-particle field, $v_\pm$, is given by $v_\pm = u_\mp$.

When matrix elements of unspecified helicities are squared and summed over spin states, the usual spin sum relation is used, converting the square into a trace over γ-matrices,

$$\sum_{spins} u(p)\bar{u}(p) = \not{p}. \tag{2.41}$$

The analogous form for spinors of definite helicity can be found by projecting eq. (2.41) with $\omega_{\pm}$,

$$u_{\pm}(p)\bar{u}_{\pm}(p) = \omega_{\pm}\ \not{p}. \tag{2.42}$$

A spinor representation for the polarization vectors of massless gauge bosons can also be found. For a polarization vector $\varepsilon^{\mu}_{\lambda}(p)$, of momentum p and helicity λ, this representation must obey the following conditions.

$$\begin{aligned} \varepsilon_{\pm}(p)\cdot p = 0, \qquad & \varepsilon_{\pm}(p)\cdot\varepsilon_{\pm}(p) = 0, \\ (\varepsilon_{\pm}(p))^{*} = \varepsilon_{\mp}(p), \qquad & \varepsilon_{\pm}(p)\cdot\varepsilon_{\mp}(p) = -1. \end{aligned} \tag{2.43}$$

It is usual to choose

$$\varepsilon^{\mu}_{\pm}(p) = \pm\frac{\bar{u}_{\pm}(p)\gamma^{\mu}u_{\pm}(k)}{\sqrt{2}\bar{u}_{\mp}(k)u_{\pm}(p)}, \tag{2.44}$$

where k is a reference momentum which can be chosen to simplify the result.

Two relations are useful for manipulating spin lines:

- **Line Reversal:** This inter-relates different helicity amplitudes, reducing the number which must be calculated. It is given by,

$$\bar{u}_{\lambda_1}(p_1)\Gamma u_{\lambda_2}(p_2) = \lambda_1\lambda_2\bar{u}_{-\lambda_2}(p_2)\Gamma^{R}u_{-\lambda_1}(p_1), \tag{2.45}$$

  where Γ is an arbitrary string of γ-matrices, and Γ^{R} its reverse.

- **The Chisholm Identity:** In its usual form, this is given by,

$$\bar{u}_{\lambda}(p_1)\gamma^{\mu}u_{\lambda}(p_2)\gamma_{\mu} = 2\left[u_{\lambda}(p_2)\bar{u}_{\lambda}(p_1) + u_{-\lambda}(p_1)\bar{u}_{-\lambda}(p_2)\right]. \tag{2.46}$$

  This is a special case of the more useful relation,

$$\bar{u}_{\lambda}(p_1)\Gamma_1\gamma^{\mu}\Gamma_2u_{\lambda}(p_2)\gamma_{\mu} = 2\left[\Gamma_2u_{\lambda}(p_2)\bar{u}_{\lambda}(p_1)\Gamma_1 + \Gamma_1^{R}u_{-\lambda}(p_1)\bar{u}_{-\lambda}(p_2)\Gamma_2^{R}\right], \tag{2.47}$$

where Γ_i are again arbitrary strings of γ-matrices, with Γ_i^R their reverse. This identity should be used to remove repeated indices. Since the second γ-matrix on the left-hand-side of eq. (2.47) must always be contained in a spin line, only one of the terms on the right-hand-side will contribute. Therefore, repeated indices can be removed without increasing the number of terms in the expression.

Indices which are repeated in the same spin line can also be removed by anti-commuting[4] their γ-matrices along the line until they are next to each other, and using,

$$\gamma^\mu \gamma_\mu = 4. \tag{2.48}$$

However, this anti-commutation will generate many terms and it is much more economical to use the generalized Chisholm identity.

By specifying the helicity of the spinor on the end of a spin line, the projection operator can be anticommuted along the line and each spinor will adopt a definite helicity. Any γ-matrix contracted with a massless momentum can be written as a spinor product using eq. (2.42), and any repeated indices are removed by using the Chisholm identity. In this way, all helicity amplitudes can be written in terms of the spinor products,

$$[ij] \equiv \bar{u}_+(p_i)u_-(p_j), \tag{2.49}$$

$$\langle ij \rangle \equiv \bar{u}_-(p_i)u_+(p_j). \tag{2.50}$$

These spinor products are antisymmetric (seen using the line reversal trick) and are related to each other by complex conjugation.

$$[ij] = -[ji], \qquad \langle ij \rangle = -\langle ji \rangle, \tag{2.51}$$

$$\langle ij \rangle = [ji]^*. \tag{2.52}$$

It is clear that these are the only non-zero scalars which are possible since,

$$\bar{u}_\pm(p_i)u_\pm(p_j) = \bar{u}(p_i)\omega_\mp\omega_\pm u(p_j) = 0. \tag{2.53}$$

[4]The definition $\gamma_5 = i\gamma_0\gamma_1\gamma_2\gamma_3$ gives $\{\gamma_5, \gamma^\mu\} = 0$.

Furthermore, their modulus squared returns twice the dot product of the two momenta.

$$\begin{aligned} |[ij]|^2 &= \frac{1}{2}\left([ij]\langle ji\rangle + \langle ij\rangle[ji]\right) \\ &= \frac{1}{2}\sum_{\lambda_1,\lambda_2} \bar{u}_{\lambda_1}(p_i)u_{\lambda_2}(p_j)\bar{u}_{\lambda_2}(p_j)u_{\lambda_1}(p_i) \\ &= \frac{1}{2}Tr(\not{p}_i\ \not{p}_j) \\ &= 2p_i\cdot p_j. \end{aligned} \tag{2.54}$$

The following example, where $p_i^2 = 0$, demonstrates some of these techniques.

$$\mathcal{M} = \varepsilon_\mu^+(p_5)\left[\bar{u}_+(p_1)\gamma^\mu(\not{p}_1 + \not{p}_5)\gamma^\nu u(p_2)\right].\bar{u}_+(p_3)\gamma_\nu u(p_4) \tag{2.55}$$

Using the definition of eq. (2.44) for the polarization vector, and eq. (2.42) to write $\not{p}$ as spinors, this becomes,

$$\mathcal{M} = \frac{\bar{u}_+(p_5)\gamma_\mu u_+(k)}{\sqrt{2}\bar{u}_-(k)u_+(p_5)}\left[\bar{u}_+(p_1)\gamma^\mu\{u_+(p_1)\bar{u}_+(p_1) + u_+(p_5)\bar{u}_+(p_5)\}\gamma^\nu u_+(p_2)\right]\bar{u}_+(p_3)\gamma_\nu u_+(p_4).$$

The negative helicity spinors in the decomposition of $\not{p}$ have been cancelled by helicity conservation. The Chisholm identity can be used to remove the repeated indices,

$$\mathcal{M} = \frac{\bar{u}_+(p_1)u_-(p_5)}{\sqrt{2}\bar{u}_-(k)u_+(p_5)}\bar{u}_-(k)\left\{u_+(p_1)\bar{u}_+(p_1) + u_+(p_5)\bar{u}_+(p_5)\right\}u_-(p_3)\bar{u}_-(p_4)u_+(p_2).$$

Now, the expression is written completely in terms of spinor products and the notation of eqs. (2.49) and (2.50) can be used,

$$\mathcal{M} = \frac{[15]}{\sqrt{2}\langle k5\rangle}\{\langle k1\rangle[13] + \langle k5\rangle[53]\}\langle 42\rangle.$$

Finally, the reference momentum, k, can be chosen for example to be p_1,

$$\mathcal{M} = \frac{1}{\sqrt{2}}[15][53]\langle 42\rangle. \tag{2.56}$$

2.7 Summary

This chapter has presented a brief overview of some of the theoretical aspects of Quantum Chromo-Dynamics required for a study of next-to-leading order QCD calculations.

In particular, the theory is described by the QCD Lagrange density from which the Feynman rules of Appendix D can be derived. It has been seen that the resulting Feynman diagrams often contain ultra-violet singularities which can be removed by a process of renormalization. This leads to a strong coupling constant which runs with energy.

In addition, the $SU(3)$ structure of QCD results in products of colour matrices multiplying QCD Feynman diagrams. The algebra of these colour matrices and how such products can be simplified in practice has been demonstrated.

Finally, an overview of spinor helicity methods has been given. This involves the calculation of matrix elements where the helicities of the external particles are specified.

The following chapter will discuss how QCD is realized in experiment and how a phenomenological connection between theory and experiment can be made.

Chapter 3

Jet Physics

3.1 QCD in Electron-Positron Annihilation

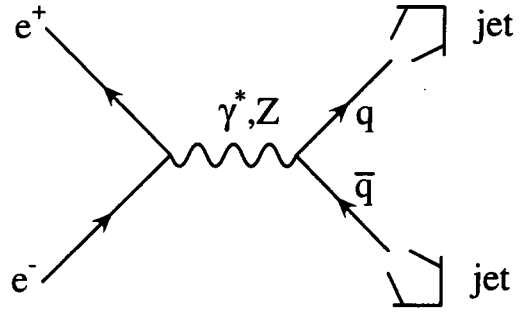

Figure 3.1: Electron-Positron Annihilation to Jets.

In order to test QCD as the theory of the strong interaction, it must be compared with experiment. One particularly effective way of doing this is via *electron-positron annihilation.* Electrons and positrons are collided together at high energies, producing a virtual photon or a Z boson, which subsequently decays into a quark-antiquark pair, see fig. (3.1). However, due to the QCD property of colour confinement, these quarks are not directly observed in experiment but form *jets* of colourless hadrons by a process of *hadronization.* These jets, and how they can be used to compare the theory of QCD with experiment, will be the subject of this chapter.

Electron-positron annihilation has several advantages over other scattering processes such as hadron-hadron collisions or electron-nucleon scattering.

- The couplings of quarks and gluons to gauge bosons are point-like and well understood. This is contrary to processes with initial state nucleons where the quarks are buried deep within the nucleon and their momentum distributions are described by universal *parton density functions*. In order to obtain physical results, the interesting small distance interactions must be convoluted with these parton densities.
- The detector sits in the centre of mass frame of the electron-positron pair, and unlike collisions involving nucleons, there is no target remnant. This allows any missing energy or momentum in the event to be easily spotted, helping to reduce unwanted backgrounds.
- Experimental data is available over a very broad range of energy, allowing QCD to be comprehensively tested. In addition, the presence of the Z boson resonance provides large cross-sections, and therefore increased statistics.

For these reasons, and because the results of Chapter 6 are most readily applied to e^+e^- collisions, this chapter will consider quark and gluon jets from the perspective of electron-positron annihilation. Of course, jets are present in any process containing quarks or gluons in the final state and the principles described here can equally well be applied to hadron-hadron collisions or lepton-nucleon scattering.

3.2 From Partons to Hadrons

The hadrons observed in the detectors of hard scattering experiments are seen to form collimated jets. A typical example of a three jet event seen in the ALEPH detector of the LEP collider at CERN, Geneva, is given in fig. (3.2). However, perturbative QCD calculations give matrix elements where the final states are partons, *not* hadrons. In order to use perturbative QCD to make experimental predictions it is necessary to make a link

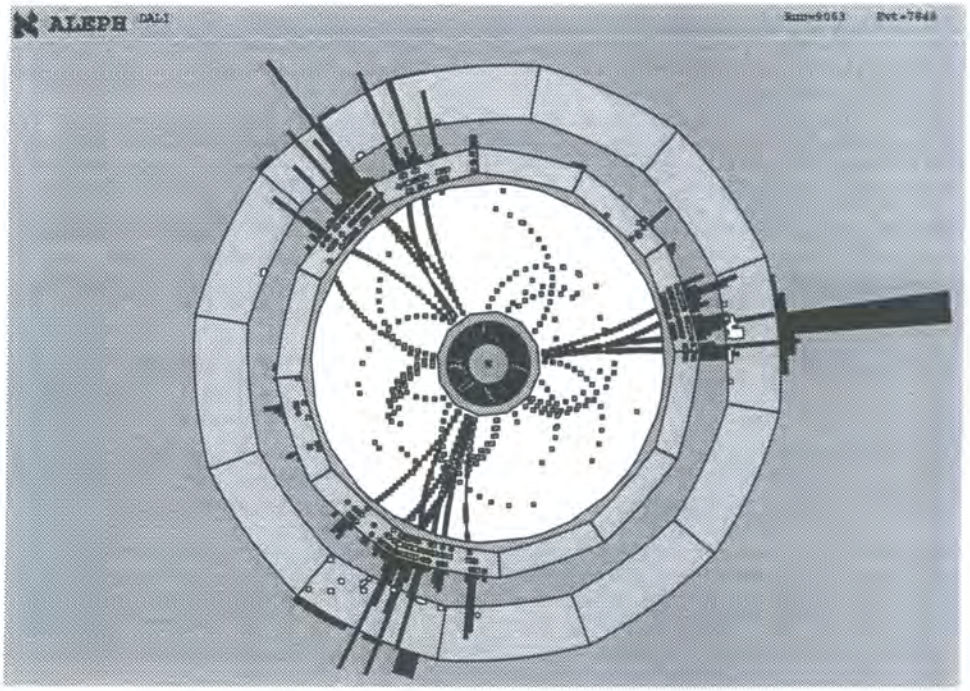

Figure 3.2: Three Jet Production at ALEPH.

between the partons of perturbative QCD calculations and the experimentally observed hadrons. Jets are instrumental in making this connection.

The three jet structure of fig. (3.2) is fairly clear. However, if quantitative experimental studies of jet production are to be made, it is necessary to have an exact definition of a hadron jet. This definition is known as the *jet algorithm*, and it describes how the final state hadrons should be combined together to form jets.

The jet algorithm can be applied not only to hadrons, but also at the level of partons. That is, the partons which are the final states of perturbative QCD calculations can also be grouped together into jets using the jet algorithm. The assumption of *Local Parton Hadron Duality* is then applied. This asserts that the jets formed from partons will mimic the jets of hadrons seen in the detector. In particular, the energy and momenta of the partons are well described by the energy and momenta of the final state hadrons in the jet. Furthermore, the quantum numbers of the partons are reflected in the final hadrons. In short, the properties of hadronic jets are to a large extent determined by the properties

of the original partons.

It is remarkable that this assumption works so well. *A priori*, one might expect that any correlation between parton and hadron jets would be destroyed by interactions of the partons after the time scale of the perturbative calculation, and their subsequent hadronization. However, these *coherence* and hadronization effects are relatively small and good agreement with experiment is found.

3.3 The Jet Algorithm

Jets can be defined using two principal forms of jet algorithm: *cone* algorithms and *clustering* algorithms. Cone algorithms are principally used in $p\bar{p}$ collisions, whereas clustering algorithms are now used in both e^+e^- collisions and e^-p scattering. Any jet algorithm should conform to the following requirements:

- The algorithm must be insensitive to the emission of soft (low momentum) particles. Also, a collinear pair of particles should be treated identically to a single particle with their combined momenta. These requirements ensure the cancellation of the soft and collinear divergences seen in perturbative QCD calculations, as will be outlined in section (3.4).
- The definition should be simple to use both in theory and experiment.
- Particles which have a small angle between them should be grouped into the same jet.
- The jets should be subject to only small hadronization corrections.

In addition, jets defined in hadron-hadron collisions or nucleon-lepton scattering must allow factorization of initial state collinear singularities, and minimize contamination from the underlying event.

Cone Algorithms

Cone algorithms place cones of a fixed angular size, R, around the jets. These are positioned so as to maximize the energy flowing through the cone. Although conceptually simple, these algorithms are somewhat imprecise due to their inflexible jet boundary. Moving the cone by a small amount can cause particles to fall out of (or into) the cone, considerably changing the properties of the jet. This results in them being somewhat sensitive to the emission of soft particles. Furthermore, ambiguities arise when two cones overlap. It is not clear to which jet particles in the overlap region should be allocated. These problems have not been fully solved, and some attempts are now being made to use the more precise clustering algorithms in $p\bar{p}$-collisions.

Clustering Algorithms

Clustering algorithms all follow a similar pattern:

- For every pair of hadrons or partons observed in the final state, a resolution parameter, y_{ij}, is calculated. The definition of y_{ij} is dependent on the jet algorithm used.
- The smallest value of y_{ij} is then compared to a predefined jet resolution scale, y_{cut}. If $y_{ij} < y_{cut}$, the two particles are regarded as being *unresolved* and are placed in the same jet. For comparison with other particles, they are then recombined to form a *pseudo-particle* with energy and momentum which is again dependent on the algorithm.
- This process is repeated until the resolution parameters, y_{ij}, of all particle or pseudo-particle pairs are greater than y_{cut}.

There are many clustering jet algorithms, differing in resolution criteria and methods for recombining the two particles to form a pseudo-particle. Some of the most commonly used are detailed in table (3.1).

Algorithm	Resolution y_{ij}	Recombination
E	$\frac{(p_i+p_j)^2}{s}$	$p_k = p_i + p_j$
P	$\frac{(p_i+p_j)^2}{s}$	$\vec{p_k} = \vec{p_i} + \vec{p_j}$ $E_k = \lvert\vec{p_k}\rvert$
E0	$\frac{(p_i+p_j)^2}{s}$	$\vec{p_k} = \frac{E_k(\vec{p_i}+\vec{p_j})}{\lvert\vec{p_i}+\vec{p_j}\rvert}$ $E_k = E_i + E_j$
JADE	$\frac{2E_iE_j(1-\cos\theta_{ij})}{s}$	$p_k = p_i + p_j$
DURHAM (k_T)	$\frac{2\min(E_i^2,E_j^2)(1-\cos\theta_{ij})}{s}$	$p_k = p_i + p_j$

Table 3.1: Some of the jet algorithms most commonly used in e^+e^- collisions. The momenta and energy of the two hadrons are given by p_i, p_j, E_i and E_j, and θ_{ij} is the angle between them. The recombined pseudo-particle has momenta and energy p_k and E_k. s is the total invariant mass for the event.

Clearly, cluster algorithms are more precisely defined than cone algorithms and have several advantages. Unlike cone algorithms, the jets of cluster algorithms have flexible boundaries. The algorithm is most sensitive to the particles in the centre of the jet (as compared to cone algorithms where all areas are treated equally), making it insensitive to soft particles at the edge of the cone. This helps reduce hadronization corrections. Also, the flexible cone size allows higher energy jets to be narrower, which seems physically sensible. Furthermore, to which jet a particle belongs is now precisely defined. The jets cannot overlap and there is no ambiguity.

However, $p\bar{p}$ collisions and e^-p scattering contain particles from the proton remnant which should not be combined into jets (since they have not participated in the hard scattering). This is problematic for clustering algorithms which combine *all* particles into jets. To overcome this problem, an extra particle must be added in the direction of the incoming particle beams [12].

Table (3.1) demonstrates the large variety in clustering algorithms. In particular, the first three algorithms shown (ie. E, P, and E0) are modifications of the JADE algorithm motivated by the conflicting desires for Lorentz invariance and masslessness of the recombined pseudo-particle. In perturbative QCD calculations, quarks and gluons are usually taken to be massless, and it is desirable for the pseudo-particle to also have zero invariant mass ($p_k^2 = 0$). However this is not possible while maintaining Lorentz invariance. The E-scheme maintains Lorentz invariance, whereas the P and E0 schemes scale energy and momentum of the pseudo-particle respectively in order to keep its invariant mass zero.

Unfortunately, the JADE algorithm (and its modifications) tends to group soft particles separated by large angles into the same jet. This undesirable feature is overcome by the DURHAM (or k_T) algorithm, which groups soft particles together with the hard particle which is closest in angle. As a consequence, this allows leading and next-to-leading infrared logarithms to be resummed.

3.4 Calculating Jet Rates

It has been seen that the partons of perturbative QCD cannot be directly compared with the hadrons seen in experiment. Instead, partons and hadrons must be organised into jets using a jet algorithm and these theoretical and experimental jets can then be compared.

As an illustrative example, consider the production of three jets at leading order and two jets at next-to-leading order. This will demonstrate how partonic matrix elements must be combined to form jet cross-sections, and outline the appearance and ultimate cancellation of soft and collinear divergences.

3.4.1 The Tree-Level Three Jet Rate

At tree level everything is particularly straightforward. The tree level three jet rate has only one contributing process: $e^+e^- \to q\bar{q}g$, fig. (3.3). However, only the parts of phase space where all three partons are resolved as separate jets, ie. $y_{qg} > y_{cut}$ and

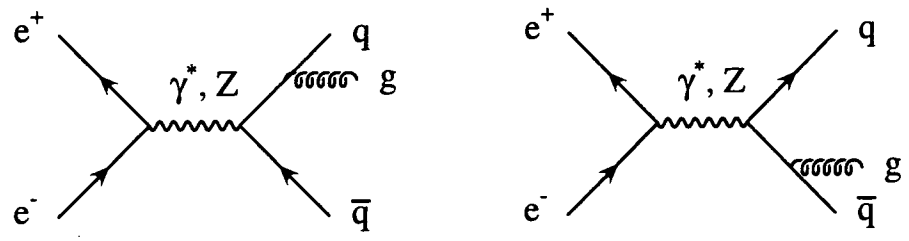

Figure 3.3: The Tree-Level Feynman Diagrams for $e^+e^- \rightarrow q\bar{q}g$.

$y_{\bar{q}g} > y_{cut}$, should be included. These cuts keep the matrix elements well away from the regions of phase space where the gluon is soft or collinear to the quark or antiquark, and the resulting cross-section is finite. Each jet is modelled by one parton and there is little sensitivity to the jet algorithm.

3.4.2 The Two Jet Rate at Next-to-Leading Order

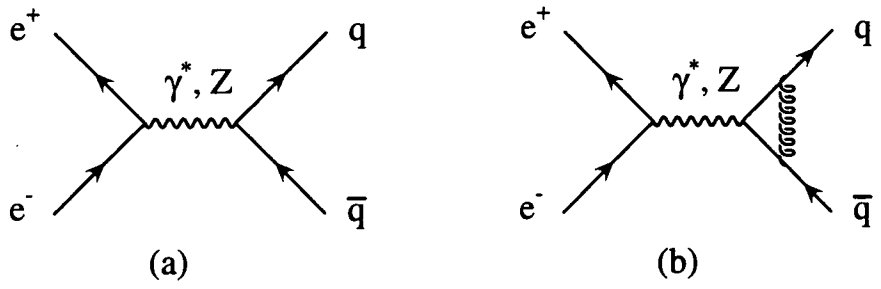

Figure 3.4: The Feynman diagrams for the process $e^+e^- \rightarrow q\bar{q}$ at, (a) tree-level, $\mathcal{O}(1)$ and (b) one loop, $\mathcal{O}(\alpha_s)$

In calculating the rate of two jet production in e^+e^- annihilation at leading order, $\mathcal{O}(1)$, only one Feynman diagram, fig. (3.4(a)), contributes. Since momentum must be conserved, the quark and antiquark are produced back-to-back with the same energy and are always resolved as separate jets.

At next-to-leading order, α_s, there will be two contributions to the two jet rate. One contribution is given by the next-to-leading order two parton process, $e^+e^- \rightarrow q\bar{q}$. This

is the loop diagram of fig. (3.4(b)), which must be multiplied by tree-level, fig. (3.4(a)), to give a contribution of $\mathcal{O}(\alpha_s)$. [1] This is called the *virtual* contribution, because of the emission and reabsorption of a virtual gluon. Again, the quark and antiquark are always resolved as separate jets.

In addition, a contribution is given by the tree-level three parton process, $e^+e^- \to q\bar{q}g$, fig. (3.3), where one of the partons is unresolved, ie. $y_{qg} < y_{cut}$ and/or $y_{\bar{q}g} < y_{cut}$. This can happen in two ways.

- The gluon is nearly collinear to the quark or antiquark. The nearly collinear pair are then combined together to form a single jet, with the jet axis and energy defined by the resulting pseudo-particle of the jet algorithm.
- Alternatively, one of the partons may be soft enough to be undetected. Again, the details of its combination with the other partons to form jets is dependent on the algorithm. In the DURHAM algorithm, for example, the soft parton would usually be combined with the hard parton closest in angle.

This is known as the *real* contribution, because of the emission of a real gluon. In order to combine this with the two parton virtual contribution the extra degrees of freedom, ie. the collinear or soft partons, are integrated out.

Infrared Divergences

It has already been demonstrated that QCD matrix element calculations at one-loop often exhibit ultra-violet divergences, caused by small distance scale effects. These divergences are cured by renormalization. However, QCD matrix elements also contain *soft* and *collinear* divergences (collectively called *infra-red* divergences) caused by long distance scale effects. Indeed, both the virtual and real contributions to $e^+e^- \to 2$ jets contain such divergences.

[1] Diagrams with loops on the quark or antiquark legs would also contribute in general, but are zero for massless particles.

Virtual Contribution: The loop diagram of fig. (3.4(b)) contains an integration over the unconstrained loop momentum which can be written,

$$I = \int d^4k \frac{(k+p_q)^\mu (k-p_{\bar{q}})^\nu}{k^2(k+p_q)^2(k-p_{\bar{q}})^2} \tag{3.1}$$

Naïve power counting shows that this integral diverges due to the behaviour as $k \to 0$. Furthermore, it is also divergent when the virtual gluon is collinear to the quark or antiquark. It is *infra-red* divergent.

Real Contribution: The tree-level partonic matrix elements for $e^+e^- \to q\bar{q}g$ also contain soft and collinear divergences. Using the Feynman rules of Appendix D, and restricting to $e^+e^- \to \gamma^* \to q\bar{q}g$ for simplicity, the matrix elements are given by,

$$\mathcal{M} = -ig_s e Q_q \bar{u}(p_{e^-})\gamma_\mu u(p_{e^+})\bar{u}(p_q)\left[\gamma^\nu T^a \frac{[\not{p}_q + \not{p}_g]}{(p_q+p_g)^2}\gamma^\mu + \gamma^\mu \frac{[\not{p}_{\bar{q}} + \not{p}_g]}{(p_{\bar{q}}+p_g)^2}\gamma^\nu T^a\right] u(p_{\bar{q}})\epsilon_\nu^{a*}(p_g) \tag{3.2}$$

The external particles of the above process — the quark, antiquark and gluon final states — are taken to be on mass-shell[2]. Then, it is clear that $\mathcal{M}$ will diverge when the gluon is collinear to the quark or antiquark ($p_q \cdot p_g \sim 0$ or $p_{\bar{q}} \cdot p_g \sim 0$), or when it is soft ($p_g \sim 0$).

These partonic matrix elements are not physical on their own but must be combined to form jet cross sections. When combined, the soft and collinear divergences cancel between real and virtual contributions. This cancellation of the infrared divergences has been shown to hold to all orders in perturbation theory [6, 7].

Notice that these divergences are long distance effects — the matrix elements of eq. (3.2) diverge as $(p_q + p_g)^2 \to 0$ or $(p_{\bar{q}} + p_g)^2 \to 0$, implying that the quark or antiquark propagates for a long time before emitting the gluon. This is to be compared with ultra-violet divergences which are of a short distance (high energy) nature. It was seen that the success of renormalization is due to the insensitivity to physics at energy

[2]Heisenberg's uncertainty principle states that the virtuality of a particle is inversely proportional to its lifetime, and therefore, external particles are taken to be on mass-shell in order to survive beyond the time of the interaction.

scales far above that of the interaction. Similarly, one would expect the interaction to be unaffected by low energy, long distance phenomena, and with hindsight the cancellation of the infrared divergence is not surprising.

3.5 Regularization

Clearly some regularization must be performed before the divergent real and virtual contributions are calculated. The most usual way of doing this is via *dimensional regularization*, where all particle momenta and polarization vectors are analytically continued to $n = 4 - 2\epsilon$ space-time dimensions[3]. The divergences in the real and virtual contributions are then manifest as poles in ϵ which cancel when the two parts are combined. The limit $\epsilon \to 0$ can then be safely taken, returning to four dimensions.

Alternatively, a distinction can be made between observed and unobserved particles. The *unobserved* particles are the internal particles which form loops in the virtual contribution and the external particles which are soft or collinear in the real contribution. It is easy to see that it is the continuation of the momenta of these unobserved particles to a number of space-time dimensions different from four, which regulates the divergences of the real and virtual contributions. The *t' Hooft-Veltman* scheme [13] keeps the momenta and polarization vectors of the observed particles in four dimensions while analytically continuing the unobserved particles to $n = 4 - 2\epsilon$ dimensions.

It should be noted the above regularizations are incompatible with the helicity method described in section (2.6). The chiral projection operators $\frac{1}{2}(1 \pm \gamma_5)$ are not well defined away from four dimensions. To overcome this, a third regularization scheme, *dimensional reduction* [14], is sometimes used. Here only the momenta of the unobserved particles are continued to $n = 4 - 2\epsilon$ dimensions. Their polarization vectors are left in four dimensions allowing γ_5 to be used. However, this regularization procedure was originally restricted to dimension $n < 4$ ($\epsilon > 0$) in order to maintain gauge invariance. The vector field

[3]Whether ϵ is greater or less than zero is unspecified. In fact $\epsilon > 0$ would only regulate ultra-violet divergences, whereas $\epsilon < 0$ would regulate infrared divergences. By leaving ϵ free to be either, both divergences are regulated at the same time.

was decomposed into a n-dimensional vector and $(4-n)$-dimensional scalars under gauge transformations [14, 15]. This is useless for regulating infrared divergences which require the possibility of having $\epsilon < 0$. Never-the-less, dimensional reduction is often used without enforcing this restriction, and has been explicitly shown to be gauge invariant up to two loops [15]. This method has been tested by Kunszt, Signer and Trócsányi [34], by the diagrammatic evaluation of the one-loop corrections of the helicity amplitudes of all $2 \to 2$ parton processes.

3.6 Slicing and Subtraction Methods

The example of section (3.4) describes how the soft and collinear divergences associated with parton level matrix elements cancel when the real and virtual contributions are combined to give jet observables. However, in practice this cancellation is very difficult to perform, since $(m+1)$-parton matrix elements must first be projected onto the m-parton phase space by integrating out the extra degrees of freedom (ie. the soft or collinear partons).

How should this integration be done? It is impractical to perform it analytically, due to the complicated structure of the matrix elements. Furthermore, the boundary of the phase space where one parton is unresolved is dependent on the jet algorithm and the experimental configuration. Even if the integration could be performed analytically, a separate calculation would have to be done for every different algorithm or detector setup used.

Clearly, the integration must be performed numerically. It is then done automatically for any jet observable required, and the integration boundary can be easily altered to accommodate any jet algorithm or detector configuration. However, recall that the real and virtual matrix elements are divergent. This divergence cannot be cancelled numerically since the cancellation of very large numbers would lead to unacceptable errors.

To overcome these problems, methods have been developed where numerical and analytical techniques are combined. The divergence is first canceled analytically, and then

the integration is performed numerically. This can be done in two ways — *slicing* and *subtraction*. For illustrative purposes, these methods will be described with reference to a simple toy example [19]. For more complete and detailed descriptions of the slicing and subtraction methods see [16] and [18].

Consider the following expression:

$$I = \lim_{\epsilon \to 0} \left(\int_0^1 \frac{dx}{x} x^\epsilon f(x) - \frac{1}{\epsilon} f(0) \right). \tag{3.3}$$

Here $f(x)$ represents the $(m+1)$-parton real matrix elements, and x is analogous to the energy of a soft gluon or the angle between two collinear partons. The integration over the soft and collinear regions of $(m+1)$-parton phase space are then reduced to an integration over x. The first term of eq. (3.3), representing the real contribution, is regulated by the factor x^ϵ as if by dimensional regularization. However, as $\epsilon \to 0$ the integral diverges. The second term of eq. (3.3) is analogous to the virtual diagrams, and also diverges as $\epsilon \to 0$. This divergence cancels between the first and second terms, rendering I finite.

3.6.1 Slicing

One possibility is to introduce an artificial cut, slicing off the very edge of phase space where the matrix elements diverge. In this small slice at the edge of phase space, approximations can be made which simplify the matrix elements considerably. Furthermore, they exhibit soft and collinear factorizations — ie. the matrix elements can be approximated by the m-parton matrix elements multiplied by a factor containing all the extra (soft or collinear) degrees of freedom.

In terms of the toy example of eq. (3.3), the integral is divided into two regions: $0 < x < \delta$ and $\delta < x < 1$, with $\delta \ll 1$. In the first region $f(x)$ is approximated by $f(0)$. The integration can then be performed easily, extracting the pole in ϵ, which cancels with the divergence from the virtual matrix elements (represented by the second term of eq. (3.3)),

$$I = \lim_{\epsilon \to 0} \left(\int_0^\delta \frac{dx}{x} x^\epsilon f(x) + \int_\delta^1 \frac{dx}{x} x^\epsilon f(x) - \frac{1}{\epsilon} f(0) \right)$$

$$\begin{aligned} &\approx \lim_{\epsilon\to 0}\left(f(0)\int_0^\delta \frac{dx}{x}x^\epsilon - \frac{1}{\epsilon}f(0) + \int_\delta^1 \frac{dx}{x}x^\epsilon f(x)\right) \\ &= \lim_{\epsilon\to 0}\left(\frac{\delta^\epsilon}{\epsilon} - \frac{1}{\epsilon}\right)f(0) + \int_\delta^1 \frac{dx}{x}f(x) \\ &= f(0)\log\delta + \int_\delta^1 \frac{dx}{x}f(x). \end{aligned} \tag{3.4}$$

The soft and collinear factorizations of the matrix elements (and phase space) are universal and this method can be used for any process [16]. However, approximations have been made and care must be taken to choose a suitable value of the artificial cut δ. If δ is chosen too large, the approximations valid at the edge of phase space will break down, leading to a large systematic error. However, if δ is chosen too small, the remaining numerical integration will approach too close to the divergence and large cancellation errors will be present.

3.6.2 Subtraction

Alternatively, the divergent part of the $(m+1)$-parton matrix elements can be added to and subtracted from the expression, making the integration manifestly finite,

$$\begin{aligned} I &= \lim_{\epsilon\to 0}\left(\int_0^1 \frac{dx}{x}x^\epsilon f(x) - \int_0^1 \frac{dx}{x}x^\epsilon f(0) + \int_0^1 \frac{dx}{x}x^\epsilon f(0) - \frac{1}{\epsilon}f(0)\right) \\ &= \lim_{\epsilon\to 0}\left(\int_0^1 \frac{dx}{x}x^\epsilon\left[f(x)-f(0)\right] + f(0)\left[\int_0^1 \frac{dx}{x}x^\epsilon - \frac{1}{\epsilon}\right]\right) \\ &= \int_0^1 \frac{dx}{x}\left[f(x)-f(0)\right]. \end{aligned} \tag{3.5}$$

In effect, "fake" matrix elements have been found which are easily integrated analytically and which have the same divergences as the true $(m+1)$-parton matrix elements. It should be stressed that this approach is exact — no extra theoretical cuts or approximations have been imposed. However, until recently, the divergences of the $(m+1)$-parton matrix elements, and therefore the "fake" matrix elements, had to be calculated analytically for every observable (and sometimes jet algorithm) required. This was first done for the three jet case by Ellis, Ross and Terrano [20].

This problem has now been overcome by Catani and Seymour [17, 18], who have developed new universal *dipole factorization formulae.* These allow the derivation of process-independent subtraction matrix elements which can then be integrated once-and-for-all. Thus, the subtraction method has now been made fully general.

3.7 The Importance of Next-to-Leading Order

The calculation of QCD observables at next-to-leading order is rather involved — much more so than at tree-level. However, as will be demonstrated in this section, these NLO corrections are essential for a good theoretical understanding of QCD and a better comparison of theory with experiment.

It is clear that NLO calculations substantially improve the accuracy to which QCD observables can be calculated. The measured value of the strong coupling constant is around 0.12 at the scale of the Z-boson mass. Therefore one might naïvely expect that NLO QCD predictions might differ from those at tree-level by around 10%.

While the measured value, of any observable is effectively to all orders, it can only be calculated theoretically on an order by order basis,

$$A = A_1\alpha_s(\mu) + A_2\alpha_s^2(\mu) + \mathcal{O}(\alpha_s^3). \tag{3.6}$$

Truncating this series at $\mathcal{O}(\alpha_s)$ will clearly give a very different value for $\alpha_s(\mu)$ from that obtained from truncating at $\mathcal{O}(\alpha_s^2)$. Furthermore, a change of the renormalization scale[4] from μ to μ' gives, by eq. (2.22),

$$A = A_1\alpha_s(\mu') + \left(A_2 - A_1\frac{\beta_0}{4\pi}\log\left(\frac{\mu^2}{\mu'^2}\right)\right)\alpha_s^2(\mu') + \mathcal{O}(\alpha_s^3). \tag{3.7}$$

Tree-level results will therefore depend strongly on the choice of renormalization scale (due to the running of α_s). As a result, tree-level QCD calculations tend to be rather badly normalized. However, at next-to-leading order, the extra logarithm compensates for the change in α_s and the renormalization scale dependence is reduced.

[4] In dimensional regularization the renormalization scale is introduced in order to keep the coupling constant dimensionless in $(4-2\epsilon)$-dimensions, ie. $g \to g\mu^\epsilon$.

In fact, tree-level QCD calculations only produce the general shapes of observables. This is nicely demonstrated by the *thrust* of an event. This observable is given by,

$$T = \max_{\vec{n}} \left[\sum_i \frac{\vec{n} \cdot \vec{p}}{|\vec{p}|} \right], \tag{3.8}$$

where $\vec{p}_i$ is the three-momentum of the i^{th} particle in the event, and $\vec{n}$ is a unit vector called the thrust axis. The thrust axis is the direction on to which the projected momenta of the particles in greatest. The experimental distributions of thrust for events seen in the OPAL detector, along with the tree-level and next-to-leading order perturbative QCD predictions are shown in fig. (3.5).

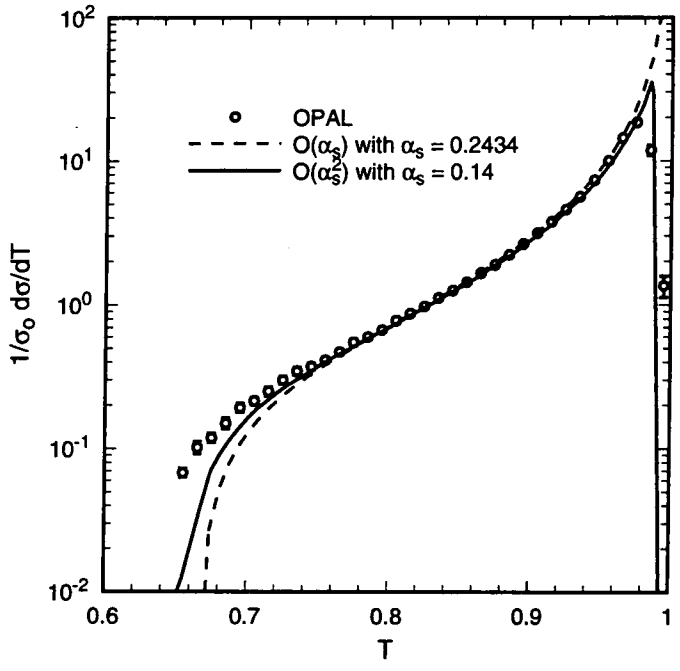

Figure 3.5: Measured distribution of Thrust, as compared to $\mathcal{O}(\alpha_s)$ and $\mathcal{O}(\alpha_s^2)$ QCD calculations.

Thrust is modelled at leading order by three parton production[5], ie. $e^+e^- \to q\bar{q}g$. Notice the large uncertainty in the normalization of this prediction — in order to get

[5]Since two parton production is always back-to-back, it will trivially give a thrust of one and is not interesting.

anywhere near the data, the value $\alpha_s = 0.2434$ must be used (for any choice of μ). Furthermore the prediction breaks down at small and large values of thrust.

For three parton production thrust has a minimum value of $\frac{2}{3}$. This mimimum is given when all three partons have the same momenta, are co-planar, and are separated in angle by $\frac{\pi}{3}$. Clearly, as the number of final particles increases the minimum will decrease, and the measured thrust can be much lower.

At high values of thrust, the leading order prediction also breaks down. This is due to the appearance of $\log(1-T)$ in the next-to-leading order correction — as $T \to 1$, the higher order corrections become increasingly important and thrust is no longer well described by only leading order.

Of course, the NLO prediction also suffers from the same deficiencies, but to a much smaller extent. Allowing more partons (up to four at NLO) allows a smaller value of thrust, and at higher thrust the inclusion of the large logarithms extends the applicability of the perturbative expansion to higher values of T. Notice now that the normalization is much better, requiring a more reasonable value of $\alpha_s(M_Z)$.

Jets are also badly modelled at leading order, especially for small values of the jet resolution parameter, y_{cut}. This is due to the appearance of $\log(y_{cut})$ in the NLO contribution. As y_{cut} becomes small, the NLO contributions become large and the perturbative expansion breaks down. Therefore in order to examine jet structures at small values of y_{cut}, NLO corrections are required. Furthermore, jets are modelled at leading order by a single parton. Consequently there is little sensitivity to the jet algorithm.

3.8 Summary.

In this chapter it has been demonstrated how jets can be used to compare parton level perturbative QCD predictions with the hadronic experimental data. Both hadrons and partons can be grouped together to form jets, and be compared using the assumption of Local Parton Hadron Duality. It has been seen that next-to-leading order QCD calcu-

lations are required for a good comparison between theory and experiment. Such NLO calculations are seen to be composed of *real* and *virtual* contributions. These contributions are individually infra-red divergent but after suitable regularization can be combined together using the subtraction or slicing methods to form infra-red safe jet quantities. The subsequent chapters will focus on the *virtual* contribution to NLO perturbative QCD calculations.

Chapter 4

Tensor Integrals

The evaluation of one loop Feynman diagrams necessarily involves integration over the unconstrained momenta flowing around the loop. It is this integration which is the principal difficulty of one loop calculations. This chapter will critically discuss some of the methods used, examining their advantages and disadvantages. In the following discussion all internal masses will be neglected.

Fig (4.1) shows a generic loop diagram, illustrating the momentum flow around the loop. The solid lines represent either fermionic or bosonic fields. Note that the arrows denote momentum flow, *not* particle flow.

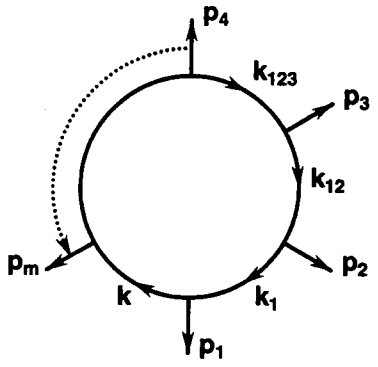

Figure 4.1: Momentum flow in a generic loop diagram with m external particles. Arrows denote momentum flow, *not* particle flow.

Such one loop diagrams with m external legs, yield integrals of the form:

$$\mathcal{I}_m^{\mu_1\cdots\mu_i} = \int \frac{d^n k}{(2\pi)^n} \frac{k^{\mu_1}\ldots k^{\mu_i}}{(k^2+i\varepsilon)(k_1^2+i\varepsilon)(k_{12}^2+i\varepsilon)\ldots(k_{1\ldots m-1}^2+i\varepsilon)} \tag{4.1}$$

where $k_{1\ldots j} = k + p_{1\ldots j}$,
$p_{1\ldots j} = p_1 + p_2 + \ldots + p_j$.

Here, k is the unconstrained momentum flowing around the loop and p_i are the momenta of the external particles. $\mathcal{I}_m^{\mu_1\cdots\mu_i}$ corresponds to the integral over a loop with m vertices (or sides). Momentum conservation ensures that $\mathcal{I}_m^{\mu_1\cdots\mu_i}$ is dependent on only $m-1$ momenta. The factors in the denominator are due to the propagators of the particles in the loop and the momenta in the numerator can arise from fermionic particles or three (or four) gluon vertices. All momenta flow *outwards*. Finally, the ε in the denominator terms is the usual infinitesimal displacement of the propagator pole away from the real axis (thus keeping the propagator finite in position space), and will be omitted from future equations.

A notation will be used where $\mathcal{I}_m$ is replaced by the m^{th} letter of the alphabet with a subscript denoting the rank of the tensor, e.g. $\mathcal{I}_3^{\mu_1\mu_2} = \mathcal{C}_2^{\mu_1\mu_2}$, etc.

The simplest form of loop integrals are those with no momenta in the numerator, ie. *scalar integrals*. Expressions for the scalar integrals are known up to the scalar five-point integral $\mathcal{E}_0$, which has recently been calculated in $n = 4 - 2\epsilon$ dimensions [21, 22] by extension to the result of Melrose [23] and independently van Neerven and Vermaseren [24] in $n = 4$ dimensions. This extension and the calculation of the other scalar integrals, can be found in Appendix C.

Several methods exist for evaluating the tensor integrals required in one loop calculations. The most usual method is to rewrite the tensor integrals as linear combinations of scalar integrals. This will be discussed in (4.1). Modifications of this method, using a vector base orthogonal to the external momenta, have been applied in recent loop calculations. Two of these variants will be described in (4.2). The problems and relative merits of these methods will be compared in (4.3). Alternatively, the tensor integrals can be obtained from the scalar integrals by using differentiation techniques. Methods of this

type will be discussed in the following chapter.

4.1 Passarino Veltman Reduction

It has been shown by Brown and Feynman [25] that tensor integrals can be written as linear combinations of scalar integrals. A general method for performing this reduction has been developed by Passarino and Veltman [26]. This Passarino Veltman reduction is the most conceptually simple method for evaluating one loop tensor integrals. Since the tensor integral can only depend on the momenta of the external particles, it can be decomposed into its tensor structure with scalar coefficients. The projection of the tensor integral onto the momenta of the external particles yields a set of simultaneous equations which can be solved to give these coefficients in terms of scalar integrals.

4.1.1 The Triangle

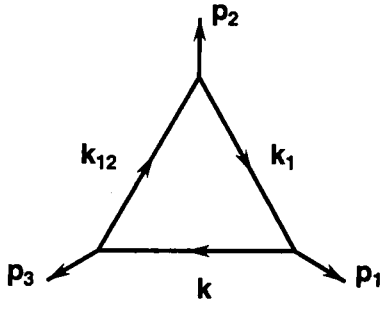

Figure 4.2: Momentum flows in a triangle loop diagram.

For illustrative purposes, consider the first rank triangle integral with all external legs off mass-shell ($p_1^2, p_2^2 \neq 0$), as shown in fig. (4.2),

$$C_1^\mu(p_1,p_2) = \int \frac{d^nk}{(2\pi)^n}\frac{k^\mu}{k^2k_1^2k_{12}^2}, \tag{4.2}$$

where $k_1 = k + p_1$,
$k_{12} = k + p_{12}$,
$p_{12} = p_1 + p_2$.

Notice that the integral depends only on two momenta since momentum conservation constrains the momentum of the third leg. Since C_1^μ depends only on p_1^μ and p_2^μ, the only possible rank one tensor structure allowed is given by,

$$C_1^\mu(p_1,p_2) = p_1^\mu c_1(p_1,p_2) + p_2^\mu c_2(p_1,p_2). \tag{4.3}$$

The scalar functions $c_1(p_1,p_2)$, $c_2(p_1,p_2)$ can be found by projecting eq. (4.3) with p_1^μ and p_2^μ, giving two simultaneous equations,

$$p_1\cdot C_1(p_1,p_2) = p_1^2c_1(p_1,p_2) + p_1\cdot p_2c_2(p_1,p_2), \tag{4.4}$$

$$p_2\cdot C_1(p_1,p_2) = p_1\cdot p_2c_1(p_1,p_2) + p_1^2c_2(p_1,p_2). \tag{4.5}$$

It is more convenient to cast these in matrix form,

$$\begin{pmatrix} p_1\cdot C_1(p_1,p_2) \\ p_2\cdot C_1(p_1,p_2) \end{pmatrix} = \begin{pmatrix} p_1^2 & p_1\cdot p_2 \\ p_1\cdot p_2 & p_2^2 \end{pmatrix} \begin{pmatrix} c_1(p_1,p_2) \\ c_2(p_1,p_2) \end{pmatrix}. \tag{4.6}$$

The entries of left hand side of the above are now scalars and easy to calculate by rewriting the scalar product in the numerator as differences of the loop propagators k_i^2,

$$p_1\cdot k = \frac{1}{2}(k_1^2 - k^2 - p_1^2), \tag{4.7}$$

$$p_2\cdot k = \frac{1}{2}(k_{12}^2 - k_1^2 - p_{12}^2 + p_1^2). \tag{4.8}$$

Using this substitution in $p_1\cdot C_1$, gives,

$$\begin{aligned} p_1\cdot C_1(p_1,p_2) &= \int \frac{d^nk}{(2\pi)^n}\frac{k\cdot p_1}{k^2k_1^2k_{12}^2} \\ &= \frac{1}{2}\int \frac{d^nk}{(2\pi)^n}\frac{k_1^2 - k^2 - p_1^2}{k^2k_1^2k_{12}^2} \end{aligned}$$

$$
\begin{aligned}
&= \frac{1}{2}\int \frac{d^nk}{(2\pi)^n}\frac{1}{k^2k_{12}^2} - \frac{1}{2}\int \frac{d^nk}{(2\pi)^n}\frac{1}{k_1^2k_{12}^2} - \frac{1}{2}p_1^2\int \frac{d^nk}{(2\pi)^n}\frac{1}{k^2k_1^2k_{12}^2} \\
&= \frac{1}{2}\mathcal{B}_0(p_{12}) - \frac{1}{2}\mathcal{B}_0(p_2) - \frac{1}{2}p_1^2\mathcal{C}_0(p_1,p_2). \qquad (4.9)
\end{aligned}
$$

To obtain the second term above the loop momenta has undergone a shift $k \to k - p_1$. Although trivial in the current example this would lead to an extra term in a higher rank tensor.

Similarly,

$$
\begin{aligned}
p_2{\cdot}\mathcal{C}_1(p_1,p_2) &= \int \frac{d^nk}{(2\pi)^n}\frac{k{\cdot}p_2}{k^2k_1^2k_{12}^2} \\
&= \frac{1}{2}\int \frac{d^nk}{(2\pi)^n}\frac{k_{12}^2 - k_1^2 - p_{12}^2 + p_1^2}{k^2k_1^2k_{12}^2} \\
&= \frac{1}{2}\int \frac{d^nk}{(2\pi)^n}\frac{1}{k^2k_1^2} - \frac{1}{2}\int \frac{d^nk}{(2\pi)^n}\frac{1}{k^2k_{12}^2} - \frac{1}{2}(p_{12}^2 - p_1^2)\int \frac{d^nk}{(2\pi)^n}\frac{1}{k^2k_1^2k_{12}^2} \\
&= \frac{1}{2}\mathcal{B}_0(p_1) - \frac{1}{2}\mathcal{B}_0(p_{12}) - \frac{1}{2}(p_{12}^2 - p_1^2)\mathcal{C}_0(p_1,p_2). \qquad (4.10)
\end{aligned}
$$

The resulting integrals are scalars and are well known (see Appendix C).

Eq. (4.6) can now be inverted to give expressions for c_1 and c_2,

$$
\begin{pmatrix} c_1(p_1,p_2) \\ c_2(p_1,p_2) \end{pmatrix} = \frac{1}{\Delta_2(p_1,p_2)}\begin{pmatrix} p_2^2 & -p_1{\cdot}p_2 \\ -p_1{\cdot}p_2 & p_1^2 \end{pmatrix}\begin{pmatrix} p_1{\cdot}\mathcal{C}_1(p_1,p_2) \\ p_2{\cdot}\mathcal{C}_1(p_1,p_2) \end{pmatrix}, \qquad (4.11)
$$

where $\Delta_2(p_1,p_2)$ is the *Gram Determinant*,

$$
\Delta_2(p_1,p_2) = \begin{vmatrix} p_1^2 & p_1{\cdot}p_2 \\ p_1{\cdot}p_2 & p_2^2 \end{vmatrix} = p_1^2p_2^2 - (p_1{\cdot}p_2)^2. \qquad (4.12)
$$

Finally, this gives $\mathcal{C}_1^\mu(p_1,p_2)$ in terms of scalar integrals:

$$
\begin{aligned}
\mathcal{C}_1^\mu(p_1,p_2) &= \frac{1}{2\Delta_2(p_1,p_2)}\times \\
&\Big[p_1^{\mu_1}\left((p_2^2p_1{\cdot}p_2 - p_1^2p_2^2 + 2(p_1{\cdot}p_2)^2)\mathcal{C}_0(p_1,p_2) + p_2{\cdot}p_{12}\mathcal{B}_0(p_{12}) - p_2^2\mathcal{B}_0(p_2) - p_1{\cdot}p_2\mathcal{B}_0(p_1)\right) \\
&+p_2^{\mu_1}\left(-p_1^2p_2{\cdot}p_{12}\mathcal{C}_0(p_1,p_2) - p_1{\cdot}p_{12}\mathcal{B}_0(p_{12}) + p_1^2\mathcal{B}_0(p_1) + p_1{\cdot}p_2\mathcal{B}_0(p_2)\right)\Big]. \qquad (4.13)
\end{aligned}
$$

Passarino Veltman Reduction has given a reasonably compact expression for $\mathcal{C}_1(p_1,p_2)$ in terms of scalar integrals.

4.1.2 The Box

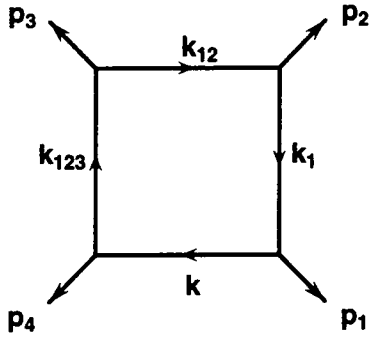

Figure 4.3: Momentum flows in a box loop diagram.

In order to demonstrate some of the difficulties inherent in the Passarino Veltman reduction of tensor integrals of higher rank or more vertices, consider the evaluation of the second rank box integral, $\mathcal{D}_2$,

$$\begin{aligned}
\mathcal{D}_2^{\mu\nu}(p_1,p_2,p_3) &= \int \frac{d^nk}{(2\pi)^n}\frac{k^\mu k^\nu}{k^2k_1^2k_{12}^2k_{123}^2} \\
&= p_1^\mu p_1^\nu d_{11}(p_1,p_2,p_3) + p_2^\mu p_2^\nu d_{22}(p_1,p_2,p_3) + p_3^\mu p_3^\nu d_{33}(p_1,p_2,p_3) \\
&+ (p_1^\mu p_2^\nu + p_2^\mu p_1^\nu) d_{12}(p_1,p_2,p_3) + (p_1^\mu p_3^\nu + p_3^\mu p_1^\nu) d_{13}(p_1,p_2,p_3) \\
&+ (p_2^\mu p_3^\nu + p_3^\mu p_2^\nu) d_{23}(p_1,p_2,p_3) \\
&+ g^{\mu\nu} d_{00}(p_1,p_2,p_3). \qquad (4.14)
\end{aligned}$$

Already, the expression for the tensor structure of $\mathcal{D}_2$ is much more complicated than that of $\mathcal{C}_1$, eq. (4.3), because $\mathcal{D}_2$ is a second rank tensor and it is dependent on an extra momentum, p_3. The scalars d_{ij} can be found by projecting eq. (4.14) with $p_i^\mu p_j^\nu$ and $g^{\mu\nu}$. This gives a set of simultaneous equations which can be solved to give d_{ij} in terms of $\mathcal{D}_1$ and $\mathcal{C}_1$. To write $\mathcal{D}_2$ as sums of scalar integrals *another* reduction must be made, rewriting $\mathcal{D}_1$ and $\mathcal{C}_1$ as $\mathcal{D}_0$, $\mathcal{C}_0$ and $\mathcal{B}_0$.

At first sight it may appear that the extra reduction from $\mathcal{D}_1$ and $\mathcal{C}_1$ to scalar integrals can be trivially performed, since $\mathcal{D}_1$ and $\mathcal{C}_1$ are now contracted with momenta, and tricks

such as eqs. (4.7) and (4.8) can be used. This is true with regard to $\mathcal{D}_1$ but not necessarily true for $\mathcal{C}_1$. In order to reduce the $\mathcal{D}_2$ to a $\mathcal{C}_1$ integral, $k{\cdot}p$ factors in the numerator of the expression have been cancelled with propagator terms in the denominator, and thus one of the propagators is now absent. If $\mathcal{C}_1$ is contracted with the momentum associated with this missing propagator then eqs. (4.7) and (4.8) are not helpful. For example $p_1\mathcal{C}_1(p_{12}, p_3)$ must be reduced in the normal way since p_1 is not contained in its arguments. Clearly this cascade of reduction after reduction will lead to a much more lengthy expression for d_{ij} than that for c_i.

Furthermore, in addition to Δ_2 introduced by the reduction of $\mathcal{C}_1$ to scalar integrals, as in (4.1.1), the reduction from $\mathcal{D}_2$ to $\mathcal{D}_1$ and $\mathcal{C}_1$ will introduce a 3×3 Gram Determinant, $\Delta_3(p_1, p_2, p_3)$, in the denominator,

$$\Delta_3(p_1, p_2, p_3) = \begin{vmatrix} p_1^2 & p_1{\cdot}p_2 & p_1{\cdot}p_3 \\ p_1{\cdot}p_2 & p_2^2 & p_2{\cdot}p_3 \\ p_1{\cdot}p_3 & p_2{\cdot}p_3 & p_3^2 \end{vmatrix}. \tag{4.15}$$

This combination of Δ_3 and Δ_2 in the denominator of the expression causes practical calculational difficulties. Often the Gram Determinant is an artifact of the method and can be cancelled with appropriate factors from the numerator. However, it is not clear (especially for long expressions) when this cancellation should be done. Indeed, complicated combinations of Gram Determinants can be made which are actually very simple when the determinants are untangled.

For example, consider factors in the denominator of the form $x + y$ and $x + z$. Even these simple factors can be combined in ways which at first sight appear much more complicated than they really are,

$$1 = \frac{x+y}{x+z} + \frac{z-y}{x+y} - \frac{(z-y)^2}{(x+y)(x+z)}. \tag{4.16}$$

Of course, Gram determinants are considerably more complicated than this simple example. Such combinations are practically impossible to spot when spread over a large number of terms.

The large size of the expressions make reduction of the higher rank tensors by hand im-

practical and must be performed using an algebraic manipulation program such as FORM [28]. This has been used extensively in the calculations found in this thesis. However, computer algebra is particularly unamenable to cancellation of factors between numerator and denominator. Packages which can in principle cancel such factors, such as MAPLE, are not sufficiently robust to handle the large number of terms coming from the reduction. This makes Passarino Veltman reduction rather impractical.

In summary, Passarino Veltman reduction allows the calculation of tensor loop integral via a decomposition into its tensor parts with coefficients given in terms of scalar integrals. However, expressions for tensor integrals evaluated in this way can be rather lengthy and complicated.

4.2 The Projective Base

Passarino Veltman reduction gives a decomposition of a tensor integral in terms of the external momenta p_i^μ and the metric $g^{\mu\nu}$. Alternatively the tensor integral can be decomposed in terms of a base which is orthogonal to the external momenta, [22, 29, 30].

4.2.1 The Naïve Projective Base

Again consider a tensor integral with m external legs:

$$\mathcal{I}_m^{\mu_1\cdots\mu_i} = \int \frac{d^n k}{(2\pi)^n} \frac{k^{\mu_1}\ldots k^{\mu_i}}{k^2 k_1^2 k_{12}^2 \ldots k_{1\ldots m-1}^2}. \tag{4.17}$$

This can be decomposed into its Lorentz structure using a new base defined by vectors, $v_i(p_1,\ldots,p_{m-1})$ and tensor $w_\nu^\mu(p_1,\ldots,p_{m-1})$, given by,

$$v_i(p_1,\ldots,p_{m-1}) = \frac{\delta^{p_1\cdots p_{i-1}\mu p_{i+1}\cdots p_{m-1}}_{p_1\cdots p_{i-1}p_i p_{i+1}\cdots p_{m-1}}}{\Delta_{m-1}(p_1,\ldots,p_{m-1})}, \tag{4.18}$$

$$w_\nu^\mu(p_1,\ldots,p_{m-1}) = \frac{\delta^{p_1\cdots p_{m-1}\mu}_{p_1\cdots p_{m-1}\nu}}{(n-m+1)\Delta_{m-1}(p_1,\ldots,p_{m-1})}. \tag{4.19}$$

The notation of eqs. (4.18) and (4.19) requires some explanation.

Firstly, the *generalised Kronecker delta* has been introduced. In an *n-dimensional* vector space, this is defined by:

$$\delta^{\mu_1\cdots\mu_n}_{\nu_1\cdots\nu_n} = \varepsilon^{\mu_1\cdots\mu_n}\varepsilon_{\nu_1\cdots\nu_n}, \tag{4.20}$$

where $\varepsilon^{\mu_1\cdots\mu_n}$ is a totally antisymmetric tensor normalised so that $\varepsilon^{12\ldots n} = 1$.

When the number of indices is less than the dimension of the vector space, the generalised Kronecker delta is assumed to have the extra indices repeated over the two corresponding ε tensors. That is,

$$\delta^{\mu_1\cdots\mu_m}_{\nu_1\cdots\nu_m} = \frac{\varepsilon^{\mu_1\cdots\mu_m\alpha_{m+1}\cdots\alpha_n}\varepsilon_{\nu_1\cdots\nu_i\alpha_{m+1}\cdots\alpha_n}}{\Gamma(n-m+1)}. \tag{4.21}$$

However, for practical purposes these extra indices can be ignored provided one temporarily assumes that the dimension of the vector space is equal to the number of indices. For example,

$$\begin{aligned}\delta^{\mu_1\nu_2}_{\nu_1\nu_2} &= \frac{\varepsilon^{\mu_1\mu_2\alpha_3\cdots\alpha_n}\varepsilon_{\nu_1\nu_2\alpha_3\cdots\alpha_n}}{\Gamma(n-1)} \\ &= \varepsilon^{\mu_1\mu_2}\varepsilon_{\nu_1\nu_2} \\ &= g^{\mu_1}_{\nu_1}g^{\mu_2}_{\nu_2} - g^{\mu_1}_{\nu_2}g^{\mu_2}_{\nu_1}.\end{aligned} \tag{4.22}$$

In this way, the definition of the generalised Kronecker delta can be extended to a non-integer number of dimensions.

Secondly, *Schoonship notation* has been used: an occurrence of a momentum where one would normally expect an index implies that the tensor is contracted with that momentum over the index which has been replaced. For example,

$$\varepsilon^{\mu_1\cdots\mu_{i-1}p\mu_{i+1}\cdots\mu_n} = \varepsilon^{\mu_1\cdots\mu_{i-1}\mu_i\mu_{i+1}\cdots\mu_n}p_{\mu_i}. \tag{4.23}$$

In this notation the Gram determinant is given by,

$$\Delta_{m-1}(p_1,\ldots,p_{m-1}) = \delta^{p_1\cdots p_{m-1}}_{p_1\cdots p_{m-1}}. \tag{4.24}$$

The new base vectors v_i^μ and $w^{\mu\nu}$ can be related to the external momenta p_i by expanding the generalised Kronecker delta,

$$\begin{aligned}\delta^{\mu_1\mu_2\ldots\mu_n}_{\nu_1\nu_2\ldots\nu_n} &= g^{\mu_1\nu_1}\delta^{\mu_2\mu_3\ldots\mu_n}_{\nu_2\nu_3\ldots\nu_n} - g^{\mu_1\nu_2}\delta^{\mu_2\mu_3\ldots\mu_n}_{\nu_1\nu_3\ldots\nu_n} + g^{\mu_1\nu_3}\delta^{\mu_2\mu_3\ldots\mu_n}_{\nu_1\nu_2\mu_4\ldots\nu_n} - \ldots \\ &\ldots + (-1)^{n+1} g^{\mu_1\nu_n}\delta^{\mu_2\mu_3\ldots\mu_n}_{\nu_1\nu_2\ldots\nu_{n-1}}. \end{aligned} \tag{4.25}$$

Note that v_i^μ and $w^{\mu\nu}$ have the following properties:

$$p_i \cdot v_j = \delta_{ij}, \tag{4.26}$$

$$w^{\mu\nu} p_{i\,\mu} = 0, \tag{4.27}$$

$$w^{\mu\nu} = w^{\nu\mu}, \tag{4.28}$$

$$w^\mu_\mu = 1. \tag{4.29}$$

The normalisation of $w^{\mu\nu}$, eq. (4.29), can be seen using eq. (4.25).

Also note that $v_i \cdot v_j$ is given by,

$$v_i(p_1,\ldots,p_{m-1})\cdot v_j(p_1,\ldots,p_{m-1}) = (-1)^{i+j}\frac{\delta^{p_1\ldots p_{i-1}p_{i+1}\ldots p_{m-1}}_{p_1\ldots p_{j-1}p_{j+1}\ldots p_{m-1}}}{\Delta_{m-1}(p_1,\ldots,p_{m-1})}. \tag{4.30}$$

This quantity is closely related to the decomposition of the Gram determinant into scalar products,

$$\Delta_{m-1}(p_1,p_2,\ldots,p_{m-1}) = \sum_{i,j} p_i\cdot p_j v_i(p_1,p_2,\ldots,p_{m-1})\cdot v_j(p_1,p_2,\ldots,p_{m-1}). \tag{4.31}$$

The tensor integrals are now decomposed in terms of this new basis and the coefficients of the Lorentz structure are found exactly as in standard Passarino Veltman reduction. However, the new base of $v_i(p_1,\ldots,p_j)$ and $w^{\mu\nu}(p_1,\ldots,p_j)$ are orthogonal to the external momenta p_i, eqs. (4.26) and (4.27), decoupling the system of equations which are obtained by projection onto the momenta. The corresponding matrix is already diagonal and can be trivially inverted.

This can be demonstrated in the example of the first rank triangle integral, $C_1(p_1,p_2)$. Firstly a decomposition in terms of $v_1(p_1,p_2)$ and $v_2(p_1,p_2)$ is made,

$$C_1^\mu(p_1,p_2) = \int \frac{d^nk}{(2\pi)^n}\frac{k^\mu}{k^2k_1^2k_{12}^2}$$

$$= v_1^\mu(p_1,p_2)c_1(p_1,p_2) + v_2^\mu(p_1,p_2)c_2(p_1,p_2). \tag{4.32}$$

Now, $C_1^\mu(p_1,p_2)$ is projected onto p_1 and p_2 yielding two *uncoupled* equations,

$$\begin{aligned} p_1\cdot C_1^\mu(p_1,p_2) &= p_1\cdot v_1(p_1,p_2)c_1(p_1,p_2) + p_1\cdot v_2(p_1,p_2)c_2(p_1,p_2) \\ &= c_1(p_1,p_2), \qquad (4.33) \\ p_2\cdot C_1^\mu(p_1,p_2) &= p_2\cdot v_1(p_1,p_2)c_1(p_1,p_2) + p_2\cdot v_2(p_1,p_2)c_2(p_1,p_2) \\ &= c_2(p_1,p_2). \qquad (4.34) \end{aligned}$$

Using eqs. (4.9) and (4.10), $C_1^\mu(p_1,p_2)$ is given by,

$$\begin{aligned} C_1^\mu(p_1,p_2) &= v_1^\mu(p_1,p_2)(\frac{1}{2}B_0(p_{12}) - \frac{1}{2}B_0(p_2) - \frac{1}{2}p_1^2C_0(p_1,p_2)) \\ &+ v_2^\mu(p_1,p_2)(\frac{1}{2}B_0(p_1) - \frac{1}{2}B_0(p_{12}) - \frac{1}{2}(p_{12}^2 - p_1^2)C_0(p_1,p_2)). \end{aligned} \tag{4.35}$$

The resulting expression for $C_1^\mu(p_1,p_2)$ is quite compact and it would seem at first sight that the Gram determinant problem has been removed, since no matrix had to be inverted. This is, of course, not the case. The determinant has been hidden away in the definition of the new base, eqs. (4.18) and (4.19). Indeed, in order to use the result for the tensor integral in a calculation of a loop diagram, v_i^μ and $w^{\mu\nu}$ must be rewritten in terms of the external momenta and, once again, the Gram determinant will become explicit (in fact eq. (4.13) will be reobtained).

For higher rank tensors or integrals over loops with more vertices, all the same problems will be encountered as in standard Passarino Veltman reduction. In fact, *the Gram determinant problem is exacerbated.* In standard Passarino Veltman reduction the number of Gram determinants in the final answer will be equal to the number of reductions made. For example, $D_2^{\mu\nu}$ will have two Gram determinants (one Δ_3 from the reduction of D_2 to C_1 and one Δ_2 from the reduction of C_1 into scalar integrals). However, with the new base of v_i^μ and $w^{\mu\nu}$, decomposing $D_2^{\mu\nu}$ into its Lorentz structure will provide terms containing two v_i^μ and thus two 3×3 Gram determinants, Δ_3. The subsequent reduction of C_1^μ will provide the 2×2 Gram determinants as before. Thus decomposition in terms of the new base will give three Gram determinants in the denominator instead of the usual two.

This extra problem can be overcome by using identities to relate products of v_i^μ to single v_i^μs. For example,

$$v_1^\mu(p_1,p_2,p_3)p_1\cdot v_1(p_2,p_3) = v_1^\mu(p_2,p_3) - v_2^\mu(p_1,p_2,p_3). \tag{4.36}$$

Hundreds of these Schouten identities can be found, in effect cancelling Gram determinants until, at most, one remains for each level of reduction. However, as with the cancellation of the Gram determinants in Passarino Veltman reduction, an ambiguity arises as to how this should be done, and complicated expressions are found.

The only advantage which has been obtained by introducing the new base is that the algorithm for reducing the tensor integrals to scalar integrals is more easily performed via computer algebra (since there is no matrix to be inverted). However, the cancellation of the extra Gram determinants using the various Schouten identities of the form of eq. (4.36) is very tedious to program due to the very large number of these identities, making this method impractical.

4.2.2 Decomposition of the Loop Momenta

A more useful application of the projective base of section (4.2.1) has been developed by van Oldenborgh and Vermaseren [29] to reduce tensor integrals to scalar integrals. As before, the base is defined by eqs. (4.18) and (4.19). However, now *the loop momenta itself* is decomposed in terms of this base [31]. This method is most easily understood by example.

The Triangle

Again consider the first rank triangle integral, eq. (4.2). The loop momenta in the numerator of the integral can themselves be decomposed in terms of v_i^μ and $w^{\mu\nu}$,

$$k^\mu = k\cdot p_1 v_1^\mu(p_1,p_2) + k\cdot p_2 v_2^\mu(p_1,p_2) + (n-2)w_\nu^\mu(p_1,p_2)k^\nu. \tag{4.37}$$

This is easily seen by expanding v_i^μ and $w^{\mu\nu}$ in terms of the external momenta p_i^μ using

eqs. (4.18), (4.19) and (4.25). For convenience of notation the following definition is made:

$$\mathcal{P}_3^\mu \equiv k\cdot p_1 v_1^\mu(p_1,p_2) + k\cdot p_2 v_2^\mu(p_1,p_2). \tag{4.38}$$

Now,

$$k^\mu = \mathcal{P}_3^\mu + (n-2)w_\nu^\mu(p_1,p_2)k^\nu. \tag{4.39}$$

Notice that the last term of eq. (4.37) will vanish when inserted into the loop integral, since w_ν^μ is orthogonal to the external momenta, eq. (4.27),

$$\begin{aligned} w_\nu^\mu(p_1,p_2)\int \frac{d^nk}{(2\pi)^n}\frac{k^\nu}{k^2k_1^2k_{12}^2} &= w_\nu^\mu(p_1,p_2)(p_1^\nu c_1(p_1,p_2) + p_2^\nu c_2(p_1,p_2)) \\ &= 0. \end{aligned} \tag{4.40}$$

Thus, single powers of k^μ and $\mathcal{P}_3^\mu$ are seen to be equivalent when inserted into a loop integral. Using the notation $\not\equiv$ to denote equality under integration,

$$k^\mu \not\equiv \mathcal{P}_3^\mu. \tag{4.41}$$

Using eqs. (4.7) and (4.8), $\mathcal{P}_3^\mu$ (and thus effectively k^μ) can be written in terms of the propagators in the denominator,

$$\mathcal{P}_3^\mu = -\frac{1}{2}k^2v_1^\mu + \frac{1}{2}k_1^2(v_1^\mu - v_2^\mu) + \frac{1}{2}k_{12}^2v_2^\mu - p_1\cdot p_2 v_2^\mu, \tag{4.42}$$

where the arguments of v_i^μ have been suppressed.

This allows C_1 to be written in terms of scalar integrals as described in section (4.1). So far there is no difference from the naïve use of the projective base described in section (4.2.1). However, the difference between the two methods becomes apparent when higher rank tensors are examined.

Now consider two powers of the loop momenta in the numerator, i.e. $C_2^\mu(p_1,p_2)$. Again, k^μ can be decomposed as in eq. (4.37),

$$\begin{aligned} k^\mu k^\nu &= \mathcal{P}_3^\mu\mathcal{P}_3^\nu + (n-2)w_\rho^\nu(p_1,p_2)k^\rho\mathcal{P}_3^\mu + (n-2)w_\rho^\mu(p_1,p_2)k^\rho\mathcal{P}_3^\nu \\ &+ (n-2)^2w_\rho^\mu(p_1,p_2)w_\sigma^\nu(p_1,p_2)k^\rho k^\sigma. \end{aligned} \tag{4.43}$$

The terms containing $w^{\mu\nu}$ will simplify considerably when inserted into the loop integral. This is because the only tensor structure of the tensor integral which can survive projection onto $w^{\mu\nu}$ is the metric $g^{\mu\nu}$. For example, consider the second term of eq. (4.43) in the numerator of the triangle,

$$\begin{aligned} w^{\mu}_{\rho}(p_1,p_2)\int \frac{d^nk}{(2\pi)^n}\frac{k^{\rho}\mathcal{P}_3^{\mu}}{k^2k_1^2k_{12}^2} &= w^{\mu}_{\rho}(p_1,p_2)(\sum_{i,j=1}^{2} a_{ij}p_i^{\mu}p_j^{\rho}+a_{00}g^{\mu\rho}) \\ &= w^{\mu}_{\rho}(p_1,p_2)a_{00}g^{\mu\rho}. \end{aligned} \tag{4.44}$$

where a_{ij} are scalar functions depending on the external momenta.

Also, using eq. (4.25), it is easy to show that,

$$w^{\mu}_{\rho}(p_1,p_2)w^{\nu}_{\sigma}(p_1,p_2)g^{\rho\sigma} = \frac{w^{\mu\nu}(p_1,p_2)}{n-2}. \tag{4.45}$$

Thus, the last three terms of eq. (4.43) can only give a tensor structure $w^{\mu\nu}$ after integration. The coefficient of $w^{\mu\nu}$ can be trivially found by projection with $g^{\mu\nu}$,

$$k^{\mu}k^{\nu} \doteqdot \mathcal{P}_3^{\mu}\mathcal{P}_3^{\nu} + (k^2-\mathcal{P}_3^2)w^{\mu\nu}(p_1,p_2). \tag{4.46}$$

This identity allows the reduction of $\mathcal{C}_2$ to scalar integrals, proceeding in a similar fashion to standard Passarino Veltman reduction. Firstly, eq. (4.42) is used to replace one $\mathcal{P}_3$ of the first term of eq. (4.46) with propagators, $k_{i\ldots j}$, and the integral is reduced to $\mathcal{C}_1$ and $\mathcal{B}_1$. The other $\mathcal{P}_3$ can be replaced by k, eq. (4.41), and the results for $\mathcal{C}_1$ and $\mathcal{B}_1$ are used to reduce further to scalar integrals.

Note the term containing $k^2-\mathcal{P}_3^2$ is most easily reduced by observing that,

$$\begin{aligned} k^2-\mathcal{P}_3^2 &= (k^{\mu}-\mathcal{P}^{\mu})(k^{\mu}+\mathcal{P}_3^{\mu}) \\ &= (n-2)w^{\mu}_{\nu}k^{\nu}(k^{\mu}+\mathcal{P}_3^{\mu}) \\ &= (n-2)w^{\mu}_{\nu}k^{\nu}k^{\mu} \\ &= \frac{\delta^{p_1p_2k}_{p_1p_2k}}{\Delta_2(p_1,p_2)}. \end{aligned} \tag{4.47}$$

This contains only scalar products $k{\cdot}p_i$ which can be trivially reduced using eqs. (4.7) and (4.8).

An important observation here is that only two Gram determinants have been introduced, one Δ_2 and a trivial Δ_1 (from the C_1 reduction). This is the same as standard Passarino Veltman reduction. However, a naïve use of the projective base would have given two Δ_2 and one trivial Δ_1.

Similar arguments can be used to reduce the third rank triangle to scalar integrals. It is easy to see that $k^\mu k^\nu k^\rho$ must have the following form when inserted into the triangle integral,

$$k^\mu k^\nu k^\rho \not\equiv \mathcal{P}_3^\mu \mathcal{P}_3^\nu \mathcal{P}_3^\rho + a(w^{\mu\nu}\mathcal{P}_3^\rho + w^{\mu\rho}\mathcal{P}_3^\nu + w^{\nu\rho}\mathcal{P}_3^\mu). \tag{4.48}$$

where a is to be determined. Contracting this with $g^{\mu\nu}\mathcal{P}_3^\rho$ and noting that $w_\nu^\mu \mathcal{P}_3^\nu = 0$ and $k\cdot\mathcal{P}_3 = \mathcal{P}_3^2$ gives,

$$k^2\mathcal{P}_3^2 \not\equiv \mathcal{P}_3^4 + a\mathcal{P}_3^2. \tag{4.49}$$

This is consistent with,

$$a \equiv k^2 - \mathcal{P}_3^2. \tag{4.50}$$

Putting everything together,

$$k^\mu k^\nu k^\rho \not\equiv \mathcal{P}_3^\mu \mathcal{P}_3^\nu \mathcal{P}_3^\rho + (k^2 - \mathcal{P}_3^2)(w^{\mu\nu}\mathcal{P}_3^\rho + w^{\mu\rho}\mathcal{P}_3^\nu + w^{\nu\rho}\mathcal{P}_3^\mu). \tag{4.51}$$

As before, eq. (4.42) can be used to replace one $\mathcal{P}_3$ with propagators, reducing the C_3 to C_2 and B_2. Next eq. (4.46) allows the remaining $\mathcal{P}_3^\mu \mathcal{P}_3^\nu$ to be rewritten as $k^\mu k^\nu$. Previously derived results for C_2 and B_2 are then used to give the final result in terms of scalar integrals.

The Box

The same procedure can be modified to evaluate box integrals. Again, k^μ is decomposed in terms of the projective base,

$$k^\mu = \mathcal{P}_4^\mu + (n-3)w_\nu^\mu(p_1,p_2,p_3)k^\nu, \tag{4.52}$$

with,

$$\mathcal{P}_4^\mu \equiv k\cdot p_1 v_1^\mu(p_1,p_2,p_3) + k\cdot p_2 v_2^\mu(p_1,p_2,p_3) + k\cdot p_3 v_3^\mu(p_1,p_2,p_3)$$

$$
\begin{aligned}
&= \frac{1}{2}k^2 v_1^\mu(p_1,p_2,p_3) + \frac{1}{2}(k_1^2 - p_1^2)(v_1^\mu(p_1,p_2,p_3) - v_2^\mu(p_1,p_2,p_3)) \\
&+ \frac{1}{2}(k_{12}^2 - p_{12}^2)(v_2^\mu(p_1,p_2,p_3) - v_3^\mu(p_1,p_2,p_3)) \\
&+ \frac{1}{2}(k_{123}^2 - p_{123}^2)v_3^\mu(p_1,p_2,p_3). \qquad (4.53)
\end{aligned}
$$

Note that v_i and w in eq. (4.52) are now dependent on three momenta and consequently the coefficient of w_ν^μ contains a factor $(n-3)$ as opposed to $(n-2)$ in the case of the triangle.

When integrated, products of the loop momenta can equivalently be written in terms of $\mathcal{P}_4$ and $w^{\mu\nu}$. For k^μ, $k^\mu k^\nu$ and $k^\mu k^\nu k^\rho$, these will be exactly as in the triangle. For $k^\mu k^\nu k^\rho k^\sigma$, eq. (4.57), the tensor structure is easy to see and the coefficients of the tensor structures can be found by projecting first with $g_{\mu\nu}g_{\rho\sigma}$ and then $g_{\mu\nu}\mathcal{P}_{4\rho}\mathcal{P}_{4\sigma}$,

$$
\begin{aligned}
k^\mu &\notin \mathcal{P}_4^\mu, && (4.54)\\
k^\mu k^\nu &\notin \mathcal{P}_4^\mu\mathcal{P}_4^\nu + (k^2 - \mathcal{P}_4^2)w^{\mu\nu}, && (4.55)\\
k^\mu k^\nu k^\rho &\notin \mathcal{P}_4^\mu\mathcal{P}_4^\nu\mathcal{P}_4^\rho + (k^2 - \mathcal{P}_4^2)(w^{\mu\nu}\mathcal{P}_4^\rho + w^{\mu\rho}\mathcal{P}_4^\nu + w^{\nu\rho}\mathcal{P}_4^\mu), && (4.56)\\
k^\mu k^\nu k^\rho k^\sigma &\notin \mathcal{P}_4^\mu\mathcal{P}_4^\nu\mathcal{P}_4^\rho\mathcal{P}_4^\sigma \\
&+ (k^2 - \mathcal{P}_4^2)(w^{\mu\nu}\mathcal{P}_4^\rho\mathcal{P}_4^\sigma + w^{\mu\rho}\mathcal{P}_4^\nu\mathcal{P}_4^\sigma + w^{\mu\sigma}\mathcal{P}_4^\nu\mathcal{P}_4^\rho \\
&+ w^{\nu\rho}\mathcal{P}_4^\mu\mathcal{P}_4^\sigma + w^{\nu\sigma}\mathcal{P}_4^\mu\mathcal{P}_4^\rho + w^{\rho\sigma}\mathcal{P}_4^\mu\mathcal{P}_4^\nu) \\
&+ \frac{n-3}{n-1}(k^2 - \mathcal{P}_4^2)^2(w^{\mu\nu}w^{\rho\sigma} + w^{\mu\rho}w^{\nu\sigma} + w^{\mu\sigma}w^{\nu\rho}). && (4.57)
\end{aligned}
$$

The arguments of $w^{\mu\nu}(p_1,p_2,p_3)$ in the above have been omitted for convenience.

These replacements are made in the numerator of the tensor box integral and eq. (4.53) is used to make the first reduction. Then the remaining $\mathcal{P}_4^\mu$ are converted back into k^μ, again using eqs. (4.54) to (4.57), and the process is repeated until only scalar integrals remain. Integrals with only $k^2 - \mathcal{P}_4^2$ in the numerator can be integrated directly.

The Pentagon

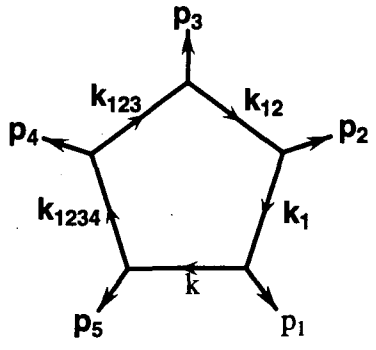

Figure 4.4: Momentum flows in a pentagon loop diagram

For the calculations described in this thesis, the only pentagon integrals which are required are those with at least four on - shell massless external particles. Also, only integrals of rank four and below are needed. In the following discussion, only such integrals will be considered, i.e. $\mathcal{E}_1$ to $\mathcal{E}_4$ with $p_1^2 = p_2^2 = p_3^2 = p_4^2 = 0$, $p_5 = -p_{1234}$,

$$\mathcal{E}_i^{\mu_1 \cdots \mu_i} = \int \frac{d^n k}{(2\pi)^n} \frac{k^{\mu_1} \ldots k^{\mu_i}}{k^2 k_1^2 k_{12}^2 k_{123}^2 k_{1234}^2}. \tag{4.58}$$

In analogy to the box and triangle integrals,

$$k^\mu = \mathcal{P}_5^\mu + (n-4) w_\nu^\mu k^\nu. \tag{4.59}$$

with,

$$\begin{aligned} \mathcal{P}_5^\mu &\equiv k\cdot p_1 v_1^\mu + k\cdot p_2 v_2^\mu + k\cdot p_2 v_2^\mu + k\cdot p_4 v_4^\mu \\ &= \frac{1}{2} k^2 v_1^\mu (p_1, p_2, p_3) + \frac{1}{2} k_1^2 (v_1^\mu - v_2^\mu) + \frac{1}{2}(k_{12}^2 - p_{12}^2)(v_2^\mu - v_3^\mu) \\ &+ \frac{1}{2}(k_{123}^2 - p_{123}^2)(v_3^\mu - v_4^\mu) + \frac{1}{2}(k_{1234}^2 - p_{1234}^2) v_4^\mu, \end{aligned} \tag{4.60}$$

where the momentum arguments of v_i^μ and $w^{\mu\nu}$ have been suppressed.

Recall the definition of $w^{\mu\nu}$, eq. (4.19). Taking $m = 5$,

$$w^{\mu}_{\nu}(p_1,p_2,p_3,p_4) = \frac{1}{n-4}\frac{\delta^{p_1p_2p_3p_4\mu}_{p_1p_2p_3p_4\nu}}{\Delta_4(p_1,p_2,p_3,p_4)} = -\frac{1}{2\epsilon}\frac{\delta^{p_1p_2p_3p_4\mu}_{p_1p_2p_3p_4\nu}}{\Delta_4(p_1,p_2,p_3,p_4)}, \tag{4.61}$$

where $n = 4 - 2\epsilon$.

It appears that $w^{\mu\nu}$ diverges in the limit $\epsilon \to 0$ (i.e in the limit of four dimensions). This is not the case because now $w^{\mu\nu}$ is dependent on four momenta which will span the four dimensional space. It is impossible to construct a non-zero totally antisymmetric fifth rank tensor in four dimensions and consequently, $\delta^{p_1p_2p_3p_4\mu}_{p_1p_2p_3p_4\nu} \sim \mathcal{O}(\epsilon)$. Thus $w^{\mu\nu}(p_1,p_2,p_3,p_4)$ is in fact of order unity.

The equations relating products of k^μ to $\mathcal{P}_5^\mu$ and $w^{\mu\nu}$ will be of exactly the same form as for the box (except for the factor $\frac{n-3}{n-1}$ in eq. (4.57) which will become $\frac{n-4}{n-2}$). However, when $k^2 - \mathcal{P}_5^2$ is inserted into the pentagon integral the result vanishes in four dimensions.

$$\int \frac{d^nk}{(2\pi)^n}\frac{k^2-\mathcal{P}_5^2}{k^2k_1^2k_{12}^2k_{123}^2k_{124}^2} \sim \mathcal{O}(\epsilon) \tag{4.62}$$

Since $w^{\mu\nu}$ is of order unity this means that all the terms containing $w^{\mu\nu}$ may be neglected. Notice that this seems reasonable without calculation because of the factor $(n-4)$ in front of w^μ_ν in eq. (4.59) making this term of $\mathcal{O}(\epsilon)$.

This makes the equations relating products of k^μ to $\mathcal{P}_5^\mu$ trivial,

$$k^\mu \not\equiv \mathcal{P}_5^\mu, \tag{4.63}$$

$$k^\mu k^\nu \not\equiv \mathcal{P}_5^\mu\mathcal{P}_5^\nu, \tag{4.64}$$

$$k^\mu k^\nu k^\rho \not\equiv \mathcal{P}_5^\mu\mathcal{P}_5^\nu\mathcal{P}_5^\rho, \tag{4.65}$$

$$k^\mu k^\nu k^\rho k^\sigma \not\equiv \mathcal{P}_5^\mu\mathcal{P}_5^\nu\mathcal{P}_5^\rho\mathcal{P}_5^\sigma. \tag{4.66}$$

Reduction of the pentagon integral then follows by analogy to the box and triangle integrals.

4.3 A Comparison of the Reduction Methods

The usual methods of reducing tensor integrals to scalar integrals via a Passarino Veltman type reduction have been described in the previous sections. In this section, the problems inherent in these methods will be discussed and compared.

It has been demonstrated that the principal difficulties inherent in Passarino Veltman reduction are:

- **Large Tensor Structure:** Loop integrals with a large number of vertices have are dependent on a large number of momenta (one less than the number of vertices). This results in a lengthy tensor decomposition. As the rank of the tensor increases this problem becomes much worse. However, this is a problem inherent in all tensor loop integral calculations and Passarino Veltman reduction, while no exception, cannot be blamed.

- **The Cascade:** The number of reductions required to reduce a tensor integral to scalar integrals is equal to the rank of a tensor integral. This reduction after reduction causes the size of the expression for a tensor integral to quickly become unmanageable when tensor integrals of higher rank are evaluated.

- **The Gram Determinant:** Each reduction introduces a *Gram determinant* into the denominator of the expression. Whether or not these determinants should be cancelled with appropriate factors in the numerator is ambiguous. Furthermore combinations of two or more Gram determinants can appear very complicated even when they are in fact rather simple. Such Gram determinants are inevitably present in all loop calculations. However, Passarino Veltman reduction results in expressions presented in an unnatural form which is manifestly more complicated than necessary. It is more desirable to have a method where the expressions, although having Gram determinants, would emerge already in the simplest form, requiring no cancellations of Gram determinants between the numerator and denominator.

- **Matrix Inversion:** In order to find the coefficients of the tensor structure, a set

of simultaneous equations must be solved, requiring the inversion of a matrix. It is from this inversion that the Gram determinant appears. Although this can be done analytically, it is not easy to perform using an algebraic program such as FORM.

The projective base was originally introduced in an attempt to remove the Gram determinant from the reduction procedure. It was thought that this would be accomplished by the removal of the need to invert the matrix seen in, for example, eq. (4.6). To this end the *projective base*, where the base vectors (and the tensor $w^{\mu\nu}$) are orthogonal to the external momenta, was introduced. This resulted in the matrix being diagonal and thus the inversion is trivial.

However, as seen in section (4.2.1) the Gram determinant is not removed from the reduction. It is merely hidden away in the definition of the projective base. Indeed, a naïve application of the projective base results in *more* Gram determinants than in the usual Passarino Veltman reduction and is impractical.

A more useful application of the projective base is in the decomposition of the *loop momenta itself* in terms of v_i^μ and $w^{\mu\nu}$. This leads to a method very similar to Passarino Veltman reduction, except that the matrix inversion has been trivialized. However, all the other problems associated with Passarino Veltman reduction remain and little is gained.

Chapter 5

Finite Functions

5.1 Introduction

It has been seen in Chapter 4 that conventional methods for evaluating the tensor integrals found in one loop calculations often lead to long, complicated expressions. To a large extent this is caused by the presence of Gram determinants in the denominator. It is unclear how these determinants should be cancelled with kinematical factors in the numerator and the resulting ambiguity can make simple results appear very complicated.

Furthermore, the presence of Gram determinants can lead to unphysical singularities. Conventionally, the tensor integral is broken down into sums over scalar integrals with kinematical coefficients — as these coefficients often contain Gram determinants in the denominator, they become singular as the Gram determinant vanishes.

This happens when two of the rows or columns of the determinant are equal. In the case of the 2×2 determinant,

$$\Delta_2(p_1, p_2) = \begin{vmatrix} p_1^2 & p_1 \cdot p_2 \\ p_1 \cdot p_2 & p_2^2 \end{vmatrix}, \tag{5.1}$$

this corresponds to two particles becoming collinear. Although at first sight this appears to be just the usual collinear divergence, it is in fact a completely unphysical artifact of the calculation. *Physical* collinear divergences can be regulated by giving the particles a non-zero mass — *this divergence cannot.*

This unphysicality of divergences in the $\Delta \to 0$ limit is easier to see in the case of the 3×3 determinant,

$$\Delta_3(p_1, p_2, p_3) = \begin{vmatrix} p_1^2 & p_1 \cdot p_2 & p_1 \cdot p_3 \\ p_1 \cdot p_2 & p_2^2 & p_2 \cdot p_3 \\ p_1 \cdot p_3 & p_2 \cdot p_3 & p_3^2 \end{vmatrix}. \tag{5.2}$$

Now $\Delta_3 = 0$ if the three momenta are co-planar, ie. $p_3 = ap_1 + bp_2$ — a divergence in this limit is clearly unphysical.

Such divergences as $\Delta \to 0$ are not surprising. In the Passarino-Veltman approach, described in section (4.1), the integral and its tensor decomposition are multiplied by all possible combinations of the external momenta and the metric tensor, resulting in a set of simultaneous equations which can be solved to give the form-factors. In the limit of vanishing Gram determinant, these equations are no longer independent and the Passarino-Veltman method breaks down. The projective base variant of Passarino-Veltman reduction is also unsatisfactory in this limit as the base vectors themselves become ill-defined.

Stuart [32] has shown that as the Gram determinant vanishes, the corresponding scalar integral can be written as a sum over lower point integrals. For example, consider the massive triangle scalar integral:

$$C_0(p_1, p_2) = \int \frac{d^n k}{(2\pi)^n} \frac{1}{k^2 k_1^2 k_{12}^2}, \tag{5.3}$$

where $k_1 = k + p_1$,
$k_{12} = k + p_{12}$,
$p_{12} = p_1 + p_2$.

The corresponding Gram determinant, $\Delta_2(p_1, p_2)$, is zero when p_1 and p_2 are collinear, ie. $p_2 = zp_1$. In this limit it is possible to write $C_0(p_1, p_2)$ as a sum over bubble integrals,

$$C_0(p_1, p_2) = \alpha B_0(p_2) + \beta B_0(p_{12}) + \gamma B_0(p_1). \tag{5.4}$$

Writing the right-hand-side as a single integral this becomes,

$$C_0(p_1, p_2) = \int \frac{d^n k}{(2\pi)^n} \frac{\alpha k^2 + \beta k_1^2 + \gamma k_{12}^2}{k^2 k_1^2 k_{12}^2}, \tag{5.5}$$

which is clearly only true if it is possible to write,

$$1 = \alpha k^2 + \beta k_1^2 + \gamma k_{12}^2, \tag{5.6}$$

Decomposing, in powers of k gives three equations:

$$\alpha + \beta + \gamma = 0, \tag{5.7}$$

$$\beta k\cdot p_1 + \gamma k\cdot p_{12} = 0, \tag{5.8}$$

$$\beta p_1^2 + \gamma p_{12}^2 = 1. \tag{5.9}$$

The second equation can be simplified by writing the loop momenta as,

$$\begin{aligned} k &= c_1 p_1 + c_2 p_2 + k_\perp \\ &= (c_1 + z c_2) p_1 + k_\perp, \end{aligned} \tag{5.10}$$

where $k_\perp$ is orthogonal to the p_1, p_2-plane. Then,

$$\beta p_1^2 + \gamma p_1\cdot p_{12} = 0. \tag{5.11}$$

In matrix form this is,

$$\begin{pmatrix} 1 & 1 & 1 \\ 0 & p_1^2 & p_1\cdot p_{12} \\ 0 & p_1^2 & p_{12}^2 \end{pmatrix} \begin{pmatrix} \alpha \\ \beta \\ \gamma \end{pmatrix} = \begin{pmatrix} 0 \\ 0 \\ 1 \end{pmatrix}. \tag{5.12}$$

Since the determinant of this matrix is non-zero, it can be inverted to give a solution for α, β and γ,

$$\begin{pmatrix} \alpha \\ \beta \\ \gamma \end{pmatrix} = \frac{1}{p_1^2 p_2\cdot p_{12}} \begin{pmatrix} p_1^2 p_2\cdot p_{12} & p_1^2 - p_{12}^2 & p_1\cdot p_2 \\ 0 & p_{12}^2 & -p_1\cdot p_{12} \\ 0 & -p_1^2 & p_1^2 \end{pmatrix} \begin{pmatrix} 0 \\ 0 \\ 1 \end{pmatrix} = \frac{1}{p_1^2 p_2\cdot p_{12}} \begin{pmatrix} p_1\cdot p_2 \\ -p_1\cdot p_{12} \\ p_1^2 \end{pmatrix}. \tag{5.13}$$

Thus in the limit of vanishing Gram determinant the scalar triangle integral can be decomposed as:

$$C_0(p_1, p_2) \longrightarrow \frac{p_1\cdot p_2}{p_1^2 p_2\cdot p_{12}} B_0(p_2) - \frac{p_1\cdot p_{12}}{p_1^2 p_2\cdot p_{12}} B_0(p_{12}) - \frac{1}{p_2\cdot p_{12}} B_0(p_1). \tag{5.14}$$

This procedure has been used to remove the Gram determinants for loop corrections to processes such as quarkonium decay where two heavy quarks are considered to travel

collinearly [32]. It demonstrates that large cancellations occur between the scalar integrals when the Gram determinant vanishes. It is clearly better to combine these scalar integrals together to form functions which are well behaved in this limit. For example, in the above case one might define a function to be,

$$\frac{1}{\Delta_2(p_1,p_2)}\left(C_0(p_1,p_2)-\frac{p_1\cdot p_2}{p_1^2 p_2\cdot p_{12}}B_0(p_2)+\frac{p_1\cdot p_{12}}{p_1^2 p_2\cdot p_{12}}B_0(p_{12})+\frac{1}{p_2\cdot p_{12}}B_0(p_1)\right), \quad (5.15)$$

rather than allowing the scalar triangle to be divided by a Gram determinant. From the discussion above, it is easy to see that this function is finite as the Gram determinant vanishes.

In fact, as will be demonstrated in this chapter, with a few notable exceptions, the tensor integrals themselves are finite as the Gram determinant vanishes. Therefore, *within individual tensor integral expressions* scalar integrals over Gram determinants can be combined together to form finite functions. Tensor integrals can then be calculated individually and expressed in terms of these new finite functions. This has several advantages:

- Since the kinematical coefficients of the functions no longer contain Gram determinants in the denominator, the matrix elements become numerically stable. The finite functions can be calculated to an arbitrary precision by making a Taylor expansion about $\Delta = 0$.

- The size of the resulting expression is reduced. Scalar integrals have been combined together to form new, more natural functions, leading to more compact expressions. For example, in the case discussed above, dilogarithms from the triangle integrals and the logarithms from the bubble integrals have been combined together in a natural way. Since final matrix elements must be finite in the limit of vanishing Gram determinant, these logarithms and dilogarithms must always come in these combinations when divided by a Gram determinant. Collecting them together into a single function will then naturally lead to more compact expressions.

- The Gram determinants are collected together in a prescribed fashion — there is no longer any ambiguity as to whether a Gram determinant should be canceled with

factors from the numerator or not, and there will be no inter-tangling of different size determinants.

In principle, the form of these finite functions can be calculated using the methods of Chapter 4. The tensor integrals can be calculated using the projective base variant of Passarino-Veltman reduction (section (4.2)) and the scalar integrals (over Gram determinants) can be rewritten in finite combinations. This was done for all the tensor integrals required for the calculation of $\gamma^* \to q\bar{q}Q\bar{Q}$, which will be discussed in Chapter (6). The finite functions were derived by making a Taylor expansion of the scalar integral about $\Delta = 0$. This could then be combined with expansions of lower point scalar integrals in such a way as to form a finite function when divided by the appropriate number of Gram determinants.

However, in practice this was rather difficult to do, because the Taylor expansions were required up to third order in the Gram determinant. Furthermore, the expressions for the tensor integrals using this method already contain the ambiguities associated with Gram determinants discussed in Chapter 4, and it is not clear how to combine the scalar integrals together in a natural way. Extra terms which are trivially finite as the Gram determinant vanishes can be arbitrarily added into the finite function.

It is perhaps easier to use the "string inspired" methods of Bern, Dixon and Kosower [21, 27] to derive the form of the tensor integrals and the subsequent finite functions. Instead of reducing the tensor integrals to sums of scalar integrals, one can differentiate the scalar integral with respect to the kinematical variables. This introduces Feynman parameters into the numerator of the integral, providing exactly the form required for the evaluation of the tensor integral. This procedure will be outlined in sections (5.2) and (5.3). These results will then be used to derive general reduction equations in section (5.4), which will be used to examine the tensor integrals on a case by case basis, and construct appropriate finite functions.

This will provide all the finite functions required for the calculation of $\gamma^* \to q\bar{q}Q\bar{Q}$ presented in Chapter 6.

5.2 Reduction by Differentiation

The general tensor integral which is to be evaluated is,

$$\mathcal{I}_m^{\mu_1\cdots\mu_R} = \int \frac{d^n k}{(2\pi)^n} \frac{k^{\mu_1}\ldots k^{\mu_R}}{k^2 k_1^2 \ldots k_{1\ldots m-1}^2}. \tag{5.16}$$

However, by performing a Feynman parameterization and integrating over the loop momenta it is possible to write $\mathcal{I}_m^{\mu_1\cdots\mu_R}$ in terms of Feynman parameter integrals given by,

$$I_m^n[\mathcal{P}\{x\}] = (-1)^m \Gamma\left(m - \frac{n}{2}\right) \int_0^1 dx_1 \ldots dx_m \frac{\delta(1 - \sum_i x_i)\mathcal{P}\{x\}}{(-\sum_{i=1}^m \sum_{j>i} s_{i\ldots(j-1)} x_i x_j)^{m-\frac{n}{2}}}, \tag{5.17}$$

where $\mathcal{P}\{x\}$ is a polynomial in the Feynman parameters and $s_{i\ldots j}$ are the generalized Mandelstam invariants,

$$s_{i\ldots j} = p_{i(i+1)\ldots j}^2 = (p_i + p_{i+1} + \ldots + p_j)^2. \tag{5.18}$$

In order to solve the tensor integrals of eq. (5.16) up to rank $R = 4$ it is sufficient to solve these integrals with up to four Feynman parameters inserted into the numerator. Relations between $\mathcal{I}_m^{\mu_1\cdots\mu_R}$ and $I_m^n[\mathcal{P}\{x\}]$ for $R \leq 4$ are derived in Appendix B.

Consider the Feynman parameter integral with no parameters in the numerator:

$$I_m^n[1] = (-1)^m \Gamma\left(m - \frac{n}{2}\right) \int_0^1 dx_1 \ldots dx_m \frac{\delta(1 - \sum_i x_i)}{(-\sum_{i=1}^m \sum_{j>i} s_{i\ldots(j-1)} x_i x_j)^{m-\frac{n}{2}}}. \tag{5.19}$$

In principle, integrals with Feynman parameters in the numerator can be obtained by differentiating $I_m^n[1]$ with respect to the kinematical variable s_{ij}. While obtaining an *even* number of parameters in the numerator is easy, obtaining an *odd* number is more tricky (but could, in principle, be done by using the δ-function to replace $x_i = 1 - \sum_{j\neq i} x_j$).

It is better to perform a further change of integration variables, suggested by 't Hooft and Veltman [33],

$$x_i = \alpha_i a_i = \frac{\alpha_i u_i}{\sum_{j=1}^n \alpha_j u_j}, \qquad \sum_{i=1}^n u_i = 1. \tag{5.20}$$

Furthermore, the matrix ρ_{ij} is introduced such that,

$$\rho_{ij} \equiv \begin{cases} -\frac{1}{2}s_{i\ldots(j-1)}\alpha_i\alpha_j, & i \neq j, \\ 0, & i = j. \end{cases} \tag{5.21}$$

The parameters α_i should be considered related to the kinematical variables, while ρ_{ij} are (in most cases) independent of them and merely parameterize the transformation. For α_i real and positive this gives,

$$I_m^n[1] = (-1)^m\Gamma\left(m - \frac{n}{2}\right)\int_0^1 d^m u_i \delta(1 - \sum_i u_i)\left(\prod_{j=1}^m \alpha_j\right)\frac{\left(\sum_{j=1}^m \alpha_j u_j\right)^{m-n}}{\left[\sum_{i,j=1}^m \rho_{ij}u_i u_j\right]^{m-\frac{n}{2}}}. \tag{5.22}$$

In addition, the integral should be rescaled to remove the product of α_j,

$$I_m^n = \left(\prod_{j=1}^m \alpha_j\right)\hat{I}_m^n. \tag{5.23}$$

With the above definitions it is now easy to obtain the integral with one Feynman parameter in the numerator by differentiating $\hat{I}_m^n[1]$ with respect to α_i,

$$\begin{aligned} \frac{\partial \hat{I}_m^n[1]}{\partial \alpha_i} &= (m-n)(-1)^m\Gamma\left(m - \frac{n}{2}\right)\int_0^1 d^m u_i \delta(1 - \sum_i u_i) u_i \frac{\left(\sum_{j=1}^m \alpha_j u_j\right)^{m-n-1}}{\left[\sum_{i,j=1}^m \rho_{ij}u_i u_j\right]^{m-n/2}} \\ &= (m-n)(-1)^m\Gamma\left(m - \frac{n}{2}\right)\int_0^1 d^m u_i \delta(1 - \sum_i u_i) a_i \frac{\left(\sum_{j=1}^m \alpha_j u_j\right)^{m-n}}{\left[\sum_{i,j=1}^m \rho_{ij}u_i u_j\right]^{m-n/2}} \\ &= (m-n)\hat{I}_m^n[a_i]. \end{aligned} \tag{5.24}$$

Therefore,

$$\hat{I}_m^n[a_i] = \frac{1}{m-n}\frac{\partial \hat{I}_m^n[1]}{\partial \alpha_i}. \tag{5.25}$$

Repeated differentiations yield integrals with an arbitrary number of Feynman parameters in the numerator.

5.3 Total Differentiation

Equations relating m and $(m-1)$-point integrals can also be derived using the *"string inspired"* methods of Bern, Dixon and Kosower [21, 27]. This involves taking the *total*

derivative of the m-point scalar integral *in* $(n+2)$ *dimensions* with respect to one of the Feynman parameters:

$$\begin{aligned}\frac{dI_m^{n+2}[1]}{dx_k} &= (-1)^m\Gamma\left(m-1-\frac{n}{2}\right)\frac{d}{dx_k}\int_0^1 dx_1\ldots dx_m\frac{\delta(1-\sum_i x_i)}{(-\sum_{i=1}^m\sum_{j>i}s_{i\ldots(j-1)}x_ix_j)^{m-1-\frac{n}{2}}}\\ &= (-1)^m\Gamma\left(m-1-\frac{n}{2}\right)\frac{d}{dx_k}\int_0^1 dx_{m-1}\int_0^{1-x_{m-1}}dx_{m-2}\cdots\int_0^{1-x_1-x_2-\ldots-x_{m-1}}dx_k\\ &\quad\times\left.\frac{1}{(-\sum_{i=1}^m\sum_{j>i}s_{i\ldots(j-1)}x_ix_j)^{m-1-\frac{n}{2}}}\right|_{x_m=1-x_1-\ldots-x_m-1},\end{aligned}\tag{5.26}$$

where the δ-function has been removed in such a way that the integration over x_k is the first which must be done.

This expression can be evaluated in two ways. The derivative with respect to x_k can be taken:

$$\begin{aligned}\frac{dI_m^{n+2}[1]}{dx_k} &= (-1)^m\Gamma\left(m-\frac{n}{2}\right)\int_0^1 dx_1\ldots dx_m\delta(1-\sum_i x_i)\frac{\sum_{j=1}^m(s_{k\ldots j-1}x_j-s_{m\ldots j-1}x_j)}{(-\sum_{i=1}^m\sum_{j>i}s_{i\ldots(j-1)}x_ix_j)^{m-\frac{n}{2}}}\\ &= \sum_{j=1}^m(s_{k\ldots j-1}-s_{m\ldots j-1})I_m^n[x_j],\end{aligned}\tag{5.27}$$

where the second term originates from the derivative of x_m.

Alternatively, the $\frac{d}{dx_k}$ can be brought inside the integral and the integration over x_k performed, giving the integrand at the two integration limits. At the lower limit, $x_k=0$, and an $(m-1)$-point integral is obtained. This integral is a *pinching* of the parent integral, removing the propagator associated with x_k, and will be written as $I_{m-1}^{n(k)}[1]$,

$$\begin{aligned}I_{m-1}^{n(k)}[1] &= (-1)^{m-1}\Gamma\left(m-1-\frac{n}{2}\right)\int dx_1\ldots dx_{k-1}dx_{k+1}\ldots dx_m\delta(1-\sum_{i\neq k}x_i)\\ &\quad\times\left(-\sum_{i\neq k}\sum_{j>i,\neq k}s_{i\ldots(j-1)}x_ix_j\right)^{-(m-1-\frac{n}{2})}.\end{aligned}\tag{5.28}$$

At the upper limit $x_m=0$ giving the pinched integral $I_{m-1}^{n(m)}[1]$. Therefore,

$$\frac{dI_m^{n+2}[1]}{dx_k} = I_{m-1}^{n(m)}[1] - I_{m-1}^{n(k)}[1]. \tag{5.29}$$

Converting the right-hand-sides of eqs. (5.27) and (5.29) into hatted quantities, using eq. (5.21) and equating gives,

$$\sum_{j=1}^{m} \left(\frac{\rho_{ij}}{\alpha_i} - \frac{\rho_{mj}}{\alpha_m} \right) \hat{I}_m^n[a_j] = \frac{1}{2} \left(\frac{\hat{I}_{m-1}^{n(m)}[1]}{\alpha_m} - \frac{\hat{I}_{m-1}^{n(i)}[1]}{\alpha_i} \right), \tag{5.30}$$

where the replacement $k \to i$ has been made.

This equation can be solved to give $\hat{I}_m^n[a_j]$ in terms of lower point integrals. However it is convenient to first introduce some extra notation. A slightly modified $(m-1) \times (m-1)$ Gram determinant is introduced. This is defined by,

$$\tilde{\Delta}_m \equiv det|2p_i \cdot p_j|, \tag{5.31}$$

where p_i and p_j run over the $(m-1)$ momenta[1]. The rescaled Gram determinant will also be useful,

$$\hat{\Delta}_m \equiv \left(\prod_{i=1}^{m} \alpha_i \right)^2 \tilde{\Delta}_m \equiv \sum_{i,j=1}^{m} \eta_{ij} \alpha_i \alpha_j. \tag{5.32}$$

The further definitions are made[2]:

$$\hat{\gamma}_i \equiv \sum_{j=1}^{m} \eta_{ij} \alpha_j, \qquad \gamma_i \equiv \hat{\gamma}_i \alpha_i = \sum_{j=1}^{m} \eta_{ij} \alpha_i \alpha_j, \tag{5.33}$$

and,

$$N_m \delta_{ij} = \sum_{k=1}^{m} \eta_{ik} \rho_{kj}, \qquad N_m = \frac{1}{2} (\det \eta)^{\frac{1}{m-1}}. \tag{5.34}$$

It is clear from the above definitions that,

$$\sum_{i=1}^{m} \alpha_i \left(\frac{\hat{\gamma}_i \hat{\gamma}_j}{\hat{\Delta}_m} - \eta_{ij} \right) = 0. \tag{5.35}$$

[1] This is related to the determinant of the previous sections by $\tilde{\Delta}_m = 2^{m-1} \Delta_{m-1}$.

[2] Note that the definition of $\hat{\gamma}$ coincides with γ of [21, 27]

Multiplying eq. (5.30) by $\left(\frac{\hat{\gamma}_k\hat{\gamma}_i}{\hat{\Delta}_m} - \eta_{ki}\right)\alpha_i$ and summing over i will therefore remove the terms which are not divided by α_i. This gives,

$$\sum_{i,j=1}^{m}\left(\frac{\hat{\gamma}_k\hat{\gamma}_i}{\hat{\Delta}_m} - \eta_{ki}\right)\rho_{ij}\hat{I}^n_m[a_j] = -\frac{1}{2}\sum_{i=1}^{m}\left(\frac{\hat{\gamma}_k\hat{\gamma}_i}{\hat{\Delta}_m} - \eta_{ki}\right)\hat{I}^{n(i)}_{m-1}[1]. \tag{5.36}$$

Using eq. (5.34) and the definition of $\hat{\gamma}_i$ on the left-hand-side of the above leads to,

$$N_m\hat{I}^n_m[a_k] - \frac{N_m}{\hat{\Delta}_m}\hat{\gamma}_k\sum_{j=1}^{m}\alpha_j\hat{I}^n_m[a_j] = \frac{1}{2}\sum_{i=1}^{m}\left(\frac{\hat{\gamma}_k\hat{\gamma}_i}{\hat{\Delta}_m} - \eta_{ki}\right)\hat{I}^{n(i)}_{m-1}[1]. \tag{5.37}$$

The second term on the left-hand-side can be simplified further by recalling that the sum over the Feynman parameters equals one and so,

$$\sum_{j=1}^{m}\alpha_j\hat{I}^n_m[a_j] = \sum_{j=1}^{m}\hat{I}^n_m[x_j] = \hat{I}^n_m[1]. \tag{5.38}$$

This gives,

$$\hat{I}^n_m[a_i] = \frac{1}{2N_m}\sum_{j=1}^{m}\left(\frac{\hat{\gamma}_i\hat{\gamma}_j}{\hat{\Delta}_m} - \eta_{ij}\right)\hat{I}^{n(i)}_{m-1}[1] + \frac{\hat{\gamma}_i}{\hat{\Delta}_m}\hat{I}^n_m[1]. \tag{5.39}$$

This equation relates Feynman parameter integrals with one parameter in the numerator (tensor integrals) to integrals with no Feynman parameters in the numerator (scalar integrals) and is the analogue of the Passarino-Veltman reduction of Chapter 4. Notice that once again the Gram determinant appears.

5.4 Tensor Integrals in Terms of Finite Functions

The above derivations have lead to two different expressions for the Feynman parameter integral with one parameter in the numerator, namely eqs. (5.25, 5.39). This section will examine the behaviour of these two equations as the Gram determinant vanishes and show how the divergent terms can be combined together into finite functions.

If the scalar integral[3] (ie. $\hat{I}^n_m[1]$) is well behaved as $\hat{\Delta}_m \to 0$ then eq. (5.25) implies that $\hat{I}^n_m[a_i]$ must also be well behaved, since the act of differentiation cannot provoke any

[3]The term "scalar integral" will be used interchangeably for $\mathcal{I}_m$ and $I^n_m[1]$.

singular behaviour. However, eq. (5.39) would appear to diverge in this limit. In fact, it does not — the appearance of $\tilde{\Delta}_m$ in the denominator is a *fake* pole. This can be seen more clearly by considering the m-point integral in $(n+2)$ dimensions,

$$\begin{aligned}\hat{I}_m^{n+2}[1] &= (-1)^m\Gamma\left(m-\frac{n+2}{2}\right)\int_0^1 d^m u_i\delta(1-\sum_i u_i)\frac{\left(\sum_{j=1}^m \alpha_j u_j\right)^{m-n-2}}{\left[\sum_{i,j=1}^m \rho_{ij}u_i u_j\right]^{m-\frac{n+2}{2}}} \\ &= \frac{1}{(n-m)(n-m-1)(m-1-\frac{n}{2})}\sum_{i,j=1}^m \rho_{ij}\frac{\partial^2 \hat{I}_m^n[1]}{\partial\alpha_i\partial\alpha_j}. \end{aligned} \tag{5.40}$$

This can be evaluated using eqs. (5.25) and (5.39),

$$\begin{aligned}&\frac{1}{m-n}\sum_{i,j=1}^m \rho_{ij}\frac{\partial^2 \hat{I}_m^n[1]}{\partial\alpha_i\partial\alpha_j} = \sum_{i,j=1}^m \rho_{ij}\frac{\partial \hat{I}_m^n[a_j]}{\partial\alpha_i} \\ &= \sum_{i,j=1}^m \rho_{ij}\frac{\partial}{\partial\alpha_i}\left(\frac{1}{2N_m}\sum_{k=1}^m\left[\frac{\hat{\gamma}_j\hat{\gamma}_k}{\hat{\Delta}_m}-\eta_{jk}\right]\hat{I}_{m-1}^{n(k)}[1]+\frac{\hat{\gamma}_j}{\hat{\Delta}_m}\hat{I}_m^n[1]\right) \\ &= \sum_{i,j=1}^m \rho_{ij}\left\{\frac{1}{2N_m}\left(\sum_{k=1}^m\left[\frac{\hat{\gamma}_j\hat{\gamma}_k}{\hat{\Delta}_m}-\eta_{jk}\right]\frac{\partial\hat{I}_{m-1}^{n(k)}[1]}{\partial\alpha_i}+\left[\frac{(\eta_{ij}\hat{\gamma}_k+\eta_{ik}\hat{\gamma}_j)}{\hat{\Delta}_m}-2\frac{\hat{\gamma}_i\hat{\gamma}_j\hat{\gamma}_k}{\hat{\Delta}_m}\right]\right)\right. \\ &\qquad \left.+\left[\frac{\eta_{ij}}{\hat{\Delta}_m}-2\frac{\hat{\gamma}_i\hat{\gamma}_j}{\hat{\Delta}_m^2}\right]\hat{I}_m^n[1]+\frac{\hat{\gamma}_j}{\hat{\Delta}_m}\frac{\partial\hat{I}_m^n[1]}{\partial\alpha_i}\right\} \\ &= \frac{1}{2}\sum_{k=1}^m\left(\sum_{i=1}^m\frac{\hat{\gamma}_k}{\hat{\Delta}_m}\alpha_i\frac{\partial\hat{I}_{m-1}^{n(k)}[1]}{\partial\alpha_i}-\frac{\partial\hat{I}_{m-1}^{n(k)}[1]}{\partial\alpha_k}+\left[\frac{(m-1)}{\hat{\Delta}_m}\hat{\gamma}_k\right]\hat{I}_{m-1}^{n(k)}[1]\right)+(m-2)\frac{N_m}{\hat{\Delta}_m}\hat{I}_m^n[1] \\ &\qquad +(m-n)\sum_{i,j=1}^m\rho_{ij}\frac{\hat{\gamma}_j}{\hat{\Delta}_m}\left(\frac{1}{2N_m}\sum_{k=1}^m\left[\frac{\hat{\gamma}_i\hat{\gamma}_k}{\hat{\Delta}_m}-\eta_{ij}\right]\hat{I}_{m-1}^{n(k)}[1]+\frac{\hat{\gamma}_i}{\hat{\Delta}_m}\hat{I}_m^n[1]\right). \end{aligned} \tag{5.41}$$

The differentiations of $\hat{I}_{m-1}^{n(k)}$ can be done by noting that $\hat{I}_{m-1}^{n(k)}[1]$ has no dependence on α_k,

$$\frac{\partial\hat{I}_{m-1}^{n(k)}[1]}{\partial\alpha_k}=0, \tag{5.42}$$

and again using eq. (5.25),

$$\sum_{i=1}^m\alpha_i\frac{\partial\hat{I}_{m-1}^{n(k)}[1]}{\partial\alpha_i}=(m-n-1)\sum_{i=1}^m\alpha_i\hat{I}_{m-1}^{n(k)}[a_i]=(m-n-1)\sum_{i=1}^m\hat{I}_{m-1}^{n(k)}[x_i]=(m-n-1)\hat{I}_{m-1}^{n(k)}[1], \tag{5.43}$$

since the Feynman parameters add to one.

This gives,

$$\frac{1}{m-n}\sum_{i,j=1}^{m}\rho_{ij}\frac{\partial^2\hat{I}_n^m[1]}{\partial\alpha_i\partial\alpha_j}=(m-1-\frac{n}{2})\frac{2N_m}{\hat{\Delta}_m}\left(\hat{I}_m^n[1]+\frac{1}{2N_m}\sum_{k=1}^{m}\hat{\gamma}_k\hat{I}_{m-1}^{n(k)}[1]\right). \tag{5.44}$$

Inserting this into eq. (5.40) gives,

$$\hat{I}_m^{n+2}[1]=\frac{1}{m-n-1}\frac{2N_m}{\hat{\Delta}_m}\left(\hat{I}_m^n[1]+\frac{1}{2N_m}\sum_{k=1}^{m}\hat{\gamma}_k\hat{I}_{m-1}^{n(k)}[1]\right), \tag{5.45}$$

so that eq. (5.39) can be written,

$$\hat{I}_m^n[a_i]=\frac{1}{2N_m}\left((m-n-1)\hat{\gamma}_i\hat{I}_m^{n+2}[1]-\sum_{j=1}^{m}\eta_{ij}\hat{I}_{m-1}^{n(j)}[1]\right). \tag{5.46}$$

This equation rewrites integrals with one Feynman parameter in the numerator in terms of higher dimensional and lower point integrals. It is important to notice that there are *no Gram determinants* in this equation. They have all been collected into the scalar integral of dimension $(n+2)$. It is clear that this higher dimensional scalar integral cannot be divergent as $\hat{\Delta}_m \to 0$ and so $\hat{I}_m^n[a_i]$ is also finite in this limit. This confirms that the divergence as $\hat{\Delta}_m \to 0$ is fake. Furthermore $\hat{I}_m^{n+2}[1]$ is an excellent candidate for a finite function — it is finite as the Gram determinant vanishes and is easily related to the Feynman parameter integrals. Of course, it may still be divergent as $\epsilon \to 0$ and before it can be used this ϵ-pole must be subtracted out.

Eq. (5.46) can be extended to two or more Feynman parameters in the numerator by differentiation (using generalizations of eq. (5.25)),

$$\begin{aligned}\hat{I}_m^n[a_ia_j] &= \frac{1}{m-n-1}\frac{\partial\hat{I}_m^n[a_i]}{\partial\alpha_j}\\ &= \frac{1}{2N_m}\left(\hat{\gamma}_i\frac{\partial\hat{I}_m^{n+2}[a_i]}{\partial\alpha_j}+\eta_{ij}\hat{I}_m^{n+2}[1]-\frac{1}{m-n-1}\sum_{k=1}^{m}\eta_{ik}\frac{\partial\hat{I}_{m-1}^{n(k)}[1]}{\partial\alpha_j}\right)\\ &= \frac{1}{2N_m}\left((m-n-2)\hat{\gamma}_i\hat{I}_m^{n+2}[a_j]+\eta_{ij}\hat{I}_m^{n+2}[1]-\sum_{k=1}^{m}\eta_{ik}\hat{I}_{m-1}^{n(k)}[a_j]\right).\end{aligned} \tag{5.47}$$

Differentiation has produced no new Gram determinants. By differentiating further it is easy to produce similar expressions for integrals with an arbitrary number of Feynman

parameters in the numerator. Converting back to the original form of eq. (5.17), ie unhatted integrals, the expressions for up to four Feynman parameters in the numerator are given by,

$$I_m^n[x_i] = \frac{1}{2N_m}\left((m-n-1)\gamma_i I_m^{n+2}[1] - \sum_{j=1}^{m}\eta_{ij}\alpha_i\alpha_j I_{m-1}^{n,(j)}[1]\right), \tag{5.48}$$

$$I_m^n[x_ix_j] = \frac{1}{2N_m}\Big((m-n-2)\gamma_i I_m^{n+2}[x_j] + \eta_{ij}\alpha_i\alpha_j I_m^{n+2}[1] - \sum_{k=1}^{m}\eta_{ik}\alpha_i\alpha_k I_{m-1}^{n,(k)}[x_j]\Big), \tag{5.49}$$

$$I_m^n[x_ix_jx_k] = \frac{1}{2N_m}\Big((m-n-3)\gamma_i I_m^{n+2}[x_jx_k] + \eta_{ij}\alpha_i\alpha_j I_m^{n+2}[x_k] + \eta_{ik}\alpha_i\alpha_k I_m^{n+2}[x_j] - \sum_{r=1}^{m}\eta_{ir}\alpha_i\alpha_r I_{m-1}^{n,(r)}[x_jx_k]\Big), \tag{5.50}$$

$$I_m^n[x_ix_jx_kx_l] = \frac{1}{2N_m}\Big((m-n-4)\gamma_i I_m^{n+2}[x_jx_kx_l] + \eta_{ij}\alpha_i\alpha_j I_m^{n+2}[x_kx_l] + \eta_{ik}\alpha_i\alpha_k I_m^{n+2}[x_jx_l] + \eta_{il}\alpha_i\alpha_l I_m^{n+2}[x_jx_k] - \sum_{r=1}^{m}\eta_{ir}\alpha_i\alpha_r I_{m-1}^{n,(r)}[x_jx_kx_l]\Big). \tag{5.51}$$

These equations can be solved recursively and related to the tensor integrals, $\mathcal{I}_m^{\mu_1\cdots\mu_R}$ using eqs. (B.22–B.25).

In summary, integrals with Feynman parameters in the numerator can be written as sums of lower point and higher dimensional scalar integrals which are well behaved in the limit of vanishing Gram determinant. In the following sections this procedure will be carried out for the tensor integrals required for the calculation of $\gamma^* \to q\bar{q}Q\bar{Q}$ in Chapter 6. Relations of the form of eqs. (5.48–5.51) can be found for each individual case. These relations are calculated once-and-for-all, and inserted where required into the matrix elements.

5.5 Triangle Integrals

The calculation of the virtual corrections to $\gamma^* \to q\bar{q}Q\bar{Q}$ in Chapter 6 will require triangle integrals with one, two and three massive legs and up to three loop momenta in the

numerator. This section will provide expressions for these integrals, presented in terms of functions which are finite as the Gram determinant vanishes.

The outgoing momenta of the three legs will be taken to be p_1, p_2 and $p_3 = -p_{12}$, as shown in fig. (5.1).

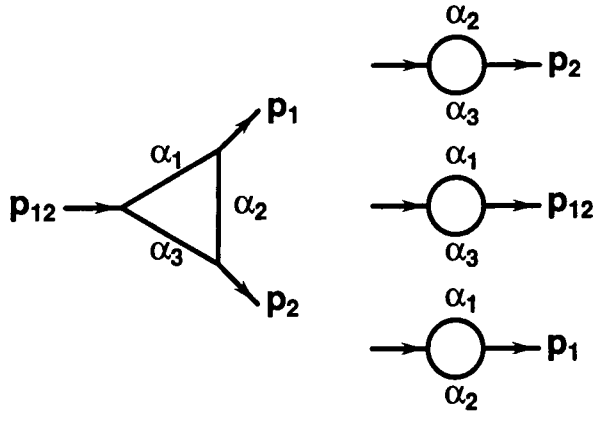

Figure 5.1: The diagrammatic form of the triangle integral and the bubbles formed by pinching. For each pinching i, the internal line corresponding to α_i is shrunk to zero length and the momenta on either end are combined.

After Feynman parameterization and integration over the loop momentum, the Feynman parameter integral is given by,

$$I_3^n[\mathcal{P}\{x\}] = -\Gamma(3-\frac{n}{2})\int_0^1 dx_1 dx_2 dx_3 \frac{\delta(1-x_1-x_2-x_3)\mathcal{P}\{x_i\}}{(-p_1^2 x_1 x_2 - p_2^2 x_2 x_3 - s_{12} x_1 x_3)^{3-\frac{n}{2}}}. \tag{5.52}$$

5.5.1 The Triangle Integral with Three Massive Legs

When p_1^2, p_2^2, $s_{12} \neq 0$, it is convenient to choose the α_i variables to satisfy,

$$\alpha_1\alpha_2 p_1^2 = -1, \quad \alpha_2\alpha_3 p_2^2 = -1, \quad \alpha_1\alpha_3 s_{12} = -1. \tag{5.53}$$

The Gram determinant and rescaled Gram determinant are given by,

$$\tilde{\Delta}_3 = -p_1^4 - p_2^4 - s_{12}^2 + 2p_1^2 p_2^2 + 2s_{12}p_1^2 + 2s_{12}p_2^2, \tag{5.54}$$

$$\hat{\Delta}_3 = -\alpha_1^2 - \alpha_2^2 - \alpha_3^2 + 2\alpha_1\alpha_2 + 2\alpha_1\alpha_3 + 2\alpha_2\alpha_3, \tag{5.55}$$

and from the bilinear form of eq. (5.32), η, and N_m are seen to be,

$$\eta = \begin{pmatrix} -1 & 1 & 1 \\ 1 & -1 & 1 \\ 1 & 1 & -1 \end{pmatrix}, \qquad N_3 = 1. \tag{5.56}$$

The γ_i variables can be written,

$$\gamma_i = \prod_{j=1}^{3} \alpha_j^2 \times \begin{cases} p_2^2(p_1^2 + s_{12} - p_2^2), & i = 1, \\ s_{12}(p_2^2 + p_1^2 - s_{12}), & i = 2, \\ p_1^2(p_2^2 + s_{12} - p_1^2), & i = 3. \end{cases} \tag{5.57}$$

The Scalar Integral

The scalar triangle integral with three massive legs is explicitly derived in Appendix C, and is finite in four dimensions. It is given by,

$$I_3^4[1] = \frac{1}{\sqrt{-\tilde{\Delta}_3}} \left(\log(a^+ a^-) \log\left(\frac{1-a^+}{1-a^-}\right) + 2\mathrm{Li}_2(a^+) - 2\mathrm{Li}_2(a^-) \right), \tag{5.58}$$

where Li_2 is the dilogarithm function defined by eq. (A.15), and the $a^\pm$ are given by,

$$a^\pm = \frac{s_{12} + p_2^2 - p_1^2 \pm \sqrt{-\tilde{\Delta}_3}}{2s_{12}}. \tag{5.59}$$

Notice the presence of the Gram determinant in the denominator. When the scalar integral is differentiated using eq. (5.25), this will lead to additional Gram determinants in the tensor integrals, as expected. As previously demonstrated, $I_3^4[1]$ is finite as $\tilde{\Delta}_3 \to 0$ and reduces to a sum of bubble integrals.

$$\lim_{\tilde{\Delta}_3 \to 0} I_3^4[1] = \frac{2}{s_{12} + p_1^2 - p_2^2} \log\left(\frac{s_{12}}{p_2^2}\right) + \frac{2}{s_{12} + p_2^2 - p_1^2} \log\left(\frac{s_{12}}{p_1^2}\right). \tag{5.60}$$

The Scalar Integral in Dimension $n > 4$

It has been seen in section (5.4) that scalar integrals in dimensions higher than four provide combinations of the scalar integrals divided by Gram determinants which are finite as $\tilde{\Delta}_m \to 0$. Furthermore, the scalar triangle integral is required in $(6 - 2\epsilon)$ dimensions

for the $g^{\mu\nu}$ coefficient of tensor triangles (eqs. (B.24) and (B.25)) and in $(8-2\epsilon)$ and $(10-2\epsilon)$ dimensions for evaluation of the box integrals using the recursive relations of eqs. (5.48-5.51).

These can be obtained by using eq. (5.45). For the triangle in $(6-2\epsilon)$ dimensions, this gives,

$$\hat{I}_3^{6-2\epsilon}[1] = \frac{1}{\epsilon-1}\frac{1}{\hat{\Delta}_3}\left[\hat{I}_3[1] + \frac{1}{2}\sum_{i=1}^{3}\hat{\gamma}_i \hat{I}_2^{4-2\epsilon(i)}[1]\right], \tag{5.61}$$

where $\hat{I}_2^{4-2\epsilon(i)}[1]$ are the bubble integrals formed by the i^{th} pinching of $\hat{I}_3^{4-2\epsilon}[1]$, shown diagrammatically in fig. (5.1). These bubble integrals are also calculated in Appendix C, and are given in terms of α_i by,

$$\hat{I}_2^{4-2\epsilon(i)} \equiv \left(\frac{\alpha_i}{\prod_{j=1}^{3}\alpha_j}\right) I_2^{4-2\epsilon(i)} = \frac{\hat{c}_\Gamma}{\epsilon(1-2\epsilon)}\left(\frac{\alpha_i}{\prod_{j=1}^{3}\alpha_j}\right)^{\epsilon-1}, \tag{5.62}$$

where $\hat{c}_\Gamma$ is given by[4]:

$$\hat{c}_\Gamma = \frac{\Gamma(1-\epsilon)\Gamma(1+\epsilon)}{\Gamma(1-2\epsilon)}. \tag{5.63}$$

The presence of the bubble integrals in the above make the expression for $\hat{I}_3^{6-2\epsilon}[1]$ divergent as $\epsilon \to 0$. However, a useful function, which is to be used as a building block of matrix element calculations, must be finite in the limits $\tilde{\Delta}_3 \to 0$ *and* $\epsilon \to 0$. The ϵ-pole must be subtracted off before defining a finite function. This can be done by adding,

$$\frac{1}{2\hat{\Delta}_3(\epsilon-1)}\left(\prod_{j=1}^{3}\alpha_j\right)^{-1}\left[\hat{\Delta}_3 - \sum_{i=1}^{3}\gamma_i\alpha_i\right]\hat{I}_2^{4-2\epsilon(2)}[1] = 0. \tag{5.64}$$

The six dimensional scalar integral is then,

$$I_3^{6-2\epsilon}[1] = \frac{1}{\epsilon-1}\frac{1}{\hat{\Delta}_3}\left[I_3^4[1] + \frac{1}{2}\sum_{i=1}^{3}\hat{\gamma}_i\alpha_i\left(I_2^{4-2\epsilon(i)}[1] - I_2^{4-2\epsilon(2)}[1]\right)\right] + \frac{1}{2(\epsilon-1)}I_2^{4-2\epsilon(2)}[1]. \tag{5.65}$$

The ϵ-pole structure lies exclusively in the last term. Returning to more conventional invariants and using the expressions for $I_2^{4-2\epsilon(i)}[1]$ gives,

$$I_3^{6-2\epsilon}[1] = Lc_{1S}(p_1,p_2) - \frac{\hat{c}_\Gamma}{2}\left[\frac{(-s_{12})^{-\epsilon}}{\epsilon} + 3\right], \tag{5.66}$$

[4]This is related to the c_Γ of eq. (C.9) by: $c_\Gamma = i(4\pi)^{\epsilon-2}\hat{c}_\Gamma$

where,

$$Lc_{1S}(p_1,p_2) \equiv \frac{1}{2\tilde{\Delta}_3}\left[2p_1^2p_2^2s_{12}I_3^4[1] - p_1^2(s_{12}+p_2^2-p_1^2)\log\left(\frac{s_{12}}{p_1^2}\right) - p_2^2(s_{12}+p_1^2-p_2^2)\log\left(\frac{s_{12}}{p_2^2}\right)\right]. \quad (5.67)$$

In a similar fashion the ϵ-pole structure can be removed from the triangle scalar integral in $(8-2\epsilon)$ and $(10-2\epsilon)$ dimensions, giving two more functions which are finite in the limits $\tilde{\Delta}_3 \to 0$ and $\epsilon \to 0$.

$$\begin{aligned} I_3^{8-2\epsilon}[1] &= Lc_{2S}(p_1,p_2) - (p_1^2+p_2^2+s_{12})\frac{c_\Gamma}{24}\left[\frac{(-s_{12})^{-\epsilon}}{\epsilon}+\frac{19}{6}\right], \\ I_3^{10-2\epsilon}[1] &= Lc_{3S}(p_1,p_2) \\ &\quad -(p_1^4+p_2^4+s_{12}^2+p_1^2p_2^2+p_1^2s_{12}+p_2^2s_{12})\frac{c_\Gamma}{360}\left[\frac{(-s_{12})^{-\epsilon}}{\epsilon}+\frac{17}{5}\right], \end{aligned} \quad (5.68)$$

where the finite functions are defined by,

$$\begin{aligned} Lc_{2S}(p_1,p_2) &= \frac{1}{4\tilde{\Delta}_3}\left[2p_1^2p_2^2s_{12}Lc_{1S}(p_1,p_2) - \frac{1}{6}\left(p_1^4(s_{12}+p_2^2-p_1^2)\log\left(\frac{s_{12}}{p_1^2}\right) + p_2^4(s_{12}+p_1^2-p_2^2)\log\left(\frac{s_{12}}{p_2^2}\right) + 2p_1^2p_2^2s_{12}\right)\right], \quad (5.69) \\ Lc_{3S}(p_1,p_2) &= \frac{1}{6\tilde{\Delta}_3}\left[(2p_1^2p_2^2s_{12}Lc_{2S}(p_1,p_2) - \frac{1}{60}\left(p_1^6(s_{12}+p_2^2-p_1^2)\log\left(\frac{s_{12}}{p_1^2}\right) + p_2^6(s_{12}+p_1^2-p_2^2)\log\left(\frac{s_{12}}{p_2^2}\right) + \frac{1}{2}p_1^2p_2^2s_{12}(p_1^2+p_2^2+s_{12})\right)\right]. \quad (5.70) \end{aligned}$$

Tensor Integrals

The triangle integral with three massive legs and one Feynman parameter in the numerator can be easily written in terms of the triangle scalar integral in $(6-2\epsilon)$ dimensions and bubble scalar integrals using eq. (5.46). In terms of unhatted quantities this gives,

$$I_3^{4-2\epsilon}[x_i] = \left[-(1-\epsilon)\gamma_i I_3^{6-2\epsilon}[1] - \frac{1}{2}\sum_{j=1}^{3}\eta_{ij}\alpha_i\alpha_j I_2^{4-2\epsilon(j)}[1]\right]. \quad (5.71)$$

Immediately a problem is apparent — γ_i in the coefficient of the scalar integral in $(6-2\epsilon)$ dimensions contains all three invariants in the denominator, eq. (5.57). Although the divergence as the Gram determinant vanishes has been removed, it has been replaced by a divergence as the invariants vanish. Problems in this limit are to be expected since even the scalar integral itself is not finite as $p_i^2 \to 0$. Since this limit is "not allowed", this decomposition of the Feynman parameter could still be used and is clearly better than the traditional decomposition of eq. (5.39). However, in this case, $I_3^{4-2\epsilon}[x_i]$ itself is particularly simple and is a better choice for a finite function.

This is most easily found by application of eq. (5.39),

$$\hat{I}_3^{4-2\epsilon}[a_i] = \frac{1}{2}\sum_{j=1}^{3}\left(\frac{\hat{\gamma}_i\hat{\gamma}_j}{\hat{\Delta}_3} - \eta_{ij}\right)\hat{I}_2^{4-2\epsilon(i)}[1] + \frac{\hat{\gamma}_i}{\hat{\Delta}_3}\hat{I}_3^4[1] + \mathcal{O}(\epsilon). \tag{5.72}$$

It is only necessary to consider the case where the Feynman parameter x_3 is inserted into the numerator, since the integral with x_1 in the numerator can be trivially obtained by swapping p_1 and p_2. Also, any appearance of x_2 can be systematically removed since the Feynman parameters must add to one. Notice that since the bubble integrals are divergent as $n \to 4$, it appears at first sight that $\hat{I}_3^n[a_i]$ diverges in four dimensions. However, since $\hat{I}_3^n[a_i]$ could also be found by differentiating the scalar integral (using eq. (5.25)), this cannot be the case. In fact, the ϵ-poles of $\hat{I}_2^{4-2\epsilon(i)}$ are independent of i and eq. (5.35) ensures that they cancel. To make this explicit it is convenient to add the following to $\hat{I}_3^n[a_i]$:

$$\frac{1}{2}\sum_{j=1}^{3}\left(\frac{\hat{\gamma}_i\hat{\gamma}_j}{\hat{\Delta}_3} - \eta_{ij}\right)\frac{\alpha_i}{\alpha_2}\hat{I}_2^{n(2)}[1] = 0. \tag{5.73}$$

This gives,

$$\hat{I}_3^4[a_i] = \frac{1}{2}\sum_{j=1}^{3}\left(\frac{\hat{\gamma}_3\hat{\gamma}_j}{\hat{\Delta}_3} - \eta_{3j}\right)\frac{\alpha_i}{\prod_{k=1}^{3}\alpha_k}\left(\hat{I}_2^{4-2\epsilon(i)}[1] - \hat{I}_2^{4-2\epsilon(2)}[1]\right) + \frac{\hat{\gamma}_i}{\hat{\Delta}_3}\hat{I}_3^4[1] + \mathcal{O}(\epsilon), \tag{5.74}$$

which simplifies after some algebra to,

$$\hat{I}_3^4[a_i] = \frac{1}{\hat{\Delta}_3}\left(\hat{\gamma}_3\hat{I}_3^4[1] - \frac{\hat{\gamma}_2}{\alpha_3}\log\left(\frac{a_2}{a_1}\right) + 2\log\left(\frac{\alpha_2}{\alpha_3}\right)\right) + \mathcal{O}(\epsilon). \tag{5.75}$$

Returning to unhatted quantities and writing α_i, $\hat{\gamma}_i$ as invariants gives,

$$I_3^4[x_3] = \frac{1}{\tilde{\Delta}_3}\left[p_1^2(s_{12}+p_2^2-p_1^2)I_3^4[1] + (p_1^2+p_2^2-s_{12})\log\left(\frac{s_{12}}{p_2^2}\right) - 2p_1^2\log\left(\frac{s_{12}}{p_1^2}\right)\right]. \quad (5.76)$$

Notice that this is just the form of the finite function suggested by eq. (5.15), multiplied by a kinematical factor. Integrals with more Feynman parameters in the numerator are most easily obtained by differentiating $\hat{I}_3^4[a_3]$,

$$I_3^4[x_i x_3^n] = -\frac{1}{n+1}\left(\prod_{j=1}^{3}\alpha_j\right)\alpha_i\alpha_3^n\frac{\partial \hat{I}_3^4[a_3^n]}{\partial \alpha_i}. \quad (5.77)$$

This gives,

$$\begin{aligned} I_3^4[x_1x_3] &= \frac{1}{2\tilde{\Delta}_3}\Big[2p_2^2(s_{12}+p_1^2-p_2^2)I_3^4[x_3] + p_1^2(s_{12}+p_2^2-p_1^2)I_3^4[x_1] \\ &\qquad -p_1^2p_2^2I_3^4[1] - p_2^2\log\left(\frac{s_{12}}{p_2^2}\right) + p_1^2+p_2^2-s_{12}\Big], \quad (5.78) \\ I_3^4[x_3^2] &= \frac{1}{2\tilde{\Delta}_3}\left[3p_1^2(s_{12}+p_2^2-p_1^2)I_3^4[x_3] + p_1^4I_3^4[1] - (s_{12}-p_2^2)\log\left(\frac{s_{12}}{p_2^2}\right) - 2p_1^2\right], \quad (5.79) \\ I_3^4[x_1x_3^2] &= \frac{1}{6\tilde{\Delta}_3}\Big[4p_2^2(s_{12}+p_1^2-p_2^2)I_3^4[x_3^2] + 6p_1^2(s_{12}+p_2^2-p_1^2)I_3^4[x_1x_3] \\ &\qquad -3p_1^2p_2^2I_3^4[x_3] + p_1^4I_3^4[x_1] - p_2^2\log\left(\frac{s_{12}}{p_2^2}\right) + p_2^2 - s_{12}\Big], \quad (5.80) \\ I_3^4[x_3^3] &= \frac{1}{3\tilde{\Delta}_3}\left[5p_1^2(s_{12}+p_2^2-p_1^2)I_3^4[x_3^2] + 2p_1^4I_3^4[x_3] - (s_{12}-p_2^2)\log\left(\frac{s_{12}}{p_2^2}\right) - p_1^2\right]. \quad (5.81) \end{aligned}$$

These integrals have several important properties:

- They are finite in four dimensions.
- They are finite as $\tilde{\Delta}_3 \to 0$. This property is inevitable since they are derivatives of $I_3^4[x_3]$ which is also finite in this limit. By expanding the integrals as a Taylor series in $\tilde{\Delta}_3$ they can be evaluated with arbitrary precision close to $\tilde{\Delta}_3 = 0$.

- They combine together the dilogarithms from the triangle integrals and the logarithms from the bubble integrals in a natural way.

To illustrate the behaviour of these integrals as the Gram determinant vanishes, they are plotted in fig. (5.2) for the case when $s_{12} = 1$, $p_1^2 = 0.2$ and p_2^2 is varied smoothly toward 0.135 — this limit corresponds to the vanishing of the Gram determinant. It is clear that as this limit is approached, the evaluation of the functions becomes unreliable. The dashed lines show the Taylor expansion about $\tilde{\Delta}_3 = 0$, keeping only the constant term, which is a reliable approximation for up to two orders of magnitude before the evaluation of the complete function breaks down.

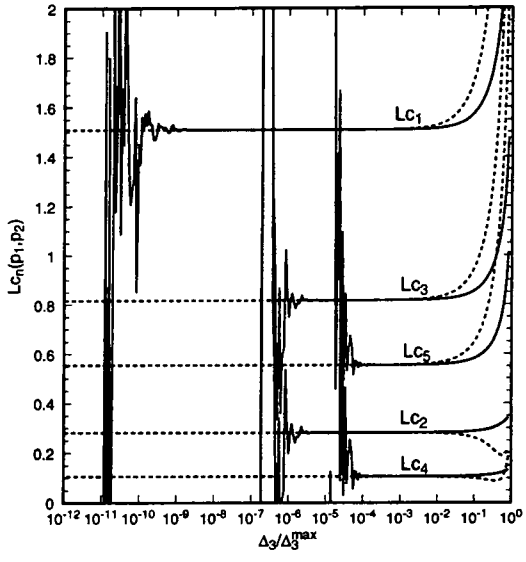

Figure 5.2: The finite functions for the triangle integral with three massive legs with $s_{12} = 1$ and $p_1^2 = 0.2$ as a function of $\tilde{\Delta}_3/\tilde{\Delta}_3^{max}$ where $\tilde{\Delta}_3^{max} = -(s_{12} - p_1^2)^2$. The dashed lines show the Taylor expansion about $\tilde{\Delta}_3 = 0$, keeping only the constant term.

The definitions of the finite functions for the massive triangle (p_1^2, $p_2^2 \neq 0$) are,

$$Lc_0(p_1, p_2) \equiv I_3^4[1], \quad Lc_{2n-1}(p_1, p_2) \equiv I_3^4[x_3^n], \quad Lc_{2n}(p_1, p_2) \equiv I_3^4[x_1 x_3^n]. \qquad (5.82)$$

These are related to the finite function derived from the scalar integral in $(6-2\epsilon)$ dimensions by,

$$Lc_{1S}(p_1,p_2) = \frac{1}{2}\left(p_1^2 Lc_1(p_2,p_1) + p_2^2 Lc_1(p_1,p_2)\right). \tag{5.83}$$

Tensor Integrals in Dimension $n > 4$

The calculation of the tensor triangle integral with three loop momenta in the numerator, eq. (B.25), also requires the integral with one Feynman parameter in the numerator in $(6-2\epsilon)$ dimensions, $I_3^{6-2\epsilon}[x_i]$. Rather than calculating this by differentiating $I_3^{6-2\epsilon}[1]$, which is divergent as $\epsilon \to 0$, it can be found more easily using eq. (5.47),

$$\begin{aligned}\hat{I}_3[a_1a_i] + \hat{I}_3[a_3a_i] &= \frac{1}{2}\Big[(2\epsilon-3)(\hat{\gamma}_1+\hat{\gamma}_3)\hat{I}_3^{6-2\epsilon}[a_i] + (\eta_{1i}+\eta_{3i})\hat{I}_3^{6-2\epsilon}[1] \\ &\qquad - \sum_{k=1}^{3}(\eta_{1k}+\eta_{3k})\hat{I}_2^{4-2\epsilon(k)}[a_i]\Big].\end{aligned} \tag{5.84}$$

However, it is clear from the definition of η_{ij}, eq. (5.56), that,

$$\eta_{1i} + \eta_{3i} = 2\delta_{2i}, \tag{5.85}$$

which simplifies the equation to,

$$\hat{I}_3[a_1a_i] + \hat{I}_3[a_3a_i] = (2\epsilon-3)\alpha_2\hat{I}_3^{6-2\epsilon}[a_i] + \delta_{2i}\hat{I}_3^{6-2\epsilon}[1] - \hat{I}_2^{4-2\epsilon(2)}[a_i]. \tag{5.86}$$

Since the Feynman parameters add to one, the case $i = 2$ is of little interest. Furthermore,

$$I_2^{4-2\epsilon(2)}[x_1] = I_2^{4-2\epsilon(2)}[x_3] = \frac{\hat{c}_\Gamma}{2}\left(\frac{(-s_{12})^{-\epsilon}}{\epsilon} + 2\right). \tag{5.87}$$

Therefore replacing the factors of α for $i = 1$ or 3 gives,

$$\frac{I_3^4[x_1x_i]}{\alpha_1\alpha_2} + \frac{I_3^4[x_3x_i]}{\alpha_2\alpha_3} = (2\epsilon-3)I_3^{6-2\epsilon}[x_i] - I_2^{4-2\epsilon(2)}[x_1]. \tag{5.88}$$

Finally,

$$\begin{aligned}I_3^{6-2\epsilon}[x_i] &= \frac{1}{3}\left(\frac{-I_3^4[x_1x_i]}{\alpha_1\alpha_2} - \frac{I_3^4[x_3x_i]}{\alpha_2\alpha_3}\right) + \frac{I_2^{4-2\epsilon(2)}[x_1]}{2\epsilon-3} \\ &= \frac{1}{3}\left[p_1^2 I_3^4[x_1x_i] + p_2^2 I_3^4[x_3x_i] - \frac{\hat{c}_\Gamma}{2}\left(\frac{(-s_{12})^{-\epsilon}}{\epsilon} + \frac{8}{3}\right)\right].\end{aligned} \tag{5.89}$$

5.5.2 Triangle Integrals with Massless Legs

Triangle integrals must also be considered where one or more external particles are massless. The scalar triangle integrals with one and two massive legs are calculated in Appendix C. When only one leg is massive, the Gram determinant becomes trivial and it is not useful to construct new functions. This case will not be discussed further here.

When two legs are massive, say p_1^2, $p_{12}^2 \neq 0$, then the scalar integral is given in terms of the α_i variables by,

$$\hat{I}_3^{4-2\epsilon}[1] = \frac{\hat{c}_\Gamma}{\epsilon^2}\left[\frac{(\alpha_1\alpha_3)^\epsilon - (\alpha_1\alpha_2)^\epsilon}{\alpha_3 - \alpha_2}\right] \tag{5.90}$$

where α_i are chosen to satisfy,

$$\alpha_1\alpha_2 p_1^2 = -1, \qquad \alpha_1\alpha_3 s_{12} = -1. \tag{5.91}$$

Notice that now there are only two equations constraining the α_i since $p_2^2 = 0$. The Gram determinant is now given by,

$$\tilde{\Delta}_3 = -(s_{12} - p_1^2)^2, \tag{5.92}$$

$$\hat{\Delta}_3 = -(\alpha_2 - \alpha_3)^2, \tag{5.93}$$

and the limit $\Delta \to 0$ corresponds to $\alpha_2 \to \alpha_3$. Notice that $\hat{\Delta}_3$ now makes no reference to α_1. Constructing η_{ij} from the Gram determinant in this case gives,

$$\eta = \begin{pmatrix} 0 & 0 & 0 \\ 0 & -1 & 1 \\ 0 & 1 & -1 \end{pmatrix}. \tag{5.94}$$

Therefore $N_3 = 0$ and the method breaks down.

However, formally one can still derive eqs. (5.48 - 5.51) in the case where $p_2^2 \neq 0$, ie. when the triangle has three massive legs, and write out $\eta_{ij}\alpha_i\alpha_j$ and γ_i in terms of invariants and $N_3 = 1$. Then the limit $p_2^2 \to 0$ can be taken and all the remaining integrals regarded as triangle integrals with $p_2^2 = 0$. It is important that one does not take the $p_2^2 \to 0$ limit of the results derived in section (5.5.1) since they have been derived *assuming that the scalar integral is finite in four dimensions.* This is obviously not true

when $p_2^2 = 0$. Formally, the limits $p_2^2 \to 0$ and $\epsilon \to 0$ do not commute. In fact, it is easiest to bypass eqs. (5.48 - 5.51) entirely and derive the tensor integrals by differentiating the scalar, ie. using eq. (5.25).

Although $\hat{I}_3^{4-2\epsilon}[1]$ is well behaved in the limit of vanishing Gram determinant ($\alpha_2 \to \alpha_3$) it is divergent as $\epsilon \to 0$. As a general rule it is not necessary to tamper with the ϵ-poles of matrix elements — they must either cancel with the infrared poles of the real matrix elements or be renormalizable. Therefore they have a prescribed form which has no Gram determinants, and finite functions are unnecessary.

However, it is possible for the tensor integral to be multiplied by a factor of ϵ in the Feynman diagram. Expanding

$$x^\epsilon = 1 + \epsilon \log x + \mathcal{O}(\epsilon),$$

it is easy to see that $\epsilon \hat{I}_3^{4-2\epsilon}[1]$ is finite as $\epsilon \to 0$:

$$\begin{aligned} \epsilon \hat{I}_3^{4-2\epsilon}[1] &= \frac{\hat{c}_\Gamma}{\epsilon}\left[\frac{(\alpha_1\alpha_3)^\epsilon - (\alpha_1\alpha_2)^\epsilon}{\alpha_3 - \alpha_2}\right] \\ &= \frac{\log\left(\frac{\alpha_3}{\alpha_2}\right)}{\alpha_3 - \alpha_2} + \mathcal{O}(\epsilon). \end{aligned} \tag{5.95}$$

Thus it is necessary to define a finite function,

$$Lc_1^{2m}(p_1, p_2) \equiv \frac{\log\left(\frac{s_{12}}{p_1^2}\right)}{s_{12} - p_1^2}, \tag{5.96}$$

where the superscript, $2m$, refers to two massive legs.

The integrals with more Feynman parameters in the numerator are easily found by differentiation, eq. (5.25), and further finite functions can be defined by,

$$Lc_n^{2m}(p_1, p_2) \equiv \lim_{\epsilon \to 0}\left(\epsilon I_3^{4-2\epsilon}[x_3^{n-1}]\right), \quad n = 1 \ldots 4. \tag{5.97}$$

In terms of invariants,

$$Lc_n^{2m}(p_1, p_2) = -\left[\frac{p_1^2 Lc_{n-1}^{2m}(p_1, p_2) - \frac{1}{n-1}}{s_{12} - p_1^2}\right], \quad n = 2, 3, 4. \tag{5.98}$$

These functions, or closely related functions, have already appeared in next-to-leading order calculations [21, 27, 34, 31].

The corresponding Feynman parameter integrals are given in terms of invariants by,

$$I_3^{4-2\epsilon}[1] = \frac{\hat{c}_\Gamma}{\epsilon^2}\left(\frac{(-s_{12})^{-\epsilon}-(-p_1^2)^{-\epsilon}}{s_{12}-p_1^2}\right), \tag{5.99}$$

$$I_3^{4-2\epsilon}[x_3] = -2Lc_2^{2m}(p_1,p_2) - \frac{\hat{c}_\Gamma}{\epsilon}\frac{(-s_{12})^{-\epsilon}}{(s_{12}-p_1^2)} - \frac{p_1^2}{s_{12}-p_1^2}I_3^{4-2\epsilon}[1] \tag{5.100}$$

$$I_3^{4-2\epsilon}[x_3^2] = -3Lc_3^{2m}(p_1,p_2) + \frac{1}{2(s_{12}-p_1^2)} - \hat{c}_\Gamma\frac{(-s_{12})^{-\epsilon}}{\epsilon}\frac{(s_{12}-3p_1^2)}{2(s_{12}-p_1^2)^2} + \frac{p_1^4}{(s_{12}-p_1^2)^2}I_3^{4-2\epsilon}[1], \tag{5.101}$$

$$I_3^{4-2\epsilon}[x_3^3] = -\frac{11}{3}Lc_4^{2m}(p_1,p_2) + \frac{(s_{12}-2p_1^2)}{2(s_{12}-p_1^2)^2} - \frac{p_1^6}{(s_{12}-p_1^2)^3}I_3^4[1] - \hat{c}_\Gamma\frac{(-s_{12})^{-\epsilon}}{\epsilon}\left(\frac{1}{3(s_{12}-p_1^2)} - \frac{p_1^2}{2(s_{12}-p_1^2)^2} + \frac{p_1^4}{(s_{12}-p_1^2)^3}\right) \tag{5.102}$$

while,

$$I_3^{4-2\epsilon}[x_1] = 2I_3^{4-2\epsilon}[x_1^2] = 3I_3^{4-2\epsilon}[x_1^3] = Lc_1^{2m}(p_1,p_2), \tag{5.103}$$

$$I_3^{4-2\epsilon}[x_1x_3] = 3I_3^{4-2\epsilon}[x_1^2x_3] = \frac{1}{2}Lc_2^{2m}(p_1,p_2), \tag{5.104}$$

$$I_3^{4-2\epsilon}[x_1x_3^2] = \frac{1}{3}Lc_3^{2m}(p_1,p_2). \tag{5.105}$$

The required integrals in $(6-2\epsilon)$ dimensions can be most easily derived by taking the $p_2^2 \to 0$ limit of the $(6-2\epsilon)$ dimensional triangle integrals with three massive legs and are given by,

$$I_3^{6-2\epsilon}[1] = \frac{1}{2}\left[p_1^2Lc_1^{2m}(p_1,p_2) - \hat{c}_\Gamma\left(\frac{(-s_{12})^{-\epsilon}}{\epsilon}+3\right)\right], \tag{5.106}$$

$$I_3^{6-2\epsilon}[x_1] = \frac{1}{6}\left[p_1^2Lc_1^{2m}(p_1,p_2) - \hat{c}_\Gamma\left(\frac{(-s_{12})^{-\epsilon}}{\epsilon}+\frac{8}{3}\right)\right], \tag{5.107}$$

$$I_3^{6-2\epsilon}[x_3] = \frac{1}{6}\left[p_1^2Lc_2^{2m}(p_1,p_2) - \hat{c}_\Gamma\left(\frac{(-s_{12})^{-\epsilon}}{\epsilon}+\frac{8}{3}\right)\right]. \tag{5.108}$$

The corresponding integrals for the case $p_1^2 = 0$, $p_2^2, s_{12} \neq 0$ are given by substituting,

$$p_1 \leftrightarrow p_2, \quad x_1 \leftrightarrow x_3. \tag{5.109}$$

5.6 Box Integrals

For the calculations of Chapter 6 it will be necessary to derive tensor box integrals and their finite functions in the case of one and two massive legs. The box integral with two massive legs can be further divided into two cases, where the massive legs are either opposite or adjacent. Throughout this section the fourth momentum will be eliminated in favour of the other three and assumed to have non-zero invariant mass, ie. $p_4^2 = -p_{123}^2 = -s_{123} \neq 0$. The momentum configuration for the box integral, together with its four triangle pinchings can be seen in fig. (5.3).

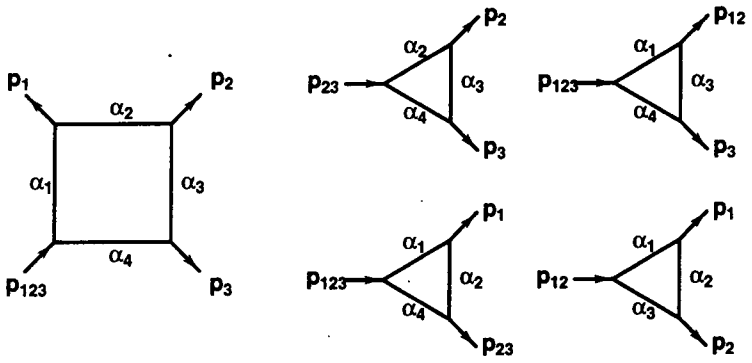

Figure 5.3: The diagrammatic form of the box integral and the triangles formed by pinching. For each pinching i, the internal line corresponding to α_i is shrunk to zero length and the momenta on either end are combined.

5.6.1 The Adjacent Box

Consider first the box integral with adjacent momenta, p_1, p_{123}, massive. One can easily see from fig. (5.3) that the α variables should be defined by,

$$\begin{aligned} \alpha_1\alpha_4 s_{123} &= -1, \quad \alpha_1\alpha_2 p_1^2 = -1, \\ \alpha_1\alpha_3 s_{12} &= -1, \quad \alpha_2\alpha_4 s_{23} = -1. \end{aligned} \tag{5.110}$$

The Gram determinant is given by,

$$\begin{aligned}\tilde{\Delta}_4 &= 2s_{23}\left[(s_{123}-s_{12})(s_{12}-p_1^2)-s_{12}s_{23}\right],\\ \hat{\Delta}_4 &= -2\left[(\alpha_3-\alpha_4)(\alpha_2-\alpha_3)-\alpha_1\alpha_3\right],\end{aligned} \tag{5.111}$$

and consequently,

$$\eta = \begin{pmatrix} 0 & 0 & 1 & 0 \\ 0 & 0 & -1 & 1 \\ 1 & -1 & 2 & -1 \\ 0 & 1 & -1 & 0 \end{pmatrix}, \qquad N_4 = \frac{1}{2}. \tag{5.112}$$

The kinematical variables γ_i are then,

$$\gamma_i = \prod_{j=1}^{4}\alpha_j \begin{cases} -s_{23} & i=1 \\ s_{123}-s_{12} & i=2 \\ p_1^2+s_{123}-s_{23}-2\frac{p_1^2 s_{123}}{s_{12}} & i=3 \\ p_1^2-s_{12} & i=4 \end{cases}. \tag{5.113}$$

Again, the scalar integral has been calculated in Appendix C, and is given in terms of the α variables as,

$$\hat{I}_4^{4-2\epsilon}[1] = \frac{\hat{c}_\Gamma}{\epsilon^2}\left[(\alpha_2\alpha_4)^\epsilon + 2(\alpha_1\alpha_3)^\epsilon - (\alpha_1\alpha_2)^\epsilon - (\alpha_1\alpha_4)^\epsilon\right] + 2Ld_0(p_1,p_2,p_3) + \mathcal{O}(\epsilon), \tag{5.114}$$

where the piece which is finite as $\epsilon \to 0$ is given by,

$$Ld_0(p_1,p_2,p_3) = \mathrm{Li}_2\left(1-\tfrac{\alpha_4}{\alpha_3}\right) - \mathrm{Li}_2\left(1-\tfrac{\alpha_3}{\alpha_2}\right) + \tfrac{1}{2}\log\left(\tfrac{\alpha_2\alpha_4}{\alpha_3^2}\right)\log\left(\tfrac{\alpha_1}{\alpha_2}\right). \tag{5.115}$$

Notice that there is no Gram determinant in eq. (5.114), and it would appear that differentiation to obtain integrals with more Feynman parameters in the numerator cannot generate any further Gram determinants. However, application of eq. (5.25) to the box integrals gives,

$$\hat{I}_4^{4-2\epsilon}[a_i] = \frac{1}{2\epsilon}\frac{\partial \hat{I}_4^{4-2\epsilon}[1]}{\partial \alpha_i}. \tag{5.116}$$

The prefactor of $\frac{1}{\epsilon}$ requires that the scalar integral be known up to $\mathcal{O}(\epsilon)$ and it is differentiation of this extra piece which leads to the Gram determinants of the tensor integrals. This phenomenon is known as the ϵ-barrier.

The Scalar Integral in Higher Dimensions

The first goal is to find a function which combines together the scalar box integral and lower point integrals over the Gram determinant in a form which is finite as the determinant vanishes. The scalar box integral in $(6-2\epsilon)$ dimensions fits this criterion. From eq. (5.45), this is given by,

$$I_4^{6-2\epsilon}[1] = \frac{1}{2\epsilon-1}\frac{1}{\hat{\Delta}_4}\left[\hat{I}_4^{4-2\epsilon}[1] + \sum_{i=1}^{4}\hat{\gamma}_i\hat{I}_3^{4-2\epsilon(i)}[1]\right]. \tag{5.117}$$

Although this appears divergent as $\epsilon \to 0$, it is actually finite. Consider the ϵ-poles of the above — the pinched integrals are given by (see Appendix C),

$$\hat{I}_3^{4-2\epsilon(1)}[1] = -\frac{\hat{c}_\Gamma}{\epsilon^2}\frac{(\alpha_2\alpha_4)^\epsilon}{\alpha_3}, \tag{5.118}$$

$$\hat{I}_3^{4-2\epsilon(2)}[1] = \frac{\hat{c}_\Gamma}{\epsilon^2}\frac{(\alpha_1\alpha_4)^\epsilon - (\alpha_1\alpha_3)^\epsilon}{\alpha_4-\alpha_3}, \tag{5.119}$$

$$\hat{I}_3^{4-2\epsilon(4)}[1] = \frac{\hat{c}_\Gamma}{\epsilon^2}\frac{(\alpha_1\alpha_3)^\epsilon - (\alpha_1\alpha_2)^\epsilon}{\alpha_3-\alpha_2}, \tag{5.120}$$

where the case $i=3$ has been omitted because the scalar integral is finite in four dimensions. The pole of eq. (5.117) is therefore,

$$\begin{aligned}\frac{1}{2\epsilon-1}\frac{\hat{c}_\Gamma}{\epsilon^2}\frac{1}{\hat{\Delta}_4}\Bigg[&(\alpha_2\alpha_4)^\epsilon + 2(\alpha_1\alpha_3)^\epsilon - (\alpha_1\alpha_2)^\epsilon - (\alpha_1\alpha_4)^\epsilon - \frac{\hat{\gamma}_1}{\alpha_3}(\alpha_2\alpha_4)^\epsilon \\ &+\frac{\hat{\gamma}_2}{\alpha_4-\alpha_3}\left((\alpha_1\alpha_4)^\epsilon - (\alpha_1\alpha_3)^\epsilon\right) + \frac{\hat{\gamma}_4}{\alpha_3-\alpha_2}\left((\alpha_1\alpha_3)^\epsilon - (\alpha_1\alpha_2)^\epsilon\right)\Bigg].\end{aligned} \tag{5.121}$$

From the definition of $\hat{\gamma}_i$ it is easy to see that this is zero and the adjacent box scalar integral is finite as $\epsilon \to 0$. Since it is clearly finite in the limit of vanishing Gram determinant (as it is a scalar integral), it is therefore an ideal candidate for a finite function:

$$\begin{aligned}&Ld_{1S}(p_1,p_2,p_3) \equiv I_4^6[1] \\ &= -\frac{2s_{12}s_{23}}{\tilde{\Delta}_4}\left[Ld_0(p_1,p_2,p_3) + \frac{1}{2}\left(s_{123} + p_1^2 - s_{23} - \frac{2p_1^2 s_{123}}{s_{12}}\right)Lc_0(p_1,p_{23})\right]\end{aligned} \tag{5.122}$$

In higher dimensions, this cancellation of the ϵ-pole does not happen and the scalar integrals in $(8-2\epsilon)$, $(10-2\epsilon)$ and $(12-2\epsilon)$ dimensions are ultra-violet divergent as $\epsilon \to 0$.

However, these ϵ-poles do not contain Gram determinants in the denominator and can be isolated by adding and subtracting lower point integrals. The explicit forms of these integrals are easily obtained from eq. (5.45).

$$I_4^{8-2\epsilon}[1] = Ld_{2S}(p_1,p_2,p_3) + \frac{\hat{c}_\Gamma}{6}\left[\frac{(-s_{123})^{-\epsilon}}{\epsilon} + \frac{11}{3}\right], \tag{5.123}$$

$$I_4^{10-2\epsilon}[1] = Ld_{3S}(p_1,p_2,p_3) + \frac{\hat{c}_\Gamma(s_{123}+s_{12}+s_{23}+p_1^2)}{120}\left[\frac{(-s_{123})^{-\epsilon}}{\epsilon} + \frac{107}{30}\right], \tag{5.124}$$

$$I_4^{12-2\epsilon}[1] = Ld_{4S}(p_1,p_2,p_3) + \frac{c_\Gamma P}{2520}\left[\frac{(-s_{123})^{-\epsilon}}{\epsilon} + \frac{129}{35}\right], \tag{5.125}$$

where,

$$P = s_{123}^2 + s_{12}^2 + s_{23}^2 + p_1^4 + s_{123}s_{12} + s_{123}s_{23} + s_{123}p_1^2 + s_{12}p_1^2 + s_{23}p_1^2 + \frac{s_{12}s_{23}}{2},$$

and the finite parts of the higher dimensional boxes are given by,

$$\begin{aligned} &Ld_{2S}(p_1,p_2,p_3) = \\ &\quad -\frac{s_{12}s_{23}}{3\tilde{\Delta}_4}\left[s_{12}s_{23}Ld_{1S}(p_1,p_2,p_3) + \left(s_{123}+p_1^2-s_{23}-\frac{2p_1^2s_{123}}{s_{12}}\right)Lc_{1S}(p_1,p_{23})\right. \\ &\quad \left.+\frac{s_{23}}{2}\log\left(\frac{s_{123}}{s_{23}}\right) + s_{12}\log\left(\frac{s_{123}}{s_{12}}\right) - \frac{p_1^2}{2}\log\left(\frac{s_{123}}{p_1^2}\right)\right], \end{aligned} \tag{5.126}$$

$$\begin{aligned} &Ld_{3S}(p_1,p_2,p_3) = \\ &\quad -\frac{s_{12}s_{23}}{5\tilde{\Delta}_4}\left[s_{12}s_{23}Ld_{2S}(p_1,p_2,p_3) + \left(s_{123}+p_1^2-s_{23}-\frac{2p_1^2s_{123}}{s_{12}}\right)Lc_{2S}(p_1,p_{23})\right. \\ &\quad \left.+\frac{s_{23}^2}{24}\log\left(\frac{s_{123}}{s_{23}}\right) + \frac{s_{12}^2}{12}\log\left(\frac{s_{123}}{s_{12}}\right) - \frac{p_1^4}{24}\log\left(\frac{s_{123}}{p_1^2}\right) + \frac{s_{12}s_{23}}{12}\right], \end{aligned} \tag{5.127}$$

$$\begin{aligned} &Ld_{4S}(p_1,p_2,p_3) = \\ &\quad -\frac{s_{12}s_{23}}{7\tilde{\Delta}_4}\left[s_{12}s_{23}Ld_{3S}(p_1,p_2,p_3) + \left(s_{123}+p_1^2-s_{23}-\frac{2p_1^2s_{123}}{s_{12}}\right)Lc_{3S}(p_1,p_{23})\right. \\ &\quad +\frac{s_{23}^3}{360}\log\left(\frac{s_{123}}{s_{23}}\right) + \frac{s_{12}^3}{180}\log\left(\frac{s_{123}}{s_{12}}\right) - \frac{p_1^6}{360}\log\left(\frac{s_{123}}{p_1^2}\right) \\ &\quad \left.+\frac{s_{12}s_{23}(s_{123}+s_{12}+s_{23}+p_1^2)}{720}\right]. \end{aligned} \tag{5.128}$$

Again, these functions are finite as $\tilde{\Delta}_4 \to 0$, and can be used as building blocks for the matrix elements. The behaviour of these functions as the Gram determinant vanishes

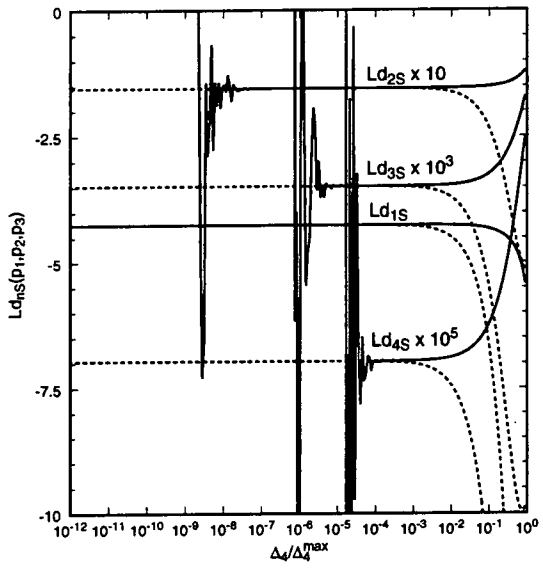

Figure 5.4: The finite functions for the box integral with two adjacent massive legs as a function of $\tilde{\Delta}_4/\tilde{\Delta}_4^{max}$, where $\tilde{\Delta}_4^{max} = 2s_{12}s_{23}(s_{123} - s_{12} - s_{23})$. Three of the invariants are fixed, $s_{123} = 1$, $s_{12} = 0.4$, $s_{23} = 0.08$, and p_1^2 is varied. The dashed lines show the Taylor expansion about $\tilde{\Delta}_4 = 0$, keeping only the constant term.

is shown in fig. (5.4) for the case where $s_{123} = 1$, $s_{12} = 0.4$, $s_{23} = 0.08$, and p_1^2 is varied. Although the stability of Ld_{1S} is remarkable, the evaluation of the other functions becomes unreliable as the limit $\tilde{\Delta}_4 \to 0$ is approached. The dashed lines show the Taylor expansion about $\tilde{\Delta}_4 = 0$, keeping only the constant term, which is a good approximation for $\tilde{\Delta}_4 < 10^{-4}\tilde{\Delta}_4^{max}$.

Tensor Integrals

Integrals with Feynman parameters in the numerator can now be expressed in terms of these finite functions using eqs. (5.48-5.51) iteratively. The integral with one Feynman parameter in the numerator becomes,

$$I_4^{4-2\epsilon}[x_i] = -\gamma_i I_4^6[1] - \sum_{j=1}^{4} \eta_{ij}\alpha_i\alpha_j I_3^{4-2\epsilon(j)}[1], \tag{5.129}$$

which is manifestly finite as $\tilde{\Delta}_4 \to 0$. Since $\sum_i x_i = 1$, this need only be calculated for three of the Feynman parameters — it is best to rewrite $x_3 = 1 - x_1 - x_2 - x_4$ since this corresponds to the most complicated column of η_{ij}. It is easy to use the definitions of η_{ij} and α_i, eqs. (5.112, 5.110) to write eq. (5.129) in terms of standard invariants for $i = 1, 2, 4$. For example,

$$I_4^{4-2\epsilon}[x_1] = \frac{1}{s_{12}} \left[Ld_{1S}(p_1, p_2, p_3) + Lc_0(p_1, p_{23}) \right]. \tag{5.130}$$

As with the triangle integrals, writing the Feynman parameter integrals in terms of the scalar integral in higher dimensions introduces an apparent divergence as one of the invariants vanishes (in this case s_{12}). However, $I_4^{4-2\epsilon}[x_1]$ is actually finite in this limit since,

$$\lim_{s_{12}\to 0} Ld_{1S}(p_1, p_2, p_3) = \lim_{s_{12}\to 0} \frac{2p_1^2 s_{123} s_{23}}{\tilde{\Delta}_4} Lc_0(p_1, p_{23}) = -Lc_0(p_1, p_{23}). \tag{5.131}$$

Instead of using $Ld_{1S}(p_1, p_2, p_3)$ as a finite function, a new function could be defined by,

$$Ld_1(p_1, p_2, p_3) \equiv I_4^{4-2\epsilon}[x_1], \tag{5.132}$$

which is finite in *all* limits. However, if such a policy is to be implemented for all the adjacent box Feynman parameter integrals, many new functions would have to be introduced. This is undesirable — it is better to have the tensor integrals written in terms of the same function to allow cancellations between them. For this reason, the calculation of Chapter 6 uses the scalar integral in higher dimensions as the building blocks for the tensor integrals. Any remaining fake poles (there are actually very few) are gathered together at the end of the calculation. This allows potential cancellations between the box integrals to happen freely.

Solving eq. (5.48-5.50) iteratively for the adjacent box then gives the Feynman parameter integrals[5],

$$I_4^{4-2\epsilon}[x_i] = (2\epsilon - 1)\gamma_i I_4^{6-2\epsilon}[1] - \sum_{j=1}^{4} \eta_{ij}\alpha_i\alpha_j I_3^{4-2\epsilon(j)}[1], \tag{5.133}$$

$$I_4^{4-2\epsilon}[x_i x_j] = (2\epsilon - 2)(2\epsilon - 3)\gamma_i\gamma_j I_4^{8-2\epsilon}[1] - (2\epsilon - 2)\gamma_i \sum_{k=1}^{4} \eta_{jk}\alpha_j\alpha_k I_4^{6-2\epsilon,(k)}[1]$$

[5]The integral with four Feynman parameters in the numerator is not required for the calculation of Chapter 6 and is not reproduced here.

$$+\eta_{ij}\alpha_i\alpha_j I_4^{6-2\epsilon}[1] - \sum_{k=1}^{4} \eta_{ij}\alpha_i\alpha_k I_3^{4-2\epsilon(k)}[x_j], \tag{5.134}$$

$$\begin{aligned} I_4^{4-2\epsilon}[x_i x_j x_k] &= (2\epsilon-3)(2\epsilon-4)(2\epsilon-5)\gamma_i\gamma_j\gamma_k I_4^{10-2\epsilon}[1] + (2\epsilon-3)\gamma_i\eta_{jk}\alpha_j\alpha_k I_4^{8-2\epsilon}[1] \\ &+(2\epsilon-3)\eta_{ij}\alpha_i\alpha_j\gamma_k I_4^{8-2\epsilon}[1] + (2\epsilon-3)\eta_{ik}\alpha_i\alpha_k\gamma_j I_4^{8-2\epsilon}[1] \\ &-(2\epsilon-3)(2\epsilon-4)\gamma_i\gamma_j \sum_{l=1}^{4} \eta_{kl}\alpha_k\alpha_l I_3^{8-2\epsilon,(l)}[1] \\ &-\eta_{ij}\alpha_i\alpha_j \sum_{l=1}^{4} \eta_{kl}\alpha_k\alpha_l I_3^{6-2\epsilon,(l)}[1] - \eta_{ik}\alpha_i\alpha_k \sum_{l=1}^{4} \eta_{jl}\alpha_j\alpha_l I_3^{6-2\epsilon,(l)}[1] \\ &-(2\epsilon-3)\gamma_i \sum_{l=1}^{4} \eta_{jl}\alpha_j\alpha_l I_3^{4-2\epsilon(l)}[x_k] - \sum_{l=1}^{4} \eta_{il}\alpha_i\alpha_l I_3^{4-2\epsilon(l)}[x_j x_k]. \end{aligned} \tag{5.135}$$

For particular i, j, k these equations can be easily written in terms of the previously defined finite functions and ϵ-pole pieces. This combines in a non trivial way the dilogarithms, logarithms and constant pieces emerging from the tensor box integrals, leading to more compact, numerically stable results.

5.6.2 The Opposite Box

This section will discuss the box integral with two massive legs at opposite edges. In the notation of fig. (5.3) this corresponds to $s_{123}, p_2^2 \neq 0$ and $p_1^2 = p_3^2 = 0$. In this case, the α_i parameters are defined by,

$$\begin{aligned} \alpha_1\alpha_4 s_{123} &= -\lambda, \qquad \alpha_2\alpha_3 p_2^2 = -1, \\ \alpha_1\alpha_3 s_{12} &= -1, \qquad \alpha_2\alpha_4 s_{23} = -1. \end{aligned} \tag{5.136}$$

Notice the appearance of λ in the first equation — this has been introduced in order to keep the α_i independent. It is given in terms of the usual invariants by,

$$\lambda = -\alpha_1\alpha_4 s_{123} = -\frac{(\alpha_1\alpha_3)(\alpha_2\alpha_4)}{\alpha_2\alpha_3} s_{123} = \frac{p_2^2 s_{123}}{s_{12}s_{23}}. \tag{5.137}$$

The Gram determinant in its normal and scaled forms can be written,

$$\tilde{\Delta}_4 = 2s_{13}(s_{12}s_{23} - p_2^2 s_{123}) = 2(1-\lambda)s_{12}s_{13}s_{23}, \tag{5.138}$$

$$\hat{\Delta}_4 = 2(1-\lambda)(\alpha_1\alpha_3 - \alpha_1\alpha_4 - \lambda\alpha_2\alpha_3 + \alpha_2\alpha_4). \tag{5.139}$$

Again, from the bilinear representation of the Gram determinant it is easy to see that the matrix η is now dependent on λ,

$$\eta = (1-\lambda)\begin{pmatrix} 0 & 0 & 1 & -1 \\ 0 & 0 & -\lambda & 1 \\ 1 & -\lambda & 0 & 0 \\ -1 & 1 & 0 & 0 \end{pmatrix}, \qquad N_4 = \frac{1}{2}(1-\lambda)^2. \tag{5.140}$$

Furthermore,

$$\gamma_i = (1-\lambda)\prod_{j=1}^{4}\alpha_j \begin{cases} p_2^2 - s_{23} & i=1 \\ s_{123} - s_{12} & i=2 \\ s_{123} - s_{23} & i=3 \\ p_2^2 - s_{12} & i=4 \end{cases}. \tag{5.141}$$

The Scalar Integral

The scalar integral has been derived in Appendix C — written in terms of α_i and λ it is,

$$\hat{I}_4^{4-2\epsilon}[1] = \frac{2}{1-\lambda}\left[\frac{\hat{c}_\Gamma}{\epsilon^2}\left((\alpha_1\alpha_3)^\epsilon + (\alpha_2\alpha_4)^\epsilon + (\alpha_2\alpha_3)^\epsilon + (\alpha_1\alpha_4)^\epsilon\lambda^{-\epsilon}\right) + Ld_0^{opp}(p_1,p_2,p_3)\right], \tag{5.142}$$

where the finite part is given by,

$$\begin{aligned} Ld_0^{opp}(p_1,p_2,p_3) &= \mathrm{Li}_2(1-\lambda) - \mathrm{Li}_2\left(1-\tfrac{\lambda\alpha_3}{\alpha_4}\right) - \mathrm{Li}_2\left(1-\tfrac{\lambda\alpha_2}{\alpha_1}\right) \\ &\quad -\mathrm{Li}_2\left(1-\tfrac{\alpha_4}{\alpha_3}\right) - \mathrm{Li}_2\left(1-\tfrac{\alpha_1}{\alpha_2}\right) - \tfrac{1}{2}\log^2\left(\tfrac{\alpha_1\alpha_3}{\alpha_2\alpha_4}\right). \end{aligned} \tag{5.143}$$

Clearly, the scalar integral is divergent as $\lambda \to 1$, ie. when the Gram determinant vanishes. Furthermore, in this limit,

$$\begin{aligned} Ld_0^{opp}(p_1,p_2,p_3) &\longrightarrow \mathrm{Li}_2(0) - \mathrm{Li}_2\left(1-\tfrac{\alpha_3}{\alpha_4}\right) - \mathrm{Li}_2\left(1-\tfrac{\alpha_2}{\alpha_1}\right) \\ &\quad -\mathrm{Li}_2\left(1-\tfrac{\alpha_4}{\alpha_3}\right) - \mathrm{Li}_2\left(1-\tfrac{\alpha_1}{\alpha_2}\right) - \tfrac{1}{2}\log^2\left(\tfrac{\alpha_1\alpha_3}{\alpha_2\alpha_4}\right) \\ &= -\log\left(\frac{\alpha_1}{\alpha_2}\right)\log\left(\frac{\alpha_3}{\alpha_4}\right), \end{aligned} \tag{5.144}$$

where the dilogarithm identity eq. (A.21) has been used. Although this is a rather simple form, it is unique to the opposite box. In creating finite functions in the previous cases the scalar integral was combined with *lower point scalar integrals* to form a function which was finite as the Gram determinant vanishes. It is easy to see from fig. (5.3) that the

only scalar integrals which are available by pinching are the triangle integrals with one and two massive legs. However, these are entirely ϵ-poles and cannot (and should not) be combined with the opposite box. There is no appropriate function which can generate the double logarithm of eq. (5.144) as $\lambda \to 1$ and consequently *no finite function can be formed.*

Since the matrix elements must be finite in the limit of vanishing Gram determinant, all occurrences of Ld_0^{opp} divided by the determinant must cancel. This provides an interesting check of the final matrix elements.

The Scalar Integral in Higher Dimensions

The scalar integrals in higher dimensions can be calculated using eq. (5.45). Since these integrals must be finite as $\lambda \to 0$, one might expect that they provide finite functions with which to build well behaved matrix elements. However, since N_4 is now effectively a Gram determinant squared (since it contains $(1-\lambda)^2$) its presence in the numerator of eq. (5.45) removes the Gram determinant from the denominator. Consequently, the scalar integrals in dimension $n > 4$ are trivially finite in this limit and are not useful as finite functions.

For example, the scalar integral in $(6-2\epsilon)$ dimensions is given by,

$$\begin{aligned}
\hat{I}_4^{6-2\epsilon}[1] &= \frac{\prod_{j=1}^4 \alpha_j}{2(2\epsilon-1)}(1-\lambda)\left[\hat{I}_4^{4-2\epsilon}[1] + \frac{1}{(1-\lambda)^2}\sum_{i=1}^4 \hat{\gamma}_i \hat{I}_3^{4-2\epsilon(i)}[1]\right] \\
&= \frac{\prod_{j=1}^4 \alpha_j}{2(2\epsilon-1)s_{13}}\Big[2Ld_0^{opp}(p_1,p_2,p_3) + 2\frac{\hat{c}_\Gamma}{\epsilon^2}\left((\alpha_1\alpha_3)^\epsilon + (\alpha_2\alpha_4)^\epsilon - (\alpha_2\alpha_3)^\epsilon - (\alpha_1\alpha_4)^\epsilon\lambda^{-\epsilon}\right) \\
&\quad + \frac{\hat{c}_\Gamma}{\epsilon^2}\left\{(\alpha_3-\alpha_4)\left[\frac{(\alpha_2\alpha_3)^\epsilon - (\alpha_2\alpha_4)^\epsilon}{\alpha_3-\alpha_4}\right] + (\alpha_4-\lambda\alpha_3)\left[\frac{(\alpha_1\alpha_4)^\epsilon\lambda^{-\epsilon} - (\alpha_1\alpha_3)^\epsilon}{\alpha_4-\lambda\alpha_3}\right]\right. \\
&\quad \left. + (\alpha_1-\lambda\alpha_2)\left[\frac{(\alpha_4\alpha_1)^\epsilon\lambda^{-\epsilon} - (\alpha_4\alpha_2)^\epsilon}{\alpha_1-\lambda\alpha_2}\right] + (\alpha_2-\alpha_1)\left[\frac{(\alpha_3\alpha_2)^\epsilon - (\alpha_3\alpha_1)^\epsilon}{\alpha_2-\alpha_1}\right]\right\}\Big], \qquad (5.145)
\end{aligned}$$

where the appropriate triangle pinchings have been inserted remembering that the definitions of α_i now involve λ (in particular $\alpha_1\alpha_4 s_{123} = -\lambda$). Clearly the ϵ-pole cancels and

the resulting (unhatted) box in six dimensions is given by,

$$I_4^6[1] = -\frac{1}{s_{13}} Ld_0^{opp}(p_1, p_2, p_3). \tag{5.146}$$

As expected, the Gram determinant has been canceled and there is no new finite function. For the third rank tensor box integral, the Feynman parameter integral in $(6-2\epsilon)$ dimensions with x_i in the numerator is also required (for the coefficient of $g_{\mu\nu}p_i^\rho$). These are given by differentiating $I_4^6[1]$, so that, for example,

$$\begin{aligned} I_4^{6-2\epsilon}[x_4] &= \frac{1}{2s_{23}}\left[\frac{s_{12}-p_2^2}{s_{12}} Ld_0^{opp}(p_1,p_2,p_3) - s_{12}Lc_1^{2m}(p_{12},p_3)\right. \\ &\quad \left. + p_2^2 Lc_1^{2m}(p_2,p_3) - \log\left(\frac{s_{123}}{s_{23}}\right)\right]. \end{aligned} \tag{5.147}$$

Similarly, the scalar integral in $(8-2\epsilon)$ dimensions is given by,

$$\begin{aligned} I_4^{8-2\epsilon}[1] &= \frac{1}{6s_{13}}\left[\frac{s_{12}s_{23}-p_2^2 s_{123}}{s_{13}} Ld_0^{opp}(p_1,p_2,p_3) - s_{12}\log\left(\frac{s_{123}}{s_{12}}\right) - s_{23}\log\left(\frac{s_{123}}{s_{23}}\right)\right. \\ &\quad \left. + p_2^2 \log\left(\frac{s_{123}}{p_2^2}\right)\right] + \frac{\hat{c}_\Gamma}{6}\left(\frac{(-s_{123})^{-\epsilon}}{\epsilon} + \frac{11}{3}\right). \end{aligned} \tag{5.148}$$

Tensor Integrals

Although the function Ld_0^{opp} cannot be grouped into a finite function, there is no reason why single logarithm terms (from the eventual bubble integrals at the end of the cascade) cannot group together in combinations which are finite as $\tilde{\Delta}_4 \to 0$. Furthermore, when the tensor integral is multiplied by a factor of ϵ in the Feynman diagram, logarithms can occur which are divided by the Gram determinant and must be combined into finite functions. For this reason it is useful to define the functions,

$$\begin{aligned} Lcd_n(p_1,p_2,p_3) &\equiv -\lim_{\epsilon\to 0} \epsilon I_4^{4-2\epsilon}[x_4^n] \\ &= -\frac{1}{1-\lambda}\lim_{\epsilon\to 0}\left(\alpha_1\alpha_4 I_3^{4-2\epsilon(1)}[x_4^{n-1}] - \alpha_2\alpha_4 I_3^{4-2\epsilon(2)}[x_4^{n-1}]\right) \\ &= \frac{2s_{13}}{\tilde{\Delta}_4}\left(s_{12}Lc_n^{2m}(p_{12},p_3) - p_2^2 Lc_n^{2m}(p_2,p_3)\right). \end{aligned} \tag{5.149}$$

Opposite box integrals with one Feynman parameter in the numerator are most easily derived using eq. (5.48)[6]. This can then be differentiated to give integrals with more than one Feynman parameter in the numerator. These derivations are straightforward but lengthy, and will not be reproduced here.

5.6.3 The One Mass Box

The box integrals with only one massive leg (ie. $s_{123} \neq 0$, $p_1^2 = p_2^2 = p_3^2 = 0$) are trivially obtained from the adjacent box integrals by taking the limit $p_1^2 \to 0$. All the integrals are well behaved in this limit and the resulting finite functions are given by,

$$Ld_{2S}^{1m}(p_1,p_2,p_3) = -\frac{2s_{12}s_{23}}{6\tilde{\Delta}_4}\left[s_{12}s_{23}Ld_{1S}^{1m}(p_1,p_2,p_3) + s_{23}\log\left(\frac{s_{123}}{s_{23}}\right) + s_{12}\log\left(\frac{s_{123}}{s_{12}}\right)\right], \tag{5.150}$$

$$Ld_{3S}^{1m}(p_1,p_2,p_3) = -\frac{2s_{12}s_{23}}{10\tilde{\Delta}_4}\left[s_{12}s_{23}Ld_{2S}^{1m}(p_1,p_2,p_3) + \frac{s_{23}^2}{12}\log\left(\frac{s_{123}}{s_{23}}\right) + \frac{s_{12}^2}{12}\log\left(\frac{s_{123}}{s_{12}}\right) + \frac{s_{12}s_{23}}{12}\right], \tag{5.151}$$

$$Ld_{4S}^{1m}(p_1,p_2,p_3) = -\frac{2s_{12}s_{23}}{14\tilde{\Delta}_4}\left[s_{12}s_{23}Ld_{3S}^{1m}(p_1,p_2,p_3) + \frac{s_{23}^3}{180}\log\left(\frac{s_{123}}{s_{23}}\right) + \frac{s_{12}^3}{180}\log\left(\frac{s_{123}}{s_{12}}\right) + \frac{s_{12}s_{23}(s_{123}+s_{12}+s_{23})}{720}\right]. \tag{5.152}$$

5.7 The Pentagon Integral

In this section the pentagon integrals with one massive leg will be examined. Since these integrals are not required for the calculation of Chapter 6 (except for the scalar integral) they are considered here only for completeness. In particular it will be demonstrated that the integrals do not contain the 4×4 determinant, Δ_5.

The particle momenta will be taken as in fig. (5.5) where $p_1^2 = p_2^2 = p_3^2 = p_4^2 = 0$ and $p_5^2 = -s_{1234} \neq 0$.

[6]Taking the derivative of the scalar integral would, as in the case of the adjacent box, require the scalar integral to order $\mathcal{O}(\epsilon)$.

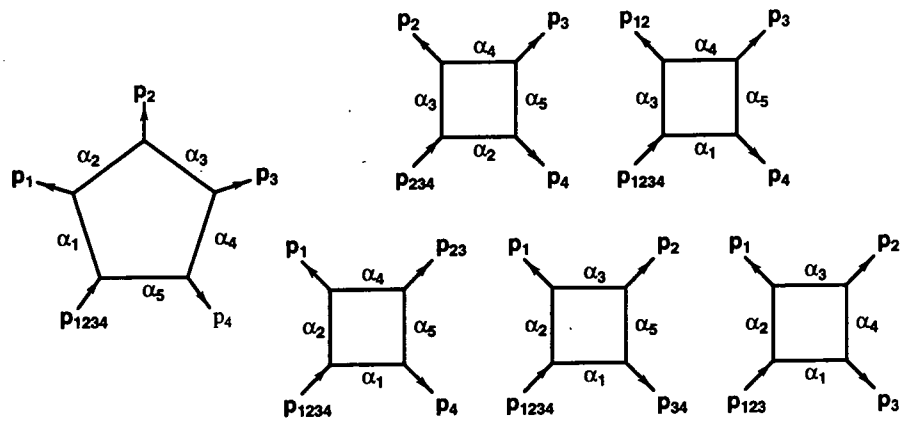

Figure 5.5: The diagrammatic form of the pentagon integral and the boxes formed by pinching. For each pinching i, the internal line corresponding to α_i is shrunk to zero length and the momenta on either end are combined.

The α_i parameters can be defined by,

$$\begin{aligned} \alpha_1\alpha_5 s_{1234} &= -\lambda, & \alpha_2\alpha_4 s_{23} &= -1, \\ \alpha_1\alpha_3 s_{12} &= -1, & \alpha_2\alpha_5 s_{234} &= -1, \\ \alpha_1\alpha_4 s_{123} &= -1, & \alpha_3\alpha_5 s_{34} &= -1, \end{aligned} \tag{5.153}$$

where

$$\lambda = -s_{1234}\frac{(\alpha_1\alpha_5)(\alpha_2\alpha_5)}{(\alpha_2\alpha_4)} = \frac{s_{1234}s_{23}}{s_{123}s_{234}}. \tag{5.154}$$

Notice that this is the same as the λ associated with the third pinching of the pentagon, ie. the opposite box, and consequently $(1-\lambda)$ can be thought of as a 3×3 Gram determinant.

The pentagon Gram determinant and its rescaled equivalent are given by,

$$\tilde{\Delta}_5 = s_{12}^2 s_{34}^2 + s_{13}^2 s_{24}^2 + s_{14}^2 s_{23}^2 - 2s_{12}s_{34}s_{13}s_{24} - 2s_{12}s_{34}s_{14}s_{23} - 2s_{13}s_{24}s_{14}s_{23}, \tag{5.155}$$

$$\begin{aligned} \hat{\Delta}_5 = {} & \alpha_1^2 + \alpha_2^2 + (1-\lambda)^2\alpha_3^2 + \alpha_4^2 + \alpha_5^2 - 2\alpha_1\alpha_2 + 2(1-\lambda)\alpha_1\alpha_3 + 2\alpha_1\alpha_4 - 2\alpha_1\alpha_5 \\ & -2(1-\lambda)\alpha_2\alpha_3 + 2(1-2\lambda)\alpha_2\alpha_4 + 2\alpha_2\alpha_5 - 2(1-\lambda)\alpha_3\alpha_4 + 2(1-\lambda)\alpha_3\alpha_5 - 2\alpha_4\alpha_5. \end{aligned} \tag{5.156}$$

With this choice of α_i the η matrix is,

$$\eta = \begin{pmatrix} 1 & -1 & 1-\lambda & 1 & -1 \\ -1 & 1 & \lambda-1 & 1-2\lambda & 1 \\ 1-\lambda & \lambda-1 & (1-\lambda)^2 & \lambda-1 & 1-\lambda \\ 1 & 1-2\lambda & \lambda-1 & 1 & -1 \\ -1 & 1 & 1-\lambda & -1 & 1 \end{pmatrix}, \tag{5.157}$$

and the normalization factor is given by,

$$N_5 = 1 - \lambda. \tag{5.158}$$

The limit $N_5 \to 0$ therefore corresponds to the vanishing of the opposite box Gram determinant.

The Scalar Integral

The pentagon scalar integral is derived in Appendix C by extension of the four dimensional result of Melrose [23], and Vermaseren and van Neerven [24], to $(4-2\epsilon)$ dimensions [22, 27]. Its decomposition into scalar box integrals can be written,

$$\hat{I}_5^{4-2\epsilon} = -\frac{1}{N_5}\sum_{i=1}^{5} \hat{\gamma}_i \hat{I}_4^{4-2\epsilon(i)}[1] + \mathcal{O}(\epsilon). \tag{5.159}$$

This is divergent in the limit $N_5 \to 0$. However, it has been demonstrated in section (5.6.2) that no finite function can be formed from the opposite box scalar integral, and it is this pinching ($i = 3$) which causes the divergence as *its* Gram determinant vanishes. The other box integrals can be combined together in such as way as to be finite as N_5 vanishes.

To make this explicit, the η matrix can be decomposed into two parts,

$$\eta_{ij} = \kappa_i \kappa_j + N_5 \tilde{\eta}_{ij}, \tag{5.160}$$

where $\kappa_i \kappa_j$ includes no opposite box pinchings,

$$\kappa_i = \begin{pmatrix} 1 \\ -1 \\ 0 \\ 1 \\ -1 \end{pmatrix}, \quad \kappa_i \kappa_j = \begin{pmatrix} 1 & -1 & 0 & 1 & -1 \\ -1 & 1 & 0 & -1 & 1 \\ 0 & 0 & 0 & 0 & 0 \\ 1 & -1 & 0 & 1 & -1 \\ -1 & 1 & 0 & -1 & 1 \end{pmatrix}, \tag{5.161}$$

and $\tilde{\eta}$ is,

$$\tilde{\eta} = \begin{pmatrix} 0 & 0 & 1 & 0 & 0 \\ 0 & 0 & -1 & 2 & 0 \\ 1 & -1 & 1-\lambda & -1 & 1 \\ 0 & 2 & -1 & 0 & 0 \\ 0 & 0 & 1 & 0 & 0 \end{pmatrix}. \tag{5.162}$$

Then the pentagon scalar integral can be written,

$$\begin{aligned} \hat{I}_5^{4-2\epsilon}[1] &= -\frac{1}{2N_5}\sum_{i,j}\eta_{ij}\alpha_j\hat{I}_4^{4-2\epsilon(i)}[1] \\ &= -\frac{1}{2N_5}\left(\sum_j \kappa_j\alpha_j\right)\sum_i \kappa_i\hat{I}_4^{4-2\epsilon(i)}[1] - \frac{1}{2}\sum_{i,j}\tilde{\eta}_{ij}\alpha_j\hat{I}_4^{4-2\epsilon(i)}[1]. \end{aligned} \tag{5.163}$$

The first term on the right-hand side in *finite* as N_5 vanishes and a new finite function can be defined,

$$\begin{aligned} Le_1(p_1,p_2,p_3,p_4) &\equiv -\frac{1}{2N_5}\sum_{i=1}^{5}\kappa_i\hat{I}_4^{4-2\epsilon(i)}[1] \\ &= \frac{s_{123}s_{234}}{s_{123}s_{234}-s_{1234}s_{23}}\left[Ld_0(p_1,p_2,p_3) - Ld_0(p_1,p_2,p_{34})\right. \\ &\qquad \left. + Ld_0(p_{12},p_3,p_4) - Ld_0(p_2,p_3,p_4)\right]. \end{aligned} \tag{5.164}$$

Although the explicit factor of N_5 in the denominator of the second term of eq. (5.163) has been cancelled, this term is still divergent as $N_5 \to 0$ since it contains the opposite box scalar integral which is itself divergent in this limit. However, since no finite function can be formed for the opposite box, this divergence must cancel explicitly in any matrix element calculation.

The scalar pentagon integral is then,

$$\hat{I}_5^{4-2\epsilon}[1] = \left(\sum_j \kappa_j\alpha_j\right) Le_1(p_1,p_2,p_3,p_4) - \frac{1}{2}\sum_{i,j}\tilde{\eta}_{ij}\alpha_j\hat{I}_4^{4-2\epsilon(i)}[1] \tag{5.165}$$

Scalar Integrals in Higher Dimensions

The scalar integral in $(6-2\epsilon)$ dimensions is given by eq. (5.45) to be,

$$\hat{I}_5^{6-2\epsilon}[1] = \frac{1}{\epsilon}\frac{N_5}{\hat{\Delta}_5}\left[\hat{I}_5^{4-2\epsilon}[1] + \frac{1}{2N_5}\sum_{k=1}^{5}\hat{\gamma}_k\hat{I}_4^{4-2\epsilon(k)}[1]\right]. \tag{5.166}$$

Therefore, in order to calculate the pentagon in six dimensions, the scalar integral in $(4-2\epsilon)$ dimensions is needed to $\mathcal{O}(\epsilon)$. However, Bern, Dixon and Kosower have shown that $\hat{I}_5^{6-2\epsilon}[1]$ always drops out of all matrix element calculations [21].

By inserting eq. (5.159) for the scalar integral in $(4-2\epsilon)$ dimensions it is at least possible to see that $\hat{I}_5^{6-2\epsilon}[1]$ in finite as $\epsilon \to 0$,

$$\hat{I}_5^{6-2\epsilon}[1] = \frac{1}{\epsilon}\frac{N_5}{\hat{\Delta}_5}\left[-\frac{1}{2N_5}\sum_{k=1}^{5}\hat{\gamma}_k\hat{I}_4^{4-2\epsilon(k)}[1] + \frac{1}{2N_5}\sum_{k=1}^{5}\hat{\gamma}_k\hat{I}_4^{4-2\epsilon(k)}[1]\right] + \mathcal{O}(1) = \mathcal{O}(1) \tag{5.167}$$

Similarly, the pentagon scalar integral in eight dimensions is also finite since $\hat{I}_5^6[1]$ and $\hat{I}_4^6[1]$ separately are, but cannot be easily calculated.

Tensor Integrals

Since the integral with one Feynman parameter in the numerator can be obtained by differentiating, ie. eq. (5.25), it is clear that the first rank pentagon integral can contain no 4×4 Gram determinants. In fact, this can be explicitly seen from eq. (5.46) where the coefficient of the pentagon integral in six dimensions is $\mathcal{O}(\epsilon)$,

$$\begin{aligned}\hat{I}_5^{4-2\epsilon}[a_i] &= \frac{1}{2N_5}\left(2\epsilon\hat{\gamma}_i\hat{I}_5^6[1] - \sum_{i=1}^{5}\eta_{ij}\hat{I}_4^{4-2\epsilon(j)}[1]\right) \\ &= -\frac{1}{2N_5}\sum_{i=1}^{5}\eta_{ij}\hat{I}_4^{4-2\epsilon(j)}[1] + \mathcal{O}(\epsilon).\end{aligned} \tag{5.168}$$

As in the scalar integral, this is divergent as $N_5 \to 0$ and can be written in terms of the finite function, Le_1 by decomposing η as in eq. (5.160). Then,

$$\begin{aligned}\hat{I}_5^{4-2\epsilon}[a_i] &= -\frac{1}{2N_5}\sum_{j=1}^{5}(\kappa_i\kappa_j + N_5\tilde{\eta}_{ij})\hat{I}_4^{4-2\epsilon(j)}[1] \\ &= \kappa_i Le_1(p_1,p_2,p_3,p_4) - \frac{1}{2}\sum_{j=1}^{5}\tilde{\eta}_{ij}\hat{I}_4^{4-2\epsilon(j)}[1]\end{aligned} \tag{5.169}$$

The Absence of $\tilde{\Delta}_5$

For the second rank tensor, the absence of $\tilde{\Delta}_5$ cannot be easily argued from the standpoint of differentiation because of the appearance of the ϵ-barrier. The generalization of eq. (5.25) to the second rank pentagon is,

$$\hat{I}_5^{4-2\epsilon}[a_i a_j] = \frac{1}{2\epsilon}\frac{\partial \hat{I}_5^{4-2\epsilon}[a_i]}{\partial \alpha_j} \tag{5.170}$$

Therefore one must again know the pentagon integral in $(4-2\epsilon)$ dimensions to $\mathcal{O}(\epsilon)$. However, eq. (5.49) can still be applied. This gives,

$$\begin{aligned}\hat{I}_5^{4-2\epsilon}[a_i a_j] &= \frac{1}{2N_5^2}\hat{\gamma}_i\hat{\gamma}_j\hat{I}_5^8[1] + \frac{1}{2N_5^2}\sum_{k=1}^{5}\eta_{ik}\hat{\gamma}_j\hat{I}_4^{6,(k)}[1] + \frac{1}{2N_5}\eta_{ij}\hat{I}_5^6[1] \\ &\quad -\frac{1}{2N_5}\sum_{k=1}^{5}\eta_{jk}\hat{I}_4^{4-2\epsilon(k)}[a_i].\end{aligned} \tag{5.171}$$

Rearranging the coefficient of $\hat{I}_5^8[1]$, $\hat{I}_5^{4-2\epsilon}[a_i a_j]$ can be written,

$$\begin{aligned}\hat{I}_5^{4-2\epsilon}[a_i a_j] &= -\frac{\hat{\Delta}_5}{N_5}\hat{c}_{ij}\hat{I}_5^8[1] - \frac{1}{2N_5^2}\eta_{ij}\hat{I}_5^8[1] + \frac{1}{2N_5^2}\sum_{k=1}^{5}\eta_{ik}\hat{\gamma}_j\hat{I}_4^{6,(k)}[1] \\ &\quad +\frac{1}{2N_5}\eta_{ij}\hat{I}_5^6[1] - \frac{1}{2N_5}\sum_{k=1}^{5}\eta_{jk}\hat{I}_4^{4-2\epsilon(k)}[a_i],\end{aligned} \tag{5.172}$$

where the definition of $\hat{c}_{ij}$ is,

$$\hat{c}_{ij} \equiv \frac{1}{2N_5}\left(\eta_{ij} - \frac{\hat{\gamma}_i\hat{\gamma}_j}{\hat{\Delta}_5}\right). \tag{5.173}$$

Now $\hat{I}_5^8[1]$ in the second term can be written in terms of the pentagon in six dimensions and boxes using eq. (5.45). This concentrates all occurrences of the Gram determinant into the first term. $\hat{I}_5^{4-2\epsilon}[a_i a_j]$ becomes,

$$\hat{I}_5^{4-2\epsilon}[a_i a_j] = -\frac{\hat{\Delta}_5}{N_5}\hat{c}_{ij}\hat{I}_5^8[1] + \frac{1}{4N_5^2}\sum_{k=1}^{5}\left(\eta_{ik}\hat{\gamma}_j - \eta_{ij}\hat{\gamma}_k\right)\hat{I}_4^{6(k)}[1] - \frac{1}{2N_5}\sum_{k=1}^{5}\eta_{ik}\hat{I}_4^{4-2\epsilon(k)}[a_i]. \tag{5.174}$$

Since $\hat{I}_5^8[1]$ contains two powers of $\hat{\Delta}_5$ this integral is divergent as the Gram determinant vanishes. However, it can be shown that $\mathcal{I}_5^{\mu\nu}$ is not.

The external momenta p_i span the four dimensional Minkowski space, giving rise to a Schouten identity which links the $p_i^\mu p_j^\nu$ and $g_{\mu\nu}$ terms of $\mathcal{I}_5^{\mu\nu}$, eq. (B.24). This can be written as,

$$\sum_{i,j=2}^{5} p^\mu_{1\ldots(i-1)} p^\nu_{1\ldots(j-1)} c_{ij} = \frac{1}{2} g^{\mu\nu}_{[4]}, \tag{5.175}$$

where $g^{\mu\nu}_{[4]}$ is the metric tensor in four dimensions, and,

$$c_{ij} = \hat{c}_{ij}\alpha_i\alpha_j. \tag{5.176}$$

Substituting eq. (5.172) into eq. (B.24) gives,

$$\begin{aligned}
\mathcal{I}_5^{\mu\nu} &= i(4\pi)^{\epsilon-2}\left(\sum_{i,j=2}^{5} p^\mu_{1\ldots(i-1)} p^\nu_{1\ldots(j-1)}\left[-\frac{\hat{\Delta}_5}{N_5} c_{ij} I_5^8[1] + boxes\right] - \frac{1}{2} g^{\mu\nu} I_5^6[1]\right) \\
&= i(4\pi)^{\epsilon-2}\left(\sum_{i,j=2}^{5} p^\mu_{1\ldots(i-1)} p^\nu_{1\ldots(j-1)}[boxes] - \frac{1}{2} g^{\mu\nu} I_5^6[1] - \frac{1}{2} g^{\mu\nu}_{[4]} \frac{\hat{\Delta}_5}{N_5} I_5^8[1]\right) \\
&= i(4\pi)^{\epsilon-2}\left(\sum_{i,j=2}^{5} p^\mu_{1\ldots(i-1)} p^\nu_{1\ldots(j-1)}[boxes] - \frac{1}{2} g^{\mu\nu}\left[I_5^6[1] + \frac{\hat{\Delta}_5}{N_5} I_5^8[1]\right]\right),
\end{aligned} \tag{5.177}$$

where the finiteness of $I_5^8[1]$ as $\epsilon \to 0$ ensures that,

$$\left(g^{\mu\nu}_{[4-2\epsilon]} - g^{\mu\nu}_{[4]}\right) I_5^8[1] = \mathcal{O}(\epsilon). \tag{5.178}$$

Expanding $I_5^8[1]$ using eq. (5.45), the coefficient of $g^{\mu\nu}$ becomes,

$$-\frac{1}{2}\left[I_5^6[1] + \left(-I_5^6[1] - \frac{1}{2N_5}\sum_{i=1}^{5}\gamma_i I_4^{6(i)}[1]\right)\right] = \frac{1}{4N_5}\sum_{i=1}^{5}\gamma_i I_4^{6(i)}[1]. \tag{5.179}$$

The second rank tensor pentagon integral has been written entirely in terms of boxes with no 4×4 Gram determinant. Since the ϵ-barrier has been passed further differentiation cannot produce any new Gram determinants and therefore Δ_5 is also absent from the third, fourth and fifth rank tensor integrals.

5.8 Summary

This chapter has presented a general method for calculating tensor loop integrals in terms of functions which are finite as the Gram determinant vanishes. It has been seen that

standard approaches produce expressions which contain fake singularities in this limit. By modifying the "string inspired" approach of Bern, Dixon and Kosower [21, 27], it is possible to collect together non-trivial combinations of scalar integrals to form these new finite functions. Not only does this improve the numerical stability of the matrix elements but also helps make the expressions more compact.

This method has been used to evaluate all the finite functions and tensor integrals required for the calculation of the virtual matrix elements for the process $\gamma^* \to q\bar{q}Q\bar{Q}$ which will be the subject of Chapter 6.

Chapter 6

Four Jet Production in e^+e^- Annihilation

6.1 Introduction

It has been seen in Chapter 3, that e^+e^- collisions provide a particularly effective laboratory for investigating the interactions of quarks and gluons. In particular, by use of a suitable jet algorithm one can compare the experimentally observed jets of hadrons with theoretical matrix element calculations at the parton level.

Therefore, in order to experimentally test QCD it is necessary to calculate the partonic matrix elements appropriate to jet production. Such matrix element calculations have been performed at lowest order (tree-level) for up to five jet production [35, 36, 37, 38, 39, 40], and at next-to-leading order for up to three jets [37]. In order to give predictions for physical observables, numerical programs have been constructed [41, 42, 16, 17] which combine together the partonic matrix elements to form infra-red safe quantities.

It is clear that the next step is to calculate the NLO radiative corrections for four jet production. This calculation involves three essential ingredients:

- **Virtual Corrections**
  The partonic matrix elements for $e^+e^- \to q\bar{q}Q\bar{Q}$ and $e^+e^- \to q\bar{q}gg$ are required

at one loop. The extremely long delay between the NLO 3-jet and 4-jet matrix element calculations has been caused by the technical difficulties encountered in the calculation of this virtual contribution. These difficulties have been outlined in the previous chapters.

- **Real Corrections**
  The tree-level matrix elements for $e^+e^- \to q\bar{q}Q\bar{Q}g$ and $e^+e^- \to q\bar{q}ggg$ are required when one of the partons is unresolved. These matrix elements are already well known in four dimensions [40].

- **Numerics**
  A Numerical program must be constructed to add together the real and virtual contributions over the appropriate phase space by implementing the jet algorithm and an appropriate method for cancelling the infra-red divergence (see section (3.6)).

This chapter will consider only the virtual corrections to four jet production. In particular the one loop partonic matrix elements for $e^+e^- \to q\bar{q}Q\bar{Q}$ are calculated using the techniques discussed in the previous chapters. This provides a first step toward the full NLO calculation of four jet production in electron-positron annihilation. Of course, the usefulness of this calculation is not restricted to e^+e^- collisions — it is also an ingredient of the next-to-leading order calculations relevant for $e^{\pm}p \to e^{\pm} + 3$ jets and $p\bar{p} \to V + 2$ jets, where V is a W or Z boson. The calculation is therefore relevant to processes seen in experiments at the major accelerators, LEP at CERN, HERA at DESY and the TEVATRON at FNAL.

In the context of e^+e^- collisions, the NLO 4-jet rate can be applied to give a more precise measurement of the QCD colour factor ratios, C_A/C_F and T_F/C_F. This will be discussed in section (6.2). Furthermore, this process is a background to the threshold production of W pairs at LEP 2.

Recently, the one-loop corrections for $e^+e^- \to q\bar{q}Q\bar{Q}$ have also been performed by Bern, Dixon and Kosower [43], providing an interesting check of the results presented here. In addition, Dixon and Signer have reported the first numerical results for the

leading colour contribution to the $e^+e^- \to 4$ jet rate at next-to-leading order [44].

6.2 The QCD Colour Factors

An important and interesting test of QCD is the experimental verification of its $SU(3)$ group structure. By describing QCD as invariant under this symmetry group, the observed hadrons can be explained in terms of colour singlet bound states of three quarks or $q\bar{q}$ pairs. However, this is a purely *static* argument — it is possible that the *dynamics* of QCD could be described by some other group. For example, the $SU(3)$ symmetry could be *spontaneously broken* to a smaller group. By measuring the QCD colour factors the group structure of QCD can be experimentally tested.

The symmetry group of a gauge theory can be completely specified by ratios of the quantities C_F, C_A and T_F, defined by,

$$\sum_{a=1}^{N_A} (T^a T^a)_{ij} \equiv \delta_{ij} C_F, \tag{6.1}$$

$$\sum_{a,b=1}^{N_A} f^{abc} f^{abd} \equiv \delta^{cd} C_A, \tag{6.2}$$

$$\sum_{i,j=1}^{N_F} T^a_{ij} T^b_{ji} \equiv \delta^{ab} T_F, \tag{6.3}$$

where T^a are the generators of the group, and N_F and N_A are the dimensions of the fundamental and adjoint representations respectively. By comparing eqs. (6.1) and (6.3), it is easy to see that N_F and N_A are related by,

$$N_F C_F = N_A T_F. \tag{6.4}$$

In the case of QCD these quantities are known as the *colour factors*, and are given by application of eqs. (2.7), (2.28) and (2.34) to be,

$$C_F = \frac{N^2 - 1}{2N}, \quad C_A = N, \quad T_F = \frac{1}{2}, \tag{6.5}$$

where N is the number of colours (ie. $N = N_F$).

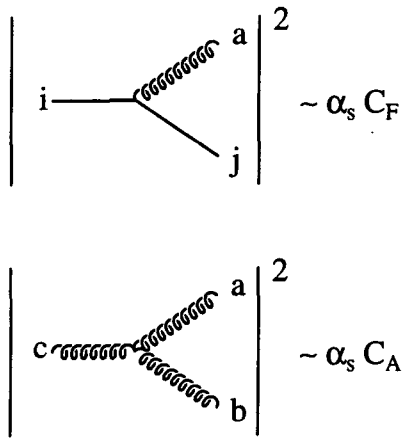

Figure 6.1: A pictorial representation of the colour factors.

The colour factors $C_{\mathcal{F}}$ and $C_{\mathcal{A}}$ can be physically interpreted as the squared *colour charges* of the quarks and gluons respectively[1]. In this way they can be identified with the quark-gluon and gluon-gluon vertices found in Feynman diagrams as seen in fig. (6.1). By measuring the colour factor ratios $C_{\mathcal{A}}/C_{\mathcal{F}}$ and $\mathcal{T}_{\mathcal{F}}/C_{\mathcal{F}}$, it is possible to distinguish between different group structures. For example, an Abelian gluon model $U(1)_3$ has no three gluon vertex and therefore has $C_{\mathcal{A}} = 0$.

Four jet production is the best place to measure these ratios, because the three gluon vertex is present at *leading order*, fig. (6.2). This is important for the measurement of $C_{\mathcal{A}}$. For three jet production this vertex is only present at next-to-leading order and its effects are suppressed by order α_s.

At leading order four jet production is described by the parton processes $e^+e^- \to q\bar{q}gg$ and $e^+e^- \to q\bar{q}Q\bar{Q}$. For *any* gauge theory with quarks in the fundamental representation and gluons in the adjoint representation of the symmetry group, the corresponding differential cross-sections will have the form:

$$\frac{1}{\sigma_0} d\sigma^{e^+e^- \to q\bar{q}gg} = \left(\frac{\alpha_s C_{\mathcal{F}}}{\pi}\right)^2 \left[F_A + \left(1 - \frac{C_{\mathcal{A}}}{2C_{\mathcal{F}}}\right) F_B + \frac{C_{\mathcal{A}}}{C_{\mathcal{F}}} F_C\right], \tag{6.6}$$

[1] $\mathcal{T}_{\mathcal{F}}$ is really just a normalization choice.

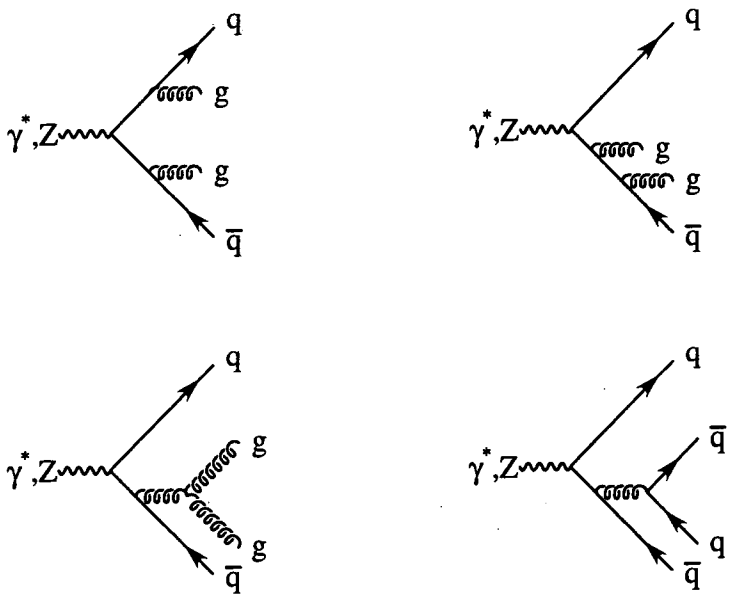

Figure 6.2: The generic leading order Feynman diagrams for $e^+e^- \to 4$ jets. Notice the presence of the three gluon vertex.

$$\frac{1}{\sigma_0} d\sigma^{e^+e^- \to q\bar{q}Q\bar{Q}} = \left(\frac{\alpha_s C_{\mathcal{F}}}{\pi}\right)^2 \left[\frac{T_{\mathcal{F}}}{C_{\mathcal{F}}} n_f F_D + \left(1 - \frac{C_{\mathcal{A}}}{2C_{\mathcal{F}}}\right) F_E\right], \tag{6.7}$$

where $F_A \ldots F_E$ are functions of the kinematic variables and independent of the group structure, n_f is the number of active quark flavours, and σ_0 is the leading order cross section for two jet production. Since the functions $F_A \ldots F_E$ are known, the differential cross section (or any other variable sensitive to the group structure) can be fitted to the experimental data to give a measurement of the colour factor ratios.

This analysis has been done by all four LEP experiments [45, 46, 47, 48], giving an average[2] result [50],

$$\frac{C_{\mathcal{A}}}{C_{\mathcal{F}}} = 2.221 \pm 0.225, \qquad \frac{T_{\mathcal{F}}}{C_{\mathcal{F}}} = 0.353 \pm 0.132, \tag{6.8}$$

which is consistent with $SU(3)$. This result is shown in fig. (6.3) together with the colour factors of some of the more usual symmetry groups.

[2]The much less accurate two and three jet analysis has also been included [49].

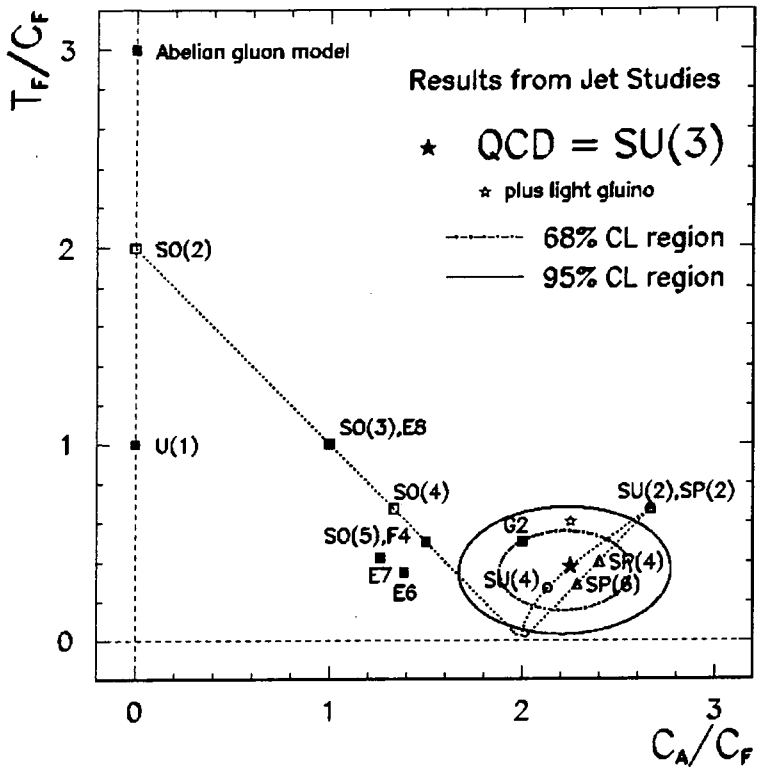

Figure 6.3: The measurement of the QCD colour factor ratios at LEP. Confidence level contours of 68% and 95% are shown, in addition to the effect of including a light gluino. This figure is reproduced from [50].

Also shown are the expected colour factor ratios for a symmetry group of $SU(3)$ in the presence of a light gluino. If this supersymmetric fermion were to exist it would contribute to the four jet cross section via the process $e^+e^- \rightarrow q\bar{q}\tilde{g}\tilde{g}$, and would therefore affect the measurement of colour factors. A light gluino has not been ruled out by this analysis.

It is clear from fig. (6.3) that the confidence boundaries are still rather large and there are many candidate symmetry groups which have not been excluded. The accuracy of the colour factor ratio measurement could be improved by the inclusion of next-to-leading order four jet production. By including NLO the perturbative expansion remains valid for lower values of the jet resolution parameter y_{cut}, and narrower jets can be used. This leads to more four jet events being seen and consequently increased statistics. Therefore,

including the next-to-leading order corrections to four jet production would improve both systematic theoretical errors and statistical errors

6.3 $\gamma^* \to q\bar{q}Q\bar{Q}$

This section will discuss the calculation of the one-loop corrections to $e^+e^- \to q\bar{q}Q\bar{Q}$. In this process, the electron and positron annihilate to form a gauge boson which subsequently decays into four quarks. Since it is the QCD part of the interaction which is of interest, it is sufficient to consider the decay of the virtual gauge boson into four quarks. In addition, the gauge boson will be restricted to vector couplings, ie. a virtual photon, because of the difficulties associated with defining γ_5 away from four dimensions. With these simplifications, the process under consideration is $\gamma^* \to q\bar{q}Q\bar{Q}$.

The momenta of the particles are chosen to be given by,

$$\gamma^*(p_{1234}) \longrightarrow q(p_1) + \bar{q}(p_2) + Q(p_3) + \bar{Q}(p_4). \tag{6.9}$$

Using momentum conservation, the photon momentum can be systematically eliminated in favour of the massless quark momenta. The cases where the quarks q and Q are of the same or different flavour are considered, and their colours are denoted by c_i, $i = 1 \ldots 4$.

Colour Decomposition

By making a colour decomposition as described in section (2.5), the tree-level matrix elements can be written as,

$$\begin{aligned} \mathcal{M}^{tree-level} = \frac{eg_s^2}{2} \Big\{ & \left(\delta_{c_1c_4}\delta_{c_3c_2} - \frac{1}{N}\delta_{c_1c_2}\delta_{c_3c_4}\right)\left(\mathcal{A}^{(0)}(1,2) + \mathcal{A}^{(0)}(3,4)\right) \\ & -\delta_{qQ}\left(\delta_{c_1c_2}\delta_{c_3c_4} - \frac{1}{N}\delta_{c_1c_4}\delta_{c_3c_2}\right)\left(\mathcal{A}^{(0)}(1,4) + \mathcal{A}^{(0)}(3,2)\right)\Big\}, \end{aligned} \tag{6.10}$$

where N is the number of colours and $\delta_{qQ} = 1$ if the quarks are of the same flavour and zero otherwise. The arguments of $\mathcal{A}$ refer to the spin line to which the virtual photon is connected, ie. $\mathcal{A}(i,j)$ has contributions from the Feynman diagrams where the photon is connected to the quark-antiquark pair i,j.

Similarly, the colour decomposition of the one-loop matrix elements gives,

$$\mathcal{M}^{one-loop} = \frac{eg_s^4}{32\pi^2} \times \Big\{ \delta_{c_1c_4}\delta_{c_3c_2}\left(\mathcal{A}_1^{(1)}(1,2)+\mathcal{A}_1^{(1)}(3,4)+\frac{\delta_{qQ}}{N}\left[\mathcal{A}_2^{(1)}(1,4)+\mathcal{A}_2^{(1)}(3,2)\right]\right) - \delta_{c_1c_2}\delta_{c_3c_4}\left(\frac{1}{N}\left[\mathcal{A}_2^{(1)}(1,2)+\mathcal{A}_2^{(1)}(3,4)\right]+\delta_{qQ}\left[\mathcal{A}_1^{(1)}(1,4)+\mathcal{A}_1^{(1)}(3,2)\right]\right)\Big\} \quad (6.11)$$

where $\mathcal{A}_1^{(1)}$ and $\mathcal{A}_2^{(1)}$ can be further decomposed as,

$$\mathcal{A}_1^{(1)}(i,j) = NA_C^{(1)}(i,j) - \frac{1}{N}\left[2A_A^{(1)}(i,j)+A_B^{(1)}(i,j)\right], \quad (6.12)$$

$$\mathcal{A}_2^{(1)}(i,j) = N\left[A_A^{(1)}(i,j)-A_C^{(1)}(i,j)\right]+\frac{1}{N}\left[A_A^{(1)}(i,j)+A_B^{(1)}(i,j)\right]. \quad (6.13)$$

The functions $A_\alpha^{(1)}(i,j)$, where α = A,B,C, have contributions from the gauge invariant sets of Feynman diagrams shown in fig. (6.5) where, again, the photon couples to the quark-antiquark pair i,j.

In addition, one would expect contributions from diagrams containing closed fermion triangles as in fig. (6.4). However, diagrams must be considered where the quark propagates both clockwise and anti-clockwise around the loop. These diagrams are exactly the same but have the opposite sign and therefore cancel. This is an application of Furry's theorem.

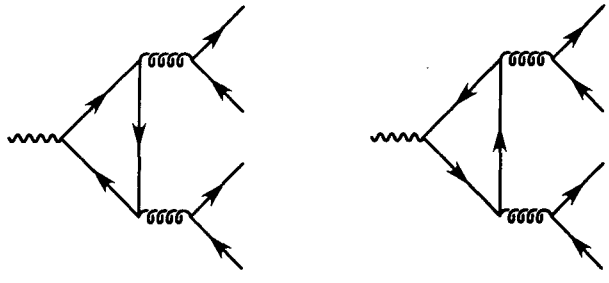

Figure 6.4: The triangle diagrams which cancel by Furry's theorem.

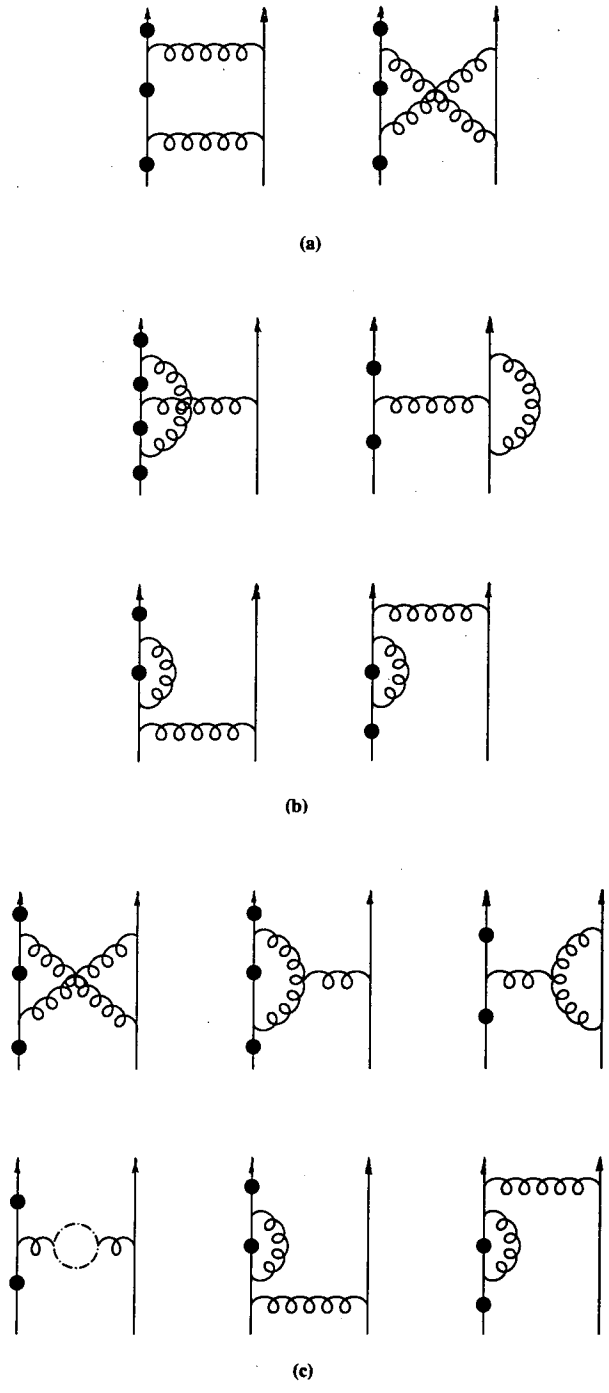

Figure 6.5: The classes of Feynman diagrams contributing to the functions $A_\alpha^{(1)}(i,j)$ for $\alpha =$ A,B,C. The solid circle shows the possible positions for attaching the off-shell photon to the quark-antiquark pair i,j.

Squared matrix elements

In principle, the matrix elements could be evaluated for external particles of definite helicity by employing the spinor helicity methods of section (2.6). As has been pointed out in section (3.5), spinor helicity methods cannot be used away from four dimensions and are therefore incompatible with dimensional regularization. To overcome this, dimensional *reduction* must be used. However, here the "squared" matrix elements are calculated, or rather the interference of the one-loop matrix elements with the tree-level in order to give $\mathcal{O}(\alpha^3)$. This has the advantage of trivially reducing the rank and point of each loop integration. Since the squared matrix elements have no tensor structure, the tensor integrals are always saturated with the external momenta. If the saturating momentum is contained in the denominator of the integrand, it can be rewritten,

$$\begin{aligned}\frac{k.p_i}{k^2k_1^2\ldots k_{1\ldots i}^2\ldots k_{1\ldots(m-1)}^2} &= \frac{1}{2}\frac{k_{1\ldots i}^2-k_{1\ldots(i-1)}^2-p_{1\ldots i}^2+p_{1\ldots(i-1)}^2}{k^2k_1^2\ldots k_{1\ldots i}^2\ldots k_{1\ldots(m-1)}^2}\\ &= \frac{1}{2}\frac{1}{k^2k_1^2\ldots k_{1\ldots(i-1)}^2k_{1\ldots(i+1)}^2\ldots k_{1\ldots(m-1)}^2}-\frac{1}{2}\frac{1}{k^2k_1^2\ldots k_{1\ldots(i-2)}^2k_{1\ldots i}^2\ldots k_{1\ldots(m-1)}^2}\\ &\quad -\frac{1}{2}\frac{p_{1\ldots i}^2-p_{1\ldots(i-1)}^2}{k^2k_1^2\ldots k_{1\ldots i}^2\ldots k_{1\ldots(m-1)}^2},\end{aligned} \tag{6.14}$$

where, as usual, $k_{1\ldots i}=k+p_{1\ldots i}=k+p_1+\ldots+p_i$. In particular, this removes all of the tensor pentagon integrals. Since helicity amplitudes are not used, the divergences are regulated using conventional dimensional regularization with the number of dimensions $n=4-2\epsilon$.

However, it should be stressed that the methods described in Chapter 5 for writing the tensor integrals in terms of finite functions are not dependent on calculating the squared matrix elements but can also be applied to spinor helicity methods. The squared matrix elements are only calculated here because of the trivial removal of the tensor pentagon integrals.

The Feynman gauge has been chosen for this calculation, and the corresponding Feynman rules are presented in Appendix D. Since the virtual photon is connected to a conserved current (the electron-positron pair) its longitudinal polarization is removed

and the spin sum over its polarization vector may be written,

$$\sum_{\text{spins}} \epsilon^{\mu}\epsilon^{*\nu} = -g^{\mu\nu}. \tag{6.15}$$

The squared matrix elements at leading order have been known for some time [37], and are of the form,

$$\begin{aligned}\sum_{\text{spins}} |\mathcal{M}^{(0)}|^2 &= \frac{e^2 g_s^4}{4}(N^2-1) \\ &\times \left\{\Big(\mathcal{T}(1,2;1,2)+\mathcal{T}(1,2;3,4)\Big) + \frac{\delta_{qQ}}{N}\Big(\mathcal{T}(1,2;1,4)+\mathcal{T}(1,2;3,2)\Big)\right\} \\ &+(1\leftrightarrow 3, 2\leftrightarrow 4) + \delta_{qQ}(2\leftrightarrow 4) + \delta_{qQ}(1\leftrightarrow 3),\end{aligned} \tag{6.16}$$

where,

$$\mathcal{T}(i,j;k,l) = \sum_{\text{spins}} |A^{(0)\dagger}(i,j)\mathcal{A}^{(0)}(k,l)|. \tag{6.17}$$

Similarly, the interference between the tree-level and one-loop amplitudes is given by,

$$\begin{aligned}\sum_{\text{spins}} 2|\mathcal{M}^{(0)\dagger}\mathcal{M}^{(1)}| &= \frac{e^2 g_s^4}{4}\left(\frac{\alpha_s N}{2\pi}\right)(N^2-1) \\ &\times \left\{\left[\Big(\mathcal{L}_C(1,2;1,2)+\mathcal{L}_C(1,2;3,4)\Big)\right.\right. \\ &\qquad \left.-\frac{1}{N^2}\Big(2\mathcal{L}_A(1,2;1,2)+2\mathcal{L}_A(1,2;3,4)+\mathcal{L}_B(1,2;1,2)+\mathcal{L}_B(1,2;3,4)\Big)\right] \\ &+\delta_{qQ}\left[\frac{1}{N}\Big(\mathcal{L}_A(1,2;1,4)+\mathcal{L}_A(1,2;3,2)-\mathcal{L}_C(1,2;1,4)-\mathcal{L}_C(1,2;3,2)\Big)\right. \\ &\qquad \left.\left.+\frac{1}{N^3}\Big(\mathcal{L}_A(1,2;1,4)+\mathcal{L}_A(1,2;3,2)+\mathcal{L}_B(1,2;1,4)+\mathcal{L}_B(1,2;3,2)\Big)\right]\right\} \\ &+(1\leftrightarrow 3, 2\leftrightarrow 4) + \delta_{qQ}(2\leftrightarrow 4) + \delta_{qQ}(1\leftrightarrow 3),\end{aligned} \tag{6.18}$$

with,

$$\mathcal{L}_\alpha(i,j;k,l) = \sum_{\text{spins}} |A_\alpha^{(1)\dagger}(i,j)\mathcal{A}^{(0)}(k,l)|. \tag{6.19}$$

Symmetries of the Matrix Elements

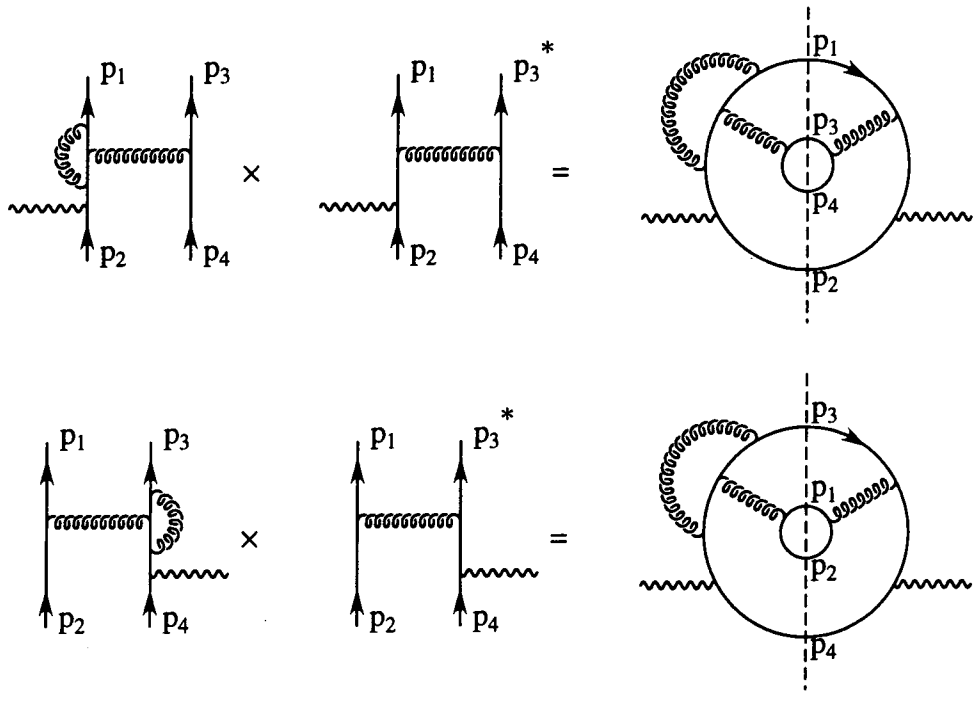

Figure 6.6: Contributions to the functions $\mathcal{L}_B(1,2;1,2)$ and $\mathcal{L}_B(3,4;3,4)$, which transform on to one another by swapping $p_1 \leftrightarrow p_3$ and $p_2 \leftrightarrow p_4$.

The symmetry properties of the above matrix elements are easy to see from the Feynman diagrams. For example, fig. (6.6) shows contributions to the functions $\mathcal{L}_B(1,2;1,2)$ and $\mathcal{L}_B(3,4;3,4)$, which transform on to one another by swapping $p_1 \leftrightarrow p_3$ and $p_2 \leftrightarrow p_4$.

Using symmetries of this form, it is only necessary to calculate one-loop diagrams where the virtual photon is attached to the p_1, p_2 spin line. Similarly, when the quarks are identical, interchanging $p_1 \leftrightarrow p_2$ and $p_3 \leftrightarrow p_4$ transforms $\mathcal{L}_\alpha(1,2;3,2)$ onto $\mathcal{L}_\alpha(1,2;1,4)$, and vice versa. The squared matrix elements are therefore described by nine independent $\mathcal{L}_\alpha$ functions.

Furthermore these functions have additional, internal symmetries. For example, it is clear that the first "squared" diagram of fig. (6.6) is symmetric under interchange of $p_3 \leftrightarrow p_4$ and the second is symmetric under interchange of $p_1 \leftrightarrow p_2$. These internal

symmetries of the $\mathcal{L}_\alpha$ functions are outlined in table (6.1).

Function	Symmetry	Anti-symmetry
$\mathcal{L}_A(1,2;1,2)$		$p_1 \leftrightarrow p_2$ $p_3 \leftrightarrow p_4$
$\mathcal{L}_A(1,2;3,4)$	$p_1 \leftrightarrow p_2$ $p_3 \leftrightarrow p_4$	
$\mathcal{L}_B(1,2;1,2)$	$p_1 \leftrightarrow p_2$ $p_3 \leftrightarrow p_4$	
$\mathcal{L}_B(1,2;3,4)$		$p_1 \leftrightarrow p_2$ $p_3 \leftrightarrow p_4$
$\mathcal{L}_C(1,2;1,2)$	$p_1 \leftrightarrow p_2$ *and* $p_3 \leftrightarrow p_4$	
$\mathcal{L}_C(1,2;3,4)$	$p_1 \leftrightarrow p_2$ *and* $p_3 \leftrightarrow p_4$	

Table 6.1: The symmetry properties of the $\mathcal{L}_\alpha$ functions. $\mathcal{L}_C(1,2;1,2)$ and $\mathcal{L}_C(1,2;3,4)$ are only symmetric under the interchange of *both* $p_1 \leftrightarrow p_2$ *and* $p_3 \leftrightarrow p_4$. $\mathcal{L}_\alpha(1,2;1,4)$ and $\mathcal{L}_\alpha(1,2;3,2)$ map onto each other under the interchange of $p_1 \leftrightarrow p_2$ *and* $p_3 \leftrightarrow p_4$ and have no internal symmetries.

Calculating $\mathcal{L}_\alpha$

The remaining nine $\mathcal{L}_\alpha$ were calculated and simplified using the algebraic manipulation package FORM [28]. Performing the algebra by computer has two clear advantages:

- Computer algebra allows the handling of very large expressions and prevents trivial algebraic errors.

- Once the manipulation program is complete, the calculation is performed automatically. This allows any changes or corrections to be made to the program, without having to recalculate the entire matrix elements by hand.

The required individual tensor integrals were calculated separately using the methods of Chapters 4 and 5. This provides expressions for the tensor integrals which are well behaved as each Gram determinant vanishes and are written in a natural, simplified form. These expressions were then included in the manipulation program and could be inserted into each Feynman diagram where required. Since the "squared" matrix elements have no remaining tensor structure, the final expressions for $\mathcal{L}_\alpha$ are written purely as dot products of the external momenta multiplying the finite functions of Chapter 5.

As previously mentioned, dimensional regularization with dimension $n = 4-2\epsilon$ is used. The infra-red and ultra-violet divergences are easily found since they must be proportional to the tree-level amplitudes. The ϵ-pole structure is given by,

$$\mathcal{L}_A(1,2;i,j) = \left(+\frac{\mathcal{P}_{13}}{\epsilon^2} - \frac{\mathcal{P}_{14}}{\epsilon^2} - \frac{\mathcal{P}_{23}}{\epsilon^2} + \frac{\mathcal{P}_{24}}{\epsilon^2}\right)\mathcal{T}(1,2;i,j) + \hat{\mathcal{T}}_A(1,2;i,j), \tag{6.20}$$

$$\mathcal{L}_B(1,2;i,j) = \left(-\frac{\mathcal{P}_{12}}{\epsilon^2} - \frac{\mathcal{P}_{34}}{\epsilon^2} - \frac{3\mathcal{P}_{34}}{\epsilon}\right)\mathcal{T}(1,2;i,j) + \hat{\mathcal{T}}_B(1,2;i,j), \tag{6.21}$$

$$\mathcal{L}_C(1,2;i,j) = \left(-\frac{\mathcal{P}_{14}}{\epsilon^2} - \frac{\mathcal{P}_{23}}{\epsilon^2} + \frac{2}{3}\frac{\mathcal{P}_{34}}{\epsilon} - \frac{2N_F}{3N}\frac{\mathcal{P}_{34}}{\epsilon}\right)\mathcal{T}(1,2;i,j) + \hat{\mathcal{T}}_C(1,2;i,j), \tag{6.22}$$

where,

$$\mathcal{P}_{ij} = \left(\frac{4\pi\mu^2}{-s_{ij}}\right)^\epsilon \frac{\Gamma^2(1-\epsilon)\Gamma(1+\epsilon)}{\Gamma(1-2\epsilon)}, \tag{6.23}$$

and $\mathcal{T}$ are the squared tree-level amplitudes of eq. (6.17) in $4-2\epsilon$ dimensions.

Of course, these ϵ-poles have a prescribed form. The infra-red poles must cancel with those from the process $\gamma^* \to q\bar{q}Q\bar{Q}g$ when one of the partons is unresolved, and the ultra-violet poles must be renormalized. This pole structure provides a check on the answer and is in agreement with the expectations of [16].

Unfortunately, the individual expressions for $\hat{\mathcal{T}}_\alpha$ are rather lengthy and their presentation here would be unilluminating. Instead they are included in a FORTRAN subroutine

which calculates the finite one-loop contribution for a given phase space point[3]. It is stressed that the $\hat{\mathcal{T}}_\alpha$ have been calculated analytically, and their numerical evaluation is performed only for the convenience of those wanting to use the results.

6.4 Outlook and Summary

This chapter has discussed the calculation of the next-to-leading order corrections to the rate $e^+e^- \to 4$ jets. This calculation is useful for improving the measurement of the measurement of the QCD colour factor ratios C_A/C_F and $\mathcal{T}_F/C_F$, which tests the group structure of QCD. The partonic matrix elements are also applicable to next-to-leading order calculations of the rates $e^\pm p \to e^\pm + 3$ jets and $p\bar{p} \to V + 2$ jets, where V is a W or Z boson.

In particular, the one-loop corrections to the process $\gamma^* \to q\bar{q}Q\bar{Q}$ have been presented. This is a first step towards the full NLO calculation of $e^+e^- \to 4$ jets. In performing this calculation, use has been made of colour decomposition and the extensive symmetries of the matrix elements. Furthermore, the results of Chapter 5 have been used to write the "squared" matrix elements in terms of functions which are well behaved as the Gram determinants vanish.

Due to the difficulties in defining γ_5 away from four dimensions, spinor helicity methods have not been used. Instead, the interference of the one-loop amplitude with tree-level has been calculated. This has two disadvantages:

- "Squaring" the matrix elements leads to longer expressions than those found using spinor helicity methods.
- Since the chiral projection operator is unavailable, the electroweak gauge boson is restricted to vector couplings. In other words, the corrections for $e^+e^- \to Z \to q\bar{q}Q\bar{Q}$ have not been included. Clearly, helicity amplitudes provide both vector and axial vector couplings.

[3]The finite functions included in the FORTRAN code may differ by factors from those of Chapter 5. However, since they are evaluated internally, these differences are unimportant.

The first objection is unimportant. Usually it is argued that compact expressions are more desirable because they are more numerically stable - fake poles cause less problems if there are few of them and they are cancelled immediately. However, since the squared matrix elements presented here are well behaved as the Gram determinants vanish, numerical stability is not an issue. Pragmatically, one is only interested in the final physical cross-section which is evaluated numerically and the analytic form of the virtual corrections is unimportant. Whether or not helicity amplitudes are more aesthetically pleasing is open to debate.

The second objection is more serious. It is clear that the Z boson cannot be neglected since it is an important channel for four jet production (even off the Z peak at LEP 2). In previous calculations, the axial contributions have been small. If the Z boson is coupled to the same spin line in both the one-loop and tree-level amplitudes there is no problem because the helicity configurations can be added incoherently (ie. they do not interfere). This leads to the usual $(g_A^2 + g_V^2)$ prefactor where g_A and g_V are the axial and vector couplings respectively. However, in the case $Z \to q\bar{q}Q\bar{Q}$, there are two spin lines and there will be contributions where the Z boson is coupled to different spin lines in the one-loop and tree-level amplitudes. It is difficult to know how important these effects are. In principle, they could be calculated by making a choice of definition of γ_5 away from four dimensions and using the methods described above. However, this is equivalent to using dimensional reduction in the first place, which, with hindsight, may have been the better option. Again, the choice is somewhat subjective.

In order to make a connection with physical observables it is still necessary to calculate the one-loop corrections to $e^+e^- \to q\bar{q}gg$. Already Bern, Dixon and Kosower have presented the leading colour contribution to this process [51], and the calculation of the remaining helicity amplitudes is in progress [52]. Once the virtual corrections are complete, they must be numerically combined with the real contribution, specifying an appropriate jet algorithm and detector cuts, etc. This has been done by Dixon and Signer for the leading colour contribution [44]. Only then can the interesting phenomenology of four jet production in e^+e^- collisions be explored.

Chapter 7

Conclusions and Summary

This thesis has discussed some new techniques for evaluating the one-loop Feynman diagrams which are generally required for the calculation of physical observables at next-to-leading order in the strong coupling constant. This evaluation involves integration over the unconstrained loop momentum, which, using traditional methods, generates Gram determinants in the denominator of the expressions. In general, the number of Gram determinants generated is equal to the rank of the tensor integral.

The appearance of these Gram determinants generates two problems:

- The presentation of the final expressions is ambiguous — complex intertangling of the Gram determinants can occur which make the expressions much more complicated than they need naturally be.
- The presence of the Gram determinants in the denominator of the expressions produces fake singularities in the regions of phase space where these Gram determinants vanish. This can lead to numerical instabilities in the Monte Carlo programs which must be constructed to combine the real and virtual contributions to the next-to-leading order cross section.

Fortunately, the second problem leads to a natural way of solving *both* problems. Since the final, physical matrix elements must be free from divergences as the Gram

determinants vanish, it must be possible to tie together the scalar integrals in such a way as to construct functions which are finite in this limit. In fact, it has been shown that the tensor integrals themselves are free from divergences in these limits and can be written in terms of these finite functions. The only notable exception is the box integral with two opposite massive legs where the scalar integral itself is divergent as the Gram determinant vanishes. However, as no finite function can be formed from this integral, the determinant must cancel from all physical matrix elements.

A general method has been presented for finding these finite combinations of scalar integrals, and writing the tensor integrals in terms of them. This is most easily done by performing a Feynman parameterization of the tensor integrals, and solving the resulting integrals with Feynman parameters in the numerator either by differentiation of the scalar integral or by applying a modification of the "string inspired" total derivative method of Bern, Dixon and Kosower [21]. The finite functions then turn out to be related to the scalar integrals in higher dimensions. In addition to removing any problems with numerical stability, this procedure combines together dilogarithms, logarithms and constants in a natural, but non-trivial way, resulting in more compact expressions for QCD matrix elements.

This procedure has been applied to all tensor triangle integrals, all tensor box integrals with up to two massive external legs, and up to second rank tensor pentagon integrals with one massive external leg. In particular it has been shown that the 4×4 pentagon Gram determinant can always be removed. Although all internal masses have been neglected in this thesis, these methods are also applicable to the general case.

These methods have been applied to the calculation of the one-loop virtual corrections to $\gamma^* \to q\bar{q}Q\bar{Q}$. This is the first step towards the calculation of the next-to-leading order corrections for $e^+e^- \to 4$ jets, which will provide a more precise measurement of the QCD colour factors and lead to a better understanding of the backgrounds to W pair production near threshold at LEP 2. In addition, it is needed for the next-to-leading order corrections for $p\bar{p} \to W/Z + 2$ jets and $e^\pm p \to e^\pm + 3$ jets.

Instead of calculating a helicity decomposition of the matrix elements, the interference

between tree-level and one-loop, giving $\mathcal{O}(\alpha_s^3)$, has been evaluated directly. By cancelling dot products of the external momenta in the numerator with the propagators, it is possible to completely remove all pentagon tensor integrals. Unfortunately, this restricts the virtual gauge boson to vector couplings with the quarks, and therefore the decay of a Z boson is not fully included. The results of this calculation, though analytic, are rather lengthy and have been included in a FORTRAN code which evaluates the matrix elements for a given phase space point.

Much work is still to be done before the calculation of the next-to-leading order corrections for $e^+e^- \to 4$ jets is complete. The one-loop matrix elements for the parton process $e^+e^- \to q\bar{q}gg$, which contributes to the virtual corrections, are still to be calculated. This can in principle be done using the methods discussed in this thesis. Furthermore, it still remains to combine the real and virtual corrections together in a numerical program evaluating infra-red safe jet quantities. Only then can the results be used for a phenomenological examination of the interactions of quarks and gluons at very small distance scales.

Appendix A

Useful Functions

This appendix will outline some of the special functions which are found in this thesis and some of their most useful properties with respect to one-loop calculations.

A.1 The Γ-Function

The Γ-function is defined for complex z with $\Re z > 0$ by:

$$\Gamma(z) \equiv \int_0^\infty \exp^{-t} t^{z-1} dt. \tag{A.1}$$

The restriction $\Re z > 0$ is necessary in order to make the integral convergent.

Integration by parts yields the useful result,

$$\begin{aligned} \Gamma(z) &= \left[-\exp^{-t} t^{z-1}\right]_0^\infty + (z-1)\int_0^\infty \exp^{-t} t^{z-2} dt & \text{(A.2)} \\ &= (z-1)\Gamma(z-1). & \text{(A.3)} \end{aligned}$$

This provides a very simple result for $\Gamma(m)$ when m is an integer,

$$\begin{aligned} \Gamma(m) &= (m-1)\Gamma(m-1) = (m-1)(m-2)\Gamma(m-2) \\ &= \ldots = (m-1)!\Gamma(1) = (m-1)!. & \text{(A.4)} \end{aligned}$$

Often this is used as a definition of the factorial function in order to extend to complex z with $\Re(z) > 0$,

$$z! \equiv \int_0^\infty \exp^{-t} t^z dt. \tag{A.5}$$

For a more comprehensive discussion of the Γ-function see [53].

A.2 The β-Function

The β-function is defined for complex m and n with $\Re m, n > 0$ by:

$$\beta(m,n) \equiv 2\int_0^{\pi/2} \cos^{2m-1}\theta \sin^{2n-1}\theta d\theta. \tag{A.6}$$

The β-function can be usefully written in terms of the Γ-function, eq. (A.1). Consider $\Gamma(m)\Gamma(n)$ with $\Re(m,n) > 0$,

$$\Gamma(m)\Gamma(n) = \int_0^\infty du \int_0^\infty dv \exp^{-u-v} u^{m-1}v^{n-1}. \tag{A.7}$$

Making the substitution $u = r^2\cos^2\theta$, $v = r^2\sin^2\theta$, ie. transforming to polar coordinates, gives,

$$\begin{aligned}\Gamma(m)\Gamma(n) &= \int_0^\infty dr \int_0^{\frac{\pi}{2}} d\theta \exp^{-r^2} r^{2m+2n-1}\cos^{2m-1}\theta\sin^{2n-1}\theta \\ &= \Gamma(m+n)2\int_0^{\frac{\pi}{2}} d\theta \cos^{2m-1}\theta\sin^{2n-1}\theta. \end{aligned}\tag{A.8}$$

The integral in eq. (A.8) above is just the definition of the beta function, eq. (A.6). This leads to,

$$\beta(m,n) = \frac{\Gamma(m)\Gamma(n)}{\Gamma(m+n)}. \tag{A.9}$$

Making the substitutions $t = \cos^2\theta$ and $t = \frac{u}{1+u}$ respectively gives two more integral forms of the beta functions which will prove useful.

$$\beta(m,n) = \int_0^1 t^{m-1}(1-t)^{n-1}dt, \tag{A.10}$$

$$\beta(m,n) = \int_0^\infty \frac{u^{m-1}}{(1+u)^{m+n}}du. \tag{A.11}$$

A more comprehensive discussion of the β-function can be found in [53].

A.3 The Hypergeometric Function

The hypergeometric function can be defined for $\Re a > \Re b > 0$ and $|\arg(1-z)| < \pi$ by,

$$\mathcal{F}(a,b,c,z) = \frac{\Gamma(c)}{\Gamma(b)\Gamma(c-b)} \int_0^1 x^{b-1}(1-x)^{c-b-1}(1-zx)^{-a}dx. \tag{A.12}$$

It can be shown that $\mathcal{F}(a,b,c,z)$ is symmetric in a and b. A useful relation can be found using this symmetry and the change of variables $x \to y = 1-x$,

$$\begin{aligned}
\mathcal{F}(a,b,c,z) &= \frac{\Gamma(c)}{\Gamma(a)\Gamma(c-a)} \int_0^1 x^{a-1}(1-x)^{c-a-1}(1-zx)^{-b}dx \\
&= -\frac{\Gamma(c)}{\Gamma(a)\Gamma(c-a)} \int_1^0 (1-y)^{a-1}y^{c-a-1}(1-z(1-y))^{-b}dx \\
&= (1-z)^{-b}\frac{\Gamma(c)}{\Gamma(c-a)\Gamma(a)} \int_0^1 y^{(c-a)-1}(1-y)^{c-(c-a)-1}\left(1-\frac{yz}{z-1}\right)^{-b}dx \\
&= (1-z)^{-b}\mathcal{F}\left(c-a,b,c,\frac{z}{z-1}\right).
\end{aligned} \tag{A.13}$$

Furthermore, a simple form can be found in the case $a = b = -\epsilon$, $c = 1-\epsilon$, when ϵ is small, by expanding in powers of ϵ,

$$\begin{aligned}
\mathcal{F}(-\epsilon,-\epsilon,1-\epsilon,z) &= \frac{\Gamma(1-\epsilon)}{\Gamma(-\epsilon)\Gamma(1)} \int_0^1 x^{-1-\epsilon}(1-xz)^{\epsilon}dx \\
&= -\epsilon \int_0^1 x^{-1-\epsilon}\left[1+\epsilon\log(1-xz)+\mathcal{O}(\epsilon^2)\right]dx \\
&= -\epsilon\left[x^{-1-\epsilon}\right]_0^1 - \epsilon^2 \int_0^1 \frac{x^{-\epsilon}}{x}\log(1-xz)dx + \mathcal{O}(\epsilon^3) \\
&= 1-\epsilon^2 \int_0^1 \frac{log(1-xz)}{x}dx + \mathcal{O}(\epsilon^3) \\
&= 1-\epsilon^2 \mathrm{Li}_2(x) + \mathcal{O}(\epsilon^3).
\end{aligned} \tag{A.14}$$

This expansion is useful in evaluating the scalar box integral with two massive opposite legs.

A.4 The Dilogarithm Function

A comprehensive discussion of the dilogarithm function can be found in [54]. Some useful properties of the dilogarithm will be given here. $\mathrm{Li}_2(x)$ is defined for $0 < |x| < 1$ by,

$$\mathrm{Li}_2(x) \equiv -\int_0^x \frac{\log(1-t)}{t}dt. \tag{A.15}$$

Using the substitutions $t \to \frac{t}{x}$ and $t \to 1-t$ respectively, gives two more integral forms of the dilogarithm,

$$\begin{aligned} \mathrm{Li}_2(x) &= -\int_0^1 \frac{\log(1-xt)}{t}dt, \\ \mathrm{Li}_2(x) &= -\int_{1-x}^1 \frac{\log(t)}{1-t}dt. \end{aligned} \tag{A.16}$$

For $|x| \leq 1$, $\mathrm{Li}_2(x)$ can be written as an infinite sum,

$$\mathrm{Li}_2(x) = \int_0^x \frac{1}{t}\sum_{n=1}^{\infty}\frac{t^n}{n}dt \tag{A.17}$$

$$= \sum_{n=1}^{\infty}\frac{x^n}{n^2}. \tag{A.18}$$

Other useful dilogarithm identities are:

$$\mathrm{Li}_2(-x) + \mathrm{Li}_2(-\tfrac{1}{x}) = -\frac{\pi^2}{6} - \frac{1}{2}\log^2(x), \tag{A.19}$$

$$\mathrm{Li}_2(x) + \mathrm{Li}_2(1-x) = \frac{\pi^2}{6} - \log(x)\log(1-x), \tag{A.20}$$

$$\mathrm{Li}_2\left(1-\tfrac{1}{x}\right) + \mathrm{Li}_2(1-x) = -\frac{1}{2}\log^2(x), \tag{A.21}$$

$$\mathrm{Li}_2\left(1-\tfrac{1}{1-x}\right) + \mathrm{Li}_2(x) = -\frac{1}{2}\log^2(1-x). \tag{A.22}$$

Appendix B

Feynman Parameterization

One-loop Feynman diagrams contain tensor integrals of the form:

$$\mathcal{I}_m^{\mu_1 \cdots \mu_R}(p_1, \ldots, p_{m-1}) = \int \frac{d^n k}{(2\pi)^n} \frac{k^{\mu_1} \ldots k^{\mu_R}}{k^2 k_1^2 \ldots k_{1\ldots m-1}^2}, \tag{B.1}$$

where $k_{1\ldots i} = k + p_{1\ldots i}$,
$p_{1\ldots i} = p_1 + p_2 + \ldots + p_i$.

These integrals can be more easily calculated after a process of *Feynman parameterization.* This allows the integration over the loop momenta to be done, rewriting $\mathcal{I}_m^{\mu_1 \cdots \mu_i}$ as an integral over new variables called Feynman parameters. Although, this seems to be just replacing one integration with another, this new Feynman parameterized form is amenable to the techniques of Chapter 5. Furthermore, this is the form required for the calculation of the scalar integrals (Appendix C) which are essential even for the reduction methods of Chapter 4.

This appendix will demonstrate this Feynman parameterization and the subsequent integration over the loop momentum for tensor integrals with up to four powers of the loop momentum in the numerator. For a more complete discussion, see, for example [55].

B.1 Preliminary Integrals

In order to perform the integration over the loop momenta after Feynman parameterization, the following integrals will be required for rank $R = 0 \ldots 4$.

$$\mathcal{J}_R^{\mu_1 \cdots \mu_R}(m) = \int \frac{d^n k}{(2\pi)^n} \frac{k^{\mu_1} \ldots k^{\mu_R}}{(k^2 + 2k \cdot q + c)^m}, \tag{B.2}$$

where q is an arbitrary momentum, c and α are arbitrary constants.

B.1.1 Rank $R = 0$

Making the substitutions $r = k + q$ and $a^2 = q^2 - c$ gives,

$$\mathcal{J}_0(m) = \int \frac{d^n r}{(2\pi)^n} \frac{1}{(r^2 - a^2)^m}. \tag{B.3}$$

This integral can be written in Euclidean space by making a *Wick rotation* to a Euclidean vector $\tilde{r}$ such that $\vec{\tilde{r}} = \vec{r}$ and $\tilde{r}^0 = ir^0$. This is valid as long as $\Im(a) < 0$. The integral can then be performed in polar co-ordinates,

$$\begin{aligned} \mathcal{J}_0(m) &= i(-1)^m \int \frac{d^n \tilde{r}}{(2\pi)^n} \frac{1}{(\tilde{r}^2 + a^2)^m} \\ &= \frac{i(-1)^m}{(2\pi)^n} V_{n-1} \int_0^\infty d\tilde{r} \frac{\tilde{r}^{n-1}}{(\tilde{r}^2 + a^2)^m}, \end{aligned} \tag{B.4}$$

where V_{n-1} is the $(n-1)$-dimensional volume element. Transforming to a variable $u = \tilde{r}^2$, the integral becomes a β-function, eq. (A.11),

$$\begin{aligned} \mathcal{J}_0(m) &= \frac{i(-1)^m}{(2\pi)^n} V_{n-1} \frac{1}{2} \int_0^\infty du \frac{u^{\frac{n}{2}-1}}{(u + a^2)^m} \\ &= \frac{i(-1)^m}{(2\pi)^n} \frac{V_{n-1}}{2a^{2m-n}} \beta\left(\frac{n}{2}, m - \frac{n}{2}\right). \end{aligned} \tag{B.5}$$

The n-dimensional volume element is given by,

$$V_n = \int_0^{2\pi} d\theta_1 \int_0^\pi d\theta_2 \sin\theta_2 \ldots \int_0^\pi d\theta_n \sin^{n-1}\theta_n$$

$$
\begin{aligned}
&= 2\pi \prod_{i=1}^{n-1} \int_0^{\pi} d\theta \sin^i \theta \\
&= 2\pi \prod_{i=1}^{n-1} \beta\left(\frac{1}{2}, \frac{i+1}{2}\right) \\
&= 2\pi^{\frac{n+1}{2}} \frac{\Gamma(1)\Gamma(\frac{3}{2}) \ldots \Gamma(\frac{n}{2})}{\Gamma(\frac{3}{2})\Gamma(2) \ldots \Gamma(\frac{n}{2})\Gamma(\frac{n+1}{2})} \\
&= \frac{2\pi^{\frac{n+1}{2}}}{\Gamma(\frac{n+1}{2})},
\end{aligned} \tag{B.6}
$$

where use has been made of the β-function identities eq. (A.6) and eq. (A.9).

Putting everything together, and writing the β-function of Eq. (B.5) as Gamma functions (using Eq. (A.9)) gives the following expression for $\mathcal{J}_0$,

$$
\mathcal{J}_0(m) = i(-1)^m (4\pi)^{-\frac{n}{2}} \frac{\Gamma(m - \frac{n}{2})}{\Gamma(m)} (q^2 - c)^{\frac{n}{2} - m}. \tag{B.7}
$$

Notice that $\mathcal{J}_0(m - \alpha)$ can be related to $\mathcal{J}_0(m)$ in $(n + 2\alpha)$-dimensions. Adding a superscript to denote the dimension,

$$
\begin{aligned}
\mathcal{J}_0^{(n)}(m - \alpha) &= i(-1)^{m-\alpha} (4\pi)^{-\frac{n}{2}} \frac{\Gamma(m - \alpha - \frac{n}{2})}{\Gamma(m - \alpha)} (q^2 - c)^{\frac{n}{2} - m + \alpha} \\
&= (-4\pi)^{\alpha} i(-1)^m (4\pi)^{-\frac{n+2\alpha}{2}} \frac{\Gamma(m - \frac{n+2\alpha}{2})}{\Gamma(m - \alpha)} (q^2 - c)^{\frac{n+2\alpha}{2} - m} \\
&= (-4\pi)^{\alpha} \frac{\Gamma(m)}{\Gamma(m - \alpha)} \mathcal{J}_0^{(n+2\alpha)}(m).
\end{aligned} \tag{B.8}
$$

B.1.2 Ranks $R = 1 \ldots 4$

Expressions for $\mathcal{J}_R^{\mu_1 \ldots \mu_R}(m)$ for $R = 1 \ldots 4$ can be most easily obtained by differentiating $\mathcal{J}_{R-1}^{\mu_1 \ldots \mu_{R-1}}(m)$ with respect to q_{μ_R},

$$
\begin{aligned}
\frac{\partial \mathcal{J}_{R-1}^{\mu_1 \ldots \mu_{R-1}}(m)}{\partial q_{\mu_R}} &= -2m \int \frac{d^n k}{(2\pi)^n} \frac{k^{\mu_1} \ldots k^{\mu_{R-1}} k^{\mu_R}}{(k^2 + 2k \cdot q + c)^{m+1}} \\
&= -2m \mathcal{J}_R^{\mu_1 \ldots \mu_R}(m + 1).
\end{aligned} \tag{B.9}
$$

Therefore,

$$\mathcal{J}_R^{\mu_1\cdots\mu_R}(m) = -\frac{1}{2(m-1)}\frac{\partial \mathcal{J}_{R-1}^{\mu_1\cdots\mu_{R-1}}(m-1)}{\partial q_{\mu_R}}. \tag{B.10}$$

Repeated use of Eq. (B.10), using Eq. (B.8) to change dimension where necessary, gives,

$$\mathcal{J}_1^{\mu}(m) = -q^{\mu}\mathcal{J}_0^{(n)}(m), \tag{B.11}$$

$$\mathcal{J}_2^{\mu_1\mu_2}(m) = q^{\mu_1}q^{\mu_2}\mathcal{J}_0^{(n)}(m) - 2\pi g^{\mu_1\mu_2}\mathcal{J}_0^{(n+2)}(m), \tag{B.12}$$

$$\begin{aligned}\mathcal{J}_3^{\mu_1\mu_2\mu_3}(m) &= -q^{\mu_1}q^{\mu_2}q^{\mu_3}\mathcal{J}_0^{(n)}(m) \\ &\quad +2\pi\left(q^{\mu_1}g^{\mu_2\mu_3}+q^{\mu_2}g^{\mu_1\mu_3}+q^{\mu_3}g^{\mu_1\mu_2}\right)\mathcal{J}_0^{(n+2)}(m),\end{aligned} \tag{B.13}$$

$$\begin{aligned}\mathcal{J}_4^{\mu_1\mu_2\mu_3\mu_4}(m) &= q^{\mu_1}q^{\mu_2}q^{\mu_3}q^{\mu_4}\mathcal{J}_0^{(n)}(m) \\ &\quad -2\pi(q^{\mu_1}q^{\mu_2}g^{\mu_3\mu_4}+q^{\mu_1}q^{\mu_3}g^{\mu_2\mu_4}+q^{\mu_1}q^{\mu_4}g^{\mu_2\mu_3} \\ &\quad +q^{\mu_2}q^{\mu_3}g^{\mu_1\mu_4}+q^{\mu_2}q^{\mu_4}g^{\mu_1\mu_3}+q^{\mu_3}q^{\mu_4}g^{\mu_1\mu_2})\mathcal{J}_0^{(n+2)}(m) \\ &\quad +(2\pi)^2(g^{\mu_1\mu_2}g^{\mu_3\mu_4}+g^{\mu_1\mu_3}g^{\mu_2\mu_4}+g^{\mu_1\mu_4}g^{\mu_2\mu_3})\mathcal{J}_0^{(n+4)}(m).\end{aligned} \tag{B.14}$$

B.2 Feynman Parameterization

Feynman Parameterization uses the relation[1],

$$\frac{1}{a_1\ldots a_m} = \Gamma(m)\int_0^1 dx_1\ldots dx_m \frac{\delta(1-x_1-\ldots-x_m)}{(a_1x_1+\ldots+a_mx_m)^m}. \tag{B.15}$$

Performing this parameterization on $\mathcal{I}_m^{\mu_1\cdots\mu_R}(p_1,\ldots,p_{m-1})$ gives,

$$\begin{aligned}\mathcal{I}_m^{\mu_1\cdots\mu_R}(p_1,\ldots,p_{m-1}) &= \Gamma(m)\int_0^1 dx_1\ldots dx_m\delta(1-x_1-\ldots-x_m) \\ &\quad \times\int\frac{d^nk}{(2\pi)^n}\frac{k^{\mu_1}\ldots k^{\mu_R}}{(k^2x_1+k_1^2x_2+\ldots+k_{1\ldots(m-1)}x_m)^m}.\end{aligned} \tag{B.16}$$

The integral over the loop-momentum, k, in the right-hand-side of the above is exactly of the form $\mathcal{J}_R^{\mu_1\cdots\mu_R}(m)$ with,

$$c = \sum_{i=2}^{m} p_{1\ldots(i-1)}^2 x_i, \tag{B.17}$$

$$q^{\mu} = \sum_{i=2}^{m} p_{1\ldots(i-1)}^{\mu} x_i. \tag{B.18}$$

[1]This is easily proven by induction.

After some algebra, it can be shown that,

$$c - q^2 = \sum_{i=1}^{m} \sum_{j>i} s_{i\ldots(j-1)} x_i x_j, \tag{B.19}$$

where the generalised Mandelstam invariants have been introduced:

$$s_{i(i+1)\ldots j} = p^2_{i(i+1)\ldots j} = (p_i + p_{i+1} + \ldots + p_j)^2. \tag{B.20}$$

The integration over the loop-momentum in $\mathcal{I}_m^{\mu_1\cdots\mu_R}$ can now be done. It is convenient to define,

$$I_m^n[\mathcal{P}\{x_i\}] \equiv (-1)^m \Gamma(m - \frac{n}{2}) \int_0^1 dx_1 \ldots dx_m \frac{\delta(1 - \sum_i x_i)\mathcal{P}\{x_i\}}{(-\sum_{i=1}^m \sum_{j>i} s_{i\ldots(j-1)} x_i x_j)^{m-\frac{n}{2}}}, \tag{B.21}$$

where $\mathcal{P}\{x_i\}$ is a polynomial in x_i. This allows $\mathcal{I}_m^{\mu_1\cdots\mu_R}$ to be written in terms of integrals over only the Feynman parameters,

$$\mathcal{I}_m = i(4\pi)^{-\frac{n}{2}} I_m^n[1], \tag{B.22}$$

$$\mathcal{I}_m^{\mu_1} = -i(4\pi)^{-\frac{n}{2}} \sum_{i=2}^{m} p^{\mu_1}_{1\ldots(i-1)} I_m^n[x_i], \tag{B.23}$$

$$\mathcal{I}_m^{\mu_1\mu_2} = i(4\pi)^{-\frac{n}{2}} \left[\sum_{i,j=2}^{m} p^{\mu_1}_{1\ldots(i-1)} p^{\mu_2}_{1\ldots(j-1)} I_m^n[x_i x_j] - \frac{1}{2} g^{\mu_1\mu_2} I_m^{n+2}[1] \right], \tag{B.24}$$

$$\begin{aligned} \mathcal{I}_m^{\mu_1\mu_2\mu_3} = & -i(4\pi)^{-\frac{n}{2}} \left[\sum_{i,j,k=2}^{m} p^{\mu_1}_{1\ldots(i-1)} p^{\mu_2}_{1\ldots(j-1)} p^{\mu_3}_{1\ldots(k-1)} I_m^n[x_i x_j x_k] \right. \\ & \left. -\frac{1}{2} \sum_{i=2}^{m} (p^{\mu_1}_{1\ldots(i-1)} g^{\mu_2\mu_3} + p^{\mu_2}_{1\ldots(i-1)} g^{\mu_1\mu_3} + p^{\mu_3}_{1\ldots(i-1)} g^{\mu_1\mu_2}) I_m^{n+2}[x_i] \right], \end{aligned} \tag{B.25}$$

$$\begin{aligned} \mathcal{I}_m^{\mu_1\mu_2\mu_3\mu_4} = & \; i(4\pi)^{-\frac{n}{2}} \left[\sum_{i,j,k,l=2}^{m} p^{\mu_1}_{1\ldots(i-1)} p^{\mu_2}_{1\ldots(j-1)} p^{\mu_3}_{1\ldots(k-1)} p^{\mu_4}_{1\ldots(l-1)} I_m^n[x_i x_j x_k x_l] \right. \\ & -\frac{1}{2} \sum_{i,j=2}^{m} (p^{\mu_1}_{1\ldots(i-1)} p^{\mu_2}_{1\ldots(j-1)} g^{\mu_3\mu_4} + p^{\mu_1}_{1\ldots(i-1)} p^{\mu_3}_{1\ldots(j-1)} g^{\mu_2\mu_4} \\ & \quad + p^{\mu_1}_{1\ldots(i-1)} p^{\mu_4}_{1\ldots(j-1)} g^{\mu_2\mu_3} + p^{\mu_2}_{1\ldots(i-1)} p^{\mu_3}_{1\ldots(j-1)} g^{\mu_1\mu_4} \\ & \quad \left. + p^{\mu_2}_{1\ldots(i-1)} p^{\mu_4}_{1\ldots(j-1)} g^{\mu_1\mu_3} + p^{\mu_3}_{1\ldots(i-1)} p^{\mu_4}_{1\ldots(j-1)} g^{\mu_1\mu_2}) I_m^{n+2}[x_i x_j] \right] \\ & + \frac{1}{4} (g^{\mu_1\mu_2} g^{\mu_3\mu_4} + g^{\mu_1\mu_3} g^{\mu_2\mu_4} + g^{\mu_1\mu_4} g^{\mu_2\mu_3}) I_m^{n+4}[1]. \end{aligned} \tag{B.26}$$

Appendix C

Scalar Integrals

C.1 Introduction

It has been demonstrated that the largest obstacle to performing one-loop Feynman Diagram calculations is the integration of the free, unconstrained momenta flowing around the loop. In general, this gives rise to tensor integrals. The most important form of these integrals are the *scalar integrals*, where there are no momenta in the numerator of the integrand. Not only do these scalar integrals appear in one-loop calculations in their own right, but the evaluation of the other, higher rank tensor integrals also requires them, as demonstrated in Chapters 4 and 5. In this appendix, expressions for the scalar integrals used in the calculations of Chapter 6 will be derived.

Consider a generic m-point scalar integral in $n = 4 - 2\epsilon$ dimensions,

$$\mathcal{S}_m(p_1, \ldots, p_{m-1}) = \int \frac{d^n k}{(2\pi)^n} \frac{1}{k^2 k_1^2 \ldots k_{1\ldots m-1}^2}, \tag{C.1}$$

where $k_{1\ldots j} = k + p_{1\ldots j}$,
$p_{1\ldots j} = p_1 + p_2 + \ldots + p_j$.

It is demonstrated in Appendix B that this integral can be simplified by a process of *Feynman parameterisation.* This introduces new integrals over over the Feynman parameters which allow the integration over the loop momentum to be performed. Then all that

remains to be done are the integrations over these Feynman parameters. These Feynman parameter integrals take the form,

$$\mathcal{S}_m = i(4\pi)^{-\frac{n}{2}}\Gamma(m-\frac{n}{2})\int_0^1 dx_1\ldots dx_m \frac{\delta^{(m)}(1-x_1-\ldots-x_m)}{(-\sum_{i=1}^m\sum_{j>i} s_{i\ldots(j-1)}x_ix_j)^{m-\frac{n}{2}}}, \tag{C.2}$$

where x_i are the Feynman parameters and the generalised Mandelstam invariants are given by,

$$s_{i(i+1)\ldots j} = p^2_{i(i+1)\ldots j} = (p_i + p_{i+1} + \ldots + p_j)^2. \tag{C.3}$$

Derivations of these integrals will be provided in sections (C.2) through (C.6).

C.2 The Tadpole

Although a loop diagram with only one external leg is forbidden by momentum conservation, its corresponding integral appears in the reduction of higher point integrals. This integral is zero in the case of massless internal particles. Consider the tadpole diagram where the "particle" in the loop has a mass m which will subsequently be taken to zero,

$$\mathcal{A}_0 = \int d^nk \frac{1}{k^2-m^2}. \tag{C.4}$$

Using eq. (B.7), this gives,

$$\begin{aligned}\mathcal{A}_0 &= i(4\pi)^{-\frac{n}{2}}\Gamma(1-\frac{n}{2})(-m^2)^{\frac{n}{2}-1} \\ &\to 0 \quad as \quad m^2 \to 0.\end{aligned} \tag{C.5}$$

C.3 The Bubble

The scalar bubble integral, where the loop has two external legs, is given by,

$$\mathcal{B}_0(p) = \int d^nk \frac{1}{k^2(k+p)^2} \tag{C.6}$$

$$= i(4\pi)^{\epsilon-2}\Gamma(\epsilon)\int_0^1 dx_1 dx_2 \frac{\delta(1-x_1-x_2)}{(-p^2 x_1 x_2)^\epsilon}. \tag{C.7}$$

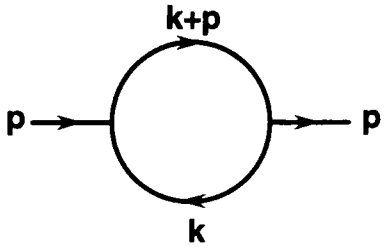

Figure C.1: Momentum flow in a bubble loop diagram.

In the above, the general result of eq. (C.2) has been used. The delta function may be used to perform one integration and the β-function identities of eq.(A.9) and eq.(A.10) to to perform the other,

$$\begin{aligned}
\mathcal{B}_0(p) &= i(4\pi)^{\epsilon-2}\Gamma(\epsilon)(-p^2)^{-\epsilon}\int_0^1 dx_1 x_1^{-\epsilon}(1-x_1)^{-\epsilon} \\
&= i(4\pi)^{\epsilon-2}\Gamma(\epsilon)(-p^2)^{-\epsilon}\frac{\Gamma^2(1-\epsilon)}{\Gamma(2-2\epsilon)} \\
&= c_\Gamma \frac{(-p^2)^{-\epsilon}}{\epsilon(1-2\epsilon)},
\end{aligned} \tag{C.8}$$

where,

$$c_\Gamma = i(4\pi)^{\epsilon-2}\frac{\Gamma(1+\epsilon)\Gamma^2(1-\epsilon)}{\Gamma(1-2\epsilon)}. \tag{C.9}$$

In the above eq. (A.3) has been used. Note that c_Γ is $\frac{i}{(4\pi)^2}$ in the four dimensional limit ($\epsilon \to 0$).

Also, $\mathcal{B}_0(p)$ will vanish for lightlike p (ie. $p^2 = 0$). This is very fortunate as a reduction of a tensor integral to scalar integrals as described in Chapter 4 and 5 can result in very large numbers of scalar bubble integrals.

C.4 The Triangle

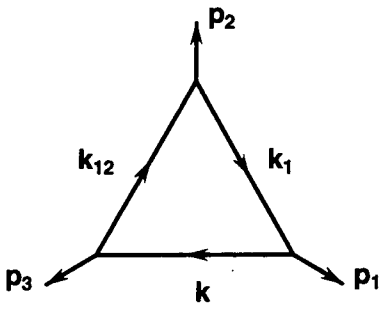

Figure C.2: Momentum flow in a triangle loop diagram.

The scalar triangle integral is given by,

$$C_0(p_1,p_2) = \int \frac{d^nk}{(2\pi)^n}\frac{1}{k^2k_1^2k_{12}^2}. \tag{C.10}$$

Using the result of eq. (C.2), a Feynman parameterisation can be done and the integration over the loop momenta performed,

$$C_0(p_1,p_2) = i(4\pi)^{\epsilon-2}\Gamma(1+\epsilon)\int dx_1dx_2dx_3\frac{\delta(1-x_1-x_2-x_3)}{(-p_{12}^2x_1x_3-p_1^2x_1x_2-p_2^2x_2x_3)^{1+\epsilon}}. \tag{C.11}$$

Two Massive Legs

Consider the triangle with two massive external legs. For convenience of notation, the momenta of the external legs will be taken to be p_1, p_{23}, and $p_4 = -p_{123}$, and the momenta p_i, with $i = 1,2,3$, will be taken to be lightlike, $p_i^2 = 0$. This allows all scalar products of external momenta to be expressed in terms of generalised Mandelstam invariants, eq. (C.3). In this notation,

$$\begin{aligned} C_0(p_1,p_{23}) &= i(4\pi)^{\epsilon-2}\Gamma(1+\epsilon)\int dx_1dx_2dx_3\frac{\delta(1-x_1-x_2-x_3)}{(s_{123}x_1x_3+s_{23}x_2x_3)^{1+\epsilon}} \\ &= i(4\pi)^{\epsilon-2}\Gamma(1+\epsilon)\int_0^1 dx_1\int_0^{1-x_1}(1-x_1-x_2)^{-(1+\epsilon)}(s_{123}x_1s_{23}x_2)^{-(1+\epsilon)}. \end{aligned} \tag{C.12}$$

This is better expressed in terms of new variables x and y given by,

$$x = x_1, \tag{C.13}$$

$$y = x_2 - x_1. \tag{C.14}$$

Using these new variables, $\mathcal{C}_0$ is now linear in x and can be easily integrated using the β-function identities of eq.(A.10) and eq.(A.9),

$$\begin{aligned}
\mathcal{C}_0(p_1, p_{23}) &= i(4\pi)^{\epsilon-2}\Gamma(1+\epsilon)\int_0^1 dy \int_0^y dx (1-y)^{-(1+\epsilon)}[x(s_{123}-s_{23})+ys_{23}]^{-(1+\epsilon)} \\
&= -i(4\pi)^{\epsilon-2}\Gamma(1+\epsilon)\int_0^1 dy (1-y)^{-(1+\epsilon)}y^{-\epsilon}\frac{1}{\epsilon}\frac{(s_{123})^{-\epsilon}-(s_{23})^{-\epsilon}}{s_{123}-s_{23}} \\
&= c_\Gamma \frac{1}{\epsilon^2}\frac{(-s_{123})^{-\epsilon}-(-s_{23})^{-\epsilon}}{s_{123}-s_{23}},
\end{aligned} \tag{C.15}$$

where c_Γ is defined by eq. (C.9).

One Massive Leg

The result derived above for the scalar triangle with two massive external legs can be easily used to give the scalar triangle with only one massive external leg, by taking the limit $s_{23} = 0$. With a slight change of notation $p_{23} \to p_2$ to conform to the notation choice described above, this gives,

$$\mathcal{C}_0(p_1, p_2) = c_\Gamma \frac{1}{\epsilon^2}\frac{(-s_{12})^{-\epsilon}}{s_{12}} \tag{C.16}$$

Three Legs Off Mass-Shell.

The scalar triangle with all three external legs off mass-shell is rather difficult to calculate in $n = 4 - 2\epsilon$ dimensions. Fortunately, it is *finite* in four dimensions. Since the only singularities which occur in loop diagrams as $\epsilon \to 0$ come from the tensor or scalar integrals, $\mathcal{C}_0$ is only needed to $\mathcal{O}(\epsilon^0)$ and the four dimensional result is sufficient,

$$\mathcal{C}_0(p_{12}, p_{34}) = i(4\pi)^{-2}\Gamma(1+\epsilon)\int dx_1 dx_2 dx_3 \frac{\delta(1-x_1-x_2-x_3)}{(s_{1234}^2 x_1 x_3 + s_{12}^2 x_1 x_2 + s_{34}^2 x_2 x_3)^{-1}}. \tag{C.17}$$

The integration over x_3 is removed and the following change of variables is made:

$$x_1 = x, \tag{C.18}$$

$$x_2 = y(1-x). \tag{C.19}$$

Using this change of variables, C_0 becomes linear in x and can be integrated,

$$\begin{aligned} C_0(p_{12},p_{34}) &= i(4\pi)^{-2}\int_0^1 dx \int_=^1 dy \frac{1-x}{[x(s_{1234}-y(s_{1234}-s_{12}+s_{34})+y^2 s_{34})+y(1-y)s_{34}]} \\ &= i(4\pi)^{-2}\int_0^1 dy \frac{\log(\frac{s_{1234}-y[s_{1234}-s_{12}]}{y(1-y)s_{34}})}{y^2 s_{34}-y[s_{1234}-s_{12}+s_{34}]+s_{1234}}. \end{aligned} \tag{C.20}$$

This integral can be done by partial fractioning. Let $a^{\pm}$ be the roots of the equation:

$$y^2 s_{34} - y[s_{1234}-s_{12}+s_{34}] + s_{1234} = 0. \tag{C.21}$$

That is,

$$a^{\pm} = \frac{s_{1234}-s_{12}+s_{34} \pm \lambda}{2s_{34}}, \tag{C.22}$$

and,

$$\lambda^2 = s_{1234}^2 + s_{12}^2 + s_{34}^2 - 2s_{1234}s_{12} - 2s_{1234}s_{34} - 2s_{12}s_{34}. \tag{C.23}$$

The integrand of eq. (C.20) can now be written,

$$\frac{\log(y[1-a^+-a^-]+a^+a^-)}{(y-a^+)(y-a^-)} = \frac{\log(y[1-a^+-a^-]+a^+a^-)}{a^+-a^-}\left(\frac{1}{y-a^+}-\frac{1}{y-a^-}\right). \tag{C.24}$$

This integrand is now in a form amenable to integration using the dilogarithm function, Li_2, eq. (A.15). After some algebra,

$$C_0^{\mu}(p_{12},p_{34}) = \frac{1}{\lambda}\left(\log(a^+a^-)\log\left(\frac{1-a^+}{1-a^-}\right)+2\mathrm{Li}_2(a^+)-2\mathrm{Li}_2(a^-)\right), \tag{C.25}$$

with $a^{\pm}$ and λ defined by Eq: (C.22) and Eq: (C.23) respectively. For a more complete discussion of this integral see [33].

C.5 The Box

The general Feynman parameterised form of the scalar box integral in $n = 4 - 2\epsilon$ dimensions is:

$$\mathcal{D}_0(p_1, p_2, p_3) = i(4\pi)^{\epsilon-2}\Gamma(2+\epsilon)\int_0^1 dx_1 dx_2 dx_3 dx_4 \delta(1 - x_1 - x_2 - x_3 - x_4)$$
$$\times(-p_1^2 x_1 x_2 - p_{12}^2 x_1 x_3 - p_{123}^2 x_1 x_4 - p_2^2 x_2 x_3 - p_{23}^2 x_2 x_4 - p_3^2 x_3 x_4)^{-(2+\epsilon)}. \quad \text{(C.26)}$$

Fortunately this simplifies in the cases of interest here.

The Opposite Mass Box

The first case of interest is the scalar box integral with two massive legs on opposite corners, fig. (C.3).

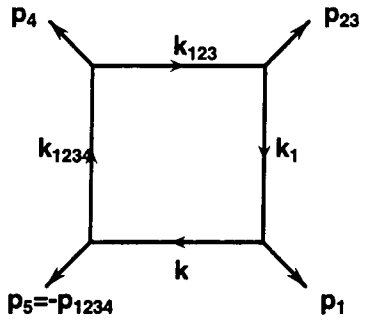

Figure C.3: Momentum flows in the opposite mass box.

In this case the box scalar integral simplifies to:

$$\mathcal{D}_0(p_1, p_{23}, p_4) = i(4\pi)^{\epsilon-2}\Gamma(2+\epsilon)\int_0^1 dx_1 dx_2 dx_3 dx_4 \delta(1 - x_1 - x_2 - x_3 - x_4)$$
$$\times(-s_{123} x_1 x_3 - s_{1234} x_1 x_4 - s_{23} x_2 x_3 - s_{234} x_2 x_4)^{-(2+\epsilon)}. \quad \text{(C.27)}$$

This is most easily done using the following change of variables:

$$x_1 = x\rho,$$

$$\begin{aligned} x_2 &= (1-x)\rho, \\ x_3 &= (1-y)\sigma, \\ x_4 &= y\sigma. \end{aligned} \tag{C.28}$$

The δ-function then ensures that $\rho = 1-\sigma \equiv z$. With this change of variables the integral the integral over z becomes a β-function, eq. (A.10),

$$\begin{aligned} \mathcal{D}_0(p_1,p_{23},p_4) &= i(4\pi)^{\epsilon-2}\Gamma(2+\epsilon)\int_0^1 dxdydz[z(1-z)]^{-(1+\epsilon)} \times \\ &\quad \times[s_{123}x(1-y)+s_{1234}y(1-x)+s_{23}(1-x)(1-y)+s_{1234}xy]^{-(2+\epsilon)} \\ &= i(4\pi)^{\epsilon-2}\Gamma(2+\epsilon)\frac{\beta(-\epsilon,-\epsilon)}{1+\epsilon}\int_0^1 dx[x(s_{1234}-s_{234}-s_{123}+s_{23})+s_{1234}-s_{23}]^{-1} \\ &\quad \times\Big([s_{123}x+s_{23}(1-x)]^{-(1+\epsilon)}-[s_{1234}x+s_{234}(1-x)]^{-(1+\epsilon)}\Big). \end{aligned} \tag{C.29}$$

The remaining integrals can be written as hypergeometric functions, eq. (A.12), giving,

$$\begin{aligned} \mathcal{D}_0(p_1,p_{23},p_4) &= c_\Gamma\frac{1}{\epsilon^2}\frac{2}{s_{1234}s_{23}-s_{123}s_{234}} \\ &\quad\times\Big[\ -(-s_{123})^{-\epsilon}\mathcal{F}\Big(1,-\epsilon,1-\epsilon,\frac{s_{123}s_{14}}{s_{1234}s_{23}-s_{123}s_{234}}\Big) \\ &\quad\ +(-s_{23})^{-\epsilon}\mathcal{F}\Big(1,-\epsilon,1-\epsilon,\frac{s_{23}s_{14}}{s_{1234}s_{23}-s_{123}s_{234}}\Big) \\ &\quad\ +(-s_{1234})^{-\epsilon}\mathcal{F}\Big(1,-\epsilon,1-\epsilon,\frac{s_{1243}s_{14}}{s_{1234}s_{23}-s_{123}s_{234}}\Big) \\ &\quad\ -(-s_{234})^{-\epsilon}\mathcal{F}\Big(1,-\epsilon,1-\epsilon,\frac{s_{234}s_{14}}{s_{1234}s_{23}-s_{123}s_{234}}\Big)\Big]. \end{aligned} \tag{C.30}$$

Further simplification can be made by expansion of the hypergeometric functions in terms of ϵ. Terms of $\mathcal{O}(\epsilon)$ can then be discarded. This is done using eq. (A.13), to rewrite the hypergeometric function in a more readily expandable form, and then eq. (A.14), to made the expansion. Terms of the form $\frac{(-s_{ij})^{-\epsilon}}{\epsilon^2}$ are left unexpanded as this is the form in which the $\frac{1}{\epsilon^2}$ poles must cancel. In this form, the $\frac{1}{\epsilon}$ pole vanishes from all box integrals.

Finally, after tidying up the dilogarithms, the result for the opposite mass box is:

$$\begin{aligned} \mathcal{D}_0(p_1,p_{23},p_4) = c_\Gamma\frac{2}{[s_{123}s_{234}-s_{1234}s_{23}]}\Big[\frac{1}{\epsilon^2}\Big(\big(-s_{123}\big)^{-\epsilon}+\big(-s_{234}\big)^{-\epsilon} \\ -\big(-s_{23}\big)^{-\epsilon}-\big(-s_{1234}\big)^{-\epsilon}\Big)+Ld_0^{opp}(p_1,p_{23},p_4)+\mathcal{O}(\epsilon)\Big], \end{aligned} \tag{C.31}$$

with,

$$Ld_0^{opp}(p_1,p_{23},p_4) = -\mathrm{Li}_2\left(1-\frac{s_{23}}{s_{123}}\right)-\mathrm{Li}_2\left(1-\frac{s_{23}}{s_{234}}\right)-\mathrm{Li}_2\left(1-\frac{s_{1234}}{s_{123}}\right) -\mathrm{Li}_2\left(1-\frac{s_{1234}}{s_{234}}\right)+\mathrm{Li}_2\left(1-\frac{s_{23}s_{1234}}{s_{123}s_{234}}\right)-\frac{1}{2}\log^2\left(\frac{s_{123}}{s_{234}}\right) \quad \text{(C.32)}$$

The Adjacent Mass Box

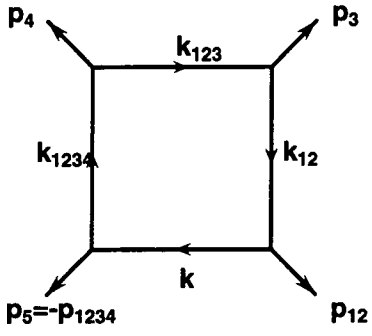

Figure C.4: Momentum flows in the adjacent mass box.

The integration over the Feynman parameters of the adjacent mass box, where two adjacent legs are massive, fig. (C.4), is rather more difficult,

$$\mathcal{D}_0(p_{12},p_3,p_4) = i(4\pi)^{\epsilon-2}\Gamma(2+\epsilon)\int_0^1 dx_1dx_2dx_3dx_4\delta(1-x_1-x_2-x_3-x_4) \times(-s_{12}x_1x_2-s_{123}x_1x_3-s_{1234}x_1x_4-s_{34}x_2x_4)^{-(2+\epsilon)}. \quad \text{(C.33)}$$

This can be solved using the same substitutions as for the opposite mass box, eq. (C.28). Then,

$$\tilde{\mathcal{D}}_0(p_{12},p_3,p_4) = i(4\pi)^{\epsilon-2}\Gamma(2+\epsilon)\int_0^1 dxdydzz^{-1-\epsilon}(1-z) \times\{x[s_{123}(1-z)-s_{12}z(1-x)]+y(1-z)[-s_{34}+x(s_{123}-s_{1234}+s_{12}]\}^{-(2+\epsilon)}. \quad \text{(C.34)}$$

As with the opposite mass box, the integral is now linear in y, allowing the y-integration to be done easily. However, this is where the comparison with the opposite

mass box ends. In that case, the integration over z was a trivial β-function - here it is not. In order to perform the z integration, terms of the form $A^{-1-\epsilon}$ must be expanded in terms of ϵ, ie.

$$A^{-1-\epsilon} = \frac{1}{A}(1 - \epsilon \log(A) + \mathcal{O}(\epsilon^2)). \tag{C.35}$$

The integrations involved are rather messy and unilluminating and will not be detailed here. Finally, with the repeated help of the dilogarithm identities eq. (A.19 - A.22), one obtains the following expression for the adjacent mass box,

$$\mathcal{D}_0(p_{12}, p_3, p_4) = \frac{c_\Gamma}{s_{123}s_{34}}\Big[\frac{1}{\epsilon^2}\Big((-s_{34})^{-\epsilon} + 2(-s_{123})^{-\epsilon} - (-s_{12})^{-\epsilon} - (-s_{1234})^{-\epsilon}\Big) + 2Ld_0(p_{12}, p_3, p_4) + \mathcal{O}(\epsilon)\Big]. \tag{C.36}$$

with,

$$Ld_0(p_{12}, p_3, p_4) = \mathrm{Li}_2\left(1 - \frac{s_{123}}{s_{1234}}\right) - \mathrm{Li}_2\left(1 - \frac{s_{12}}{s_{123}}\right) + \frac{1}{2}\log\left(\frac{s_{123}^2}{s_{12}s_{1234}}\right)\log\left(\frac{s_{34}}{s_{1234}}\right). \tag{C.37}$$

C.6 The Pentagon

The pentagon scalar integral is given by,

$$\mathcal{E}_0(p_1, p_2, p_3, p_4) = \int d^m k \frac{1}{k^2 k_1^2 k_{12}^2 k_{123}^2 k_{1234}^2}, \tag{C.38}$$

where $k_{1\ldots j} = k + p_{1\ldots j}$,
$p_{1\ldots j} = p_1 + p_2 + \ldots + p_j$.

A result for this integral is required in $n = 4 - 2\epsilon$ dimensions. Melrose [23] and independently van Neerven and Vermaseren [24] have shown that this integral in $n = 4$ dimensions can be written as a linear combination of scalar box integrals. This result will be reproduced below. The extension to $n = 4 - 2\epsilon$ dimensions is then straight forward, [21, 22].

The Scalar Pentagon Integral in Four Dimensions

Consider the integral,

$$\tilde{\mathcal{E}}_0 = \int dq^4 \frac{1}{d_0 d_1 d_2 d_3 d_4}, \tag{C.39}$$

where $d_0 = q^2 - m^2$,
$d_i = q_i^2 - m^2$,
and $q_i = q + p_i$.

This is the scalar pentagon integral in four dimensions where the particles propagating around the loop have a mass m. For convenience of notation, the usual $p_{1\ldots i}$ have been replaced with p_i. The presence of the mass, m, ensures that $\tilde{\mathcal{E}}_0$ is free from infrared and collinear singularities.

In four dimensions, the *Schouten identity* allows the loop momentum q to be decomposed in terms of the projective base,v_i^μ, defined in section (4.2), where the vectors v_i are orthogonal to p_i,

$$\begin{aligned} q^\mu &= \sum_{i=1}^{4} v_i^\mu p_i \cdot q \\ &= \frac{1}{2}\sum_{i=1}^{4} v_i^\mu (q_i^2 - q^2 - p_i^2). \end{aligned} \tag{C.40}$$

Contracting this equation with q^μ, dividing by $d_0 d_1 d_2 d_3 d_4$ and integrating over q gives,

$$\int dq^4 \frac{q^2}{d_0 d_1 d_2 d_3 d_4} = \frac{1}{2}\sum_{i=1}^{4} \int dq^4 v_i \cdot q \frac{d_i - d_0 - p_i^2}{d_0 d_1 d_2 d_3 d_4}. \tag{C.41}$$

Consider each of the terms of the right hand side of eq. (C.41) separately. It is easy to see that the first term vanishes by expressing the tensor integral in terms of its possible tensor structure. For example,

$$\begin{aligned} v_3^\mu \int dq^4 q_\mu \frac{d_3}{d_0 d_1 d_2 d_3 d_4} &= v_3^\mu \int dq^4 q_\mu \frac{1}{d_0 d_1 d_2 d_3 d_4} \\ &= v_3^\mu (p_{1\mu}\alpha_1 + p_{2\mu}\alpha_2 + p_{4\mu}\alpha_4) \\ &= 0, \end{aligned} \tag{C.42}$$

where α_i are scalar functions dependent on p_1, p_2, p_4 and m.

Similarly, the second term of the right hand side of eq. (C.41) can be simplified by first making a shift in the loop momenta, $q \to q - p_1$, and again making a tensor decomposition of the integral,

$$\begin{aligned}
&\sum_{i=1}^{4} \int dq^4 \frac{v_i \cdot q}{d_1 d_2 d_3 d_4} \\
&= \sum_{i=1}^{4} \int dq^4 \frac{v_i \cdot q - v_i \cdot p_1}{[q^2 - m^2][(q + p_2 - p_1)^2 - m^2][(q + p_3 - p_1)^2 - m^2][(q + p_4 - p_1)^2 - m^2]} \\
&= \sum_{i=1}^{4} v_i^\mu \int dq^4 \frac{q_\mu}{[q^2 - m^2][(q + p_2 - p_1)^2 - m^2][(q + p_3 - p_1)^2 - m^2][(q + p_4 - p_1)^2 - m^2]} \\
&\quad - \int dq^4 \frac{1}{[q^2 - m^2][(q + p_2 - p_1)^2 - m^2][(q + p_3 - p_1)^2 - m^2][(q + p_4 - p_1)^2 - m^2]} \\
&= \sum_{i=1}^{4} v_i^\mu [(p_2 - p_1)_\mu \beta_2 + (p_3 - p_1)_\mu \beta_3 + (p_4 - p_1)_\mu \beta_4] - \int dq^4 \frac{1}{d_1 d_2 d_3 d_4} \\
&= - \int dq^4 \frac{1}{d_1 d_2 d_3 d_4}, \qquad \text{(C.43)}
\end{aligned}$$

where the orthogonality relation $p_i \cdot v_j = \delta_{ij}$ has been used, and β_i are scalar functions dependent on the vectors $p_2 - p_1$, $p_3 - p_1$, $p_4 - p_1$ and the mass m.

For the final term, use is once again made of eq. (C.40), decomposing the loop momenta in terms of the projective base,

$$\begin{aligned}
\sum_{i=1}^{4} p_i^2 \int dq^4 \frac{v_i \cdot q}{d_0 d_1 d_2 d_3 d_4} &= \sum_{i,j=1}^{4} p_i^2 \int dq^4 \frac{v_i \cdot v_j \; q \cdot p_j}{d_0 d_1 d_2 d_3 d_4} \\
&= \frac{1}{2} \sum_{i,j=1}^{4} p_i^2 \; v_i \cdot v_j \int dq^4 \frac{d_j - d_0 - p_j^2}{d_0 d_1 d_2 d_3 d_4}. \qquad \text{(C.44)}
\end{aligned}$$

Putting this all together gives the four dimensional, massive, scalar pentagon in terms of scalar box integrals,

$$\begin{aligned}
\int d^4 q \frac{1}{d_0 d_1 d_2 d_3 d_4} &= c_0 \mathcal{D}_{1234} + c_1 \mathcal{D}_{0234} + c_2 \mathcal{D}_{0134} \\
&+ c_3 \mathcal{D}_{0124} + c_4 \mathcal{D}_{0123} + c_5 m^2 \int d^4 q \frac{1}{d_0 d_1 d_1 d_2 d_3}, \qquad \text{(C.45)}
\end{aligned}$$

where,

$$\mathcal{D}_{ijkl} = \int d^4 q \frac{1}{d_i d_j d_k d_l} \qquad \text{(C.46)}$$

and,

$$\begin{aligned} c_0 &= \frac{2-\sum_{i,j=1}^{4} p_i^2 v_i v_j}{\sum_{m,n=1}^{4} p_m^2 p_n^2 v_m v_n}, \\ c_i &= \frac{\sum_{j=1}^{4} p_j^2 v_i v_j}{\sum_{m,n=1}^{4} p_m^2 p_n^2 v_m v_n}, \quad (i = 1 \ldots 4), \\ c_5 &= \frac{4}{\sum_{m,n=1}^{4} p_m^2 p_n^2 v_m v_n}. \end{aligned} \tag{C.47}$$

Extension to $n = 4 - 2\epsilon$ Dimensions.

The extension of the above result to $n = 4 - 2\epsilon$ dimensions is now straightforward. Consider the scalar pentagon integral integral:

$$\mathcal{E}_0(p_1, p_2, p_3, p_4) = \int \frac{d^n k}{(2\pi)^n} \frac{1}{k^2 k_1^2 k_{12}^2 k_{123}^2 k_{1234}^2}, \tag{C.48}$$

where $k_{1\ldots j} = k + p_{1\ldots j}$;
$p_{1\ldots j} = p_1 + p_2 + \ldots + p_j$.

The loop momentum k is an n-dimensional vector, which can be decomposed into four dimensional and $n - 4$ dimensional components. That is, $k = q + \tilde{q}$ where q is a four dimensional vector and $\tilde{q}$ an $n - 4$ dimensional space-like Euclidean vector. Writing $\tilde{q}^2 = -m^2$, the expression for $\mathcal{E}_0$ becomes,

$$\mathcal{E}_0(p_1, p_2, p_3, p_4) = \int \frac{d^4 q d^{n-4} \tilde{q}}{(2\pi)^n} \frac{1}{d_0 d_1 d_2 d_3 d_4}, \tag{C.49}$$

where,

$$\begin{aligned} d_0 &= q^2 - m^2, \\ d_i &= (q + p_{1\ldots i})^2 - m^2. \end{aligned} \tag{C.50}$$

The integration over the trivial angles in the $n - 4$ dimensional subspace can now be performed,

$$\mathcal{E}_0(p_1, p_2, p_3, p_4) = \frac{-\epsilon}{\Gamma(1-\epsilon)2^\epsilon} \int dm^2 (m^2)^{-(1+\epsilon)} \int \frac{d^4 q}{(2\pi)^4} \frac{1}{d_0 d_1 d_2 d_3 d_4}. \tag{C.51}$$

Now eq. (C.45) can be used to rewrite the four dimensional integral over q as a sum of four dimensional, massive scalar box integrals,

$$\mathcal{E}_0(p_1,p_2,p_3,p_4) = \frac{-\epsilon}{\Gamma(1-\epsilon)2^\epsilon}\int dm^2(m^2)^{-(1+\epsilon)}\Big(c_0\mathcal{D}_{1234} + c_1\mathcal{D}_{0234} + c_2\mathcal{D}_{0134} + c_3\mathcal{D}_{0124} + c_4\mathcal{D}_{0123} + c_5 m^2\int d^4q \frac{1}{d_0d_1d_2d_3d_4}\Big), \tag{C.52}$$

where,

$$\mathcal{D}_{ijkl} = \int d^4q \frac{1}{d_i d_j d_k d_l}, \tag{C.53}$$

and,

$$\begin{aligned} c_0 &= \frac{2-\sum_{i,j=1}^4 p^2_{1\ldots i}v_iv_j}{\sum_{i,j=1}^4 p^2_{1\ldots i}p^2_{1\ldots j}v_iv_j}, \\ c_i &= \frac{\sum_{j=1}^4 p^2_{1\ldots j}v_iv_j}{\sum_{i,j=1}^4 p^2_{1\ldots i}p^2_{1\ldots j}v_iv_j}, \quad (i=1\ldots 4), \\ c_5 &= \frac{4}{\sum_{i,j=1}^4 p^2_{1\ldots i}p^2_{1\ldots j}v_iv_j}. \end{aligned} \tag{C.54}$$

(Notice that $p_{1\ldots i}$ now replaces p_i.)

The integral over the trivial angles in the $n-4$ dimensional subspace can be reconstructed, returning the integrals back into $n = 4-2\epsilon$ dimensional integrals,

$$\begin{aligned} \mathcal{E}_0(p_1,p_2,p_3,p_4) &= \Big(c_0\mathcal{D}_0(p_2,p_3,p_4) + c_1\mathcal{D}_0(p_{12},p_3,p_4) + c_2\mathcal{D}_0(p_1,p_{23},p_4) \\ &+ c_3\mathcal{D}_0(p_1,p_2,p_{34}) + c_4\mathcal{D}_0(p_1,p_2,p_3) \\ &- c_5\frac{\epsilon}{\Gamma(1-\epsilon)2^\epsilon}\int dm^2(m^2)^{-\epsilon}\int d^4q\frac{1}{d_0d_1d_2d_3d_4}\Big), \end{aligned} \tag{C.55}$$

where c_i, $i = 1\ldots 5$, are given by eq. (C.54).

The last term is $\mathcal{O}(\epsilon)$ and can be ignored. Eq. (C.55) then gives the scalar pentagon integral as a linear combination of scalar box integrals.

Appendix D

The QCD Feynman Rules

In this appendix, the Feynman rules of QCD are presented in the Feynman gauge. In the following, the quark mass is set to zero.

For each external quark or antiquark of momentum p, helicity λ and colour i, a dirac spinor is included:

- Outgoing quark: $\bar{u}_{i\lambda}(p)$.
- Incoming quark: $u_{i\lambda}(p)$.

Similarly, each external gluon of momentum p, helicity λ and colour a, must be given a polarization vector:

- Outgoing gluon: $\varepsilon^{a^*}_{\lambda}(p)$.
- Incoming gluon: $\varepsilon^{a}_{\lambda}(p)$.

The QCD propagators and vertices are given in fig.(D.1). The letters i and j label the colour of the quarks, whereas a, b and c are used to denote the colours of the gluons and ghost fields. For the vertices, all momenta are outgoing. Finally, T^a are the colour matrices, f_{abc} are the $SU(3)$ structure constants, and g_s is the coupling strength.

For closed loops, the unconstrained momentum is integrated over and the integral is divided by $(2\pi)^n$ where n is the space-time dimension. Furthermore, for closed *quark* loops, a factor of (-1) is included.

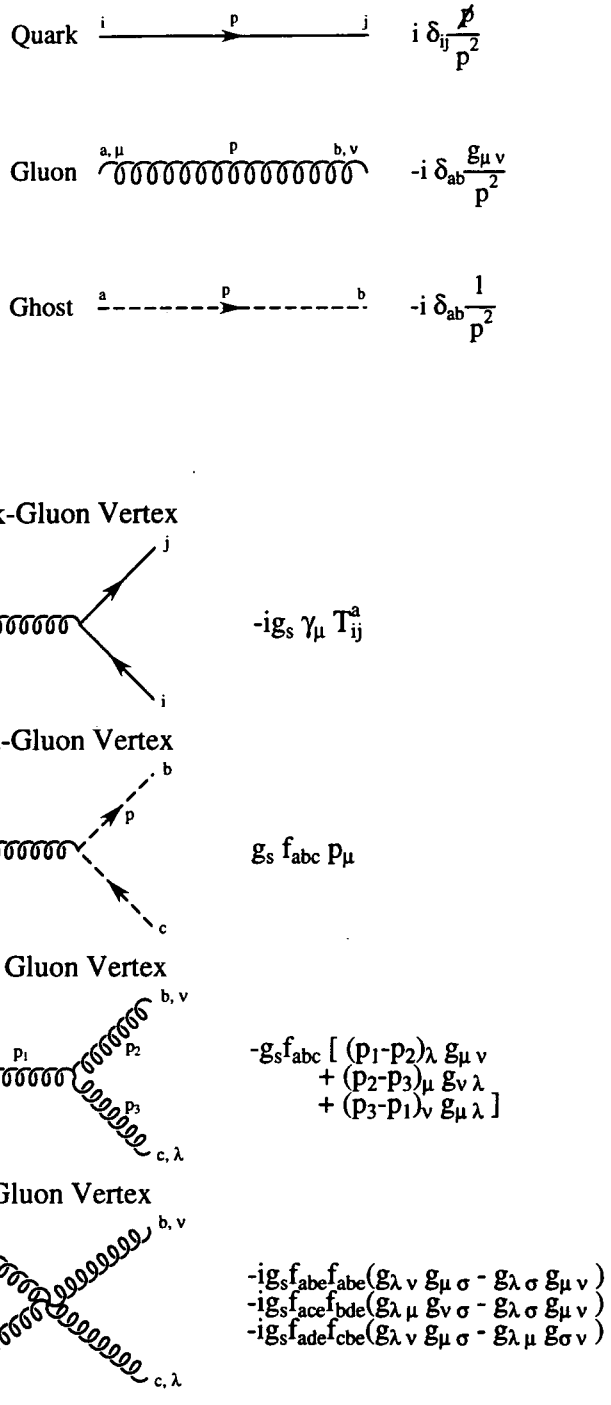

Figure D.1: The QCD propagators and vertices.

Bibliography

[1] M. Gell-Mann, Phys. Lett **8**, 412 (1964).

[2] G. Zweig, CERN preprint **TH401**, 412 (1964).

[3] A review of these experiments can be found in, J. Freidman and H. Kendall, Ann. Rev. Nucl. Sci. **22**, 203 (1972).

[4] L. H. Ryder, *Quantum Field Theory*, Cambridge University Press (1992).
M. Kaku, *Quantum Field Theory: A Modern Introduction*, Oxford University Press (1993).

[5] R. D. Field, *Applications of Perturbative* QCD, Frontiers in Physics Series, Addison-Wesley Publishing Company, Inc. (1989).

[6] F. Bloch and A. Nordsieck, Phys. Rev. **52**, 54 (1937).

[7] T. Kinoshita, J. Math. Phys, **3**, 650 (1962),
T. D. Lee and M. Nauenberg, Phys. Rev. **133**, 1549 (1964).

[8] W. A. Bardeen, A. J. Buras, D. W. Duke and T. Muta, Phys. Rev. **18**, 3998 (1978),
D. W. Duke, Rev. Mod. Phys. **52**, 199 (1980).

[9] P. N. Burrows, Cracow International Symposium on Radiative Corrections (CRAD96), Cracow, Poland, August 1996.

[10] R. Kleiss, Nucl. Phys. **B241**, 61 (1984),
R. Kleiss and W.J. Stirling, Nucl. Phys. **B262**, 235 (1985),

F. A. Berends and W.T. Giele, Nucl. Phys. **B294**, 700 (1987),
B. L. van der Waerden, Goettinger Nachrichten, 100 (1929),
H. Weyl, *Gruppentheorie und Quantummechanik*, Leipzig (1928).

[11] Z. Xu, D. Zhang, and L. Chang, Nucl. Phys. **B291** 392 (1987).

[12] S. Catani, Y.L. Dokshitzer and B.R. Webber, Phys. Lett. **B285** 291 (1992).
B.R. Webber, J. Phys **G19** 1567 (1993).

[13] G. 't Hooft and M. Veltman, Nucl. Phys. **B44**, 189 (1972).

[14] W. Seigel, Phys. Lett. **B84**, 193 (1979).

[15] D. Capper, D. Jones and P. van Nieuwenhuizen, Nucl. Phys. **B167**, 479 (1980).

[16] W.T. Giele and E.W.N. Glover, Phys. Rev. **D46**, 1980 (1992).

[17] S. Catani and M.H. Seymour, Phys. Lett. **B378**, 287 (1996).

[18] S. Catani and M.H. Seymour, CERN preprint CERN-TH/96-29, hep-ph/9605323,
S. Catani and M.H. Seymour, "QCD and QED in Higher Orders", Rheinsberg, Germany, April 1996, CERN preprint CERN-TH/96-181, hep-ph/9607318,
S. Catani and M.H. Seymour, Cracow International Symposium on Radiative Corrections (CRAD96), Cracow, Poland, August 1996, CERN preprint CERN-TH/96-342, hep-ph/9612236.

[19] Z. Kunszt and D.E. Soper, Phys. Rev. **D46**, 192 (1992).

[20] R. K. Ellis, D. A. Ross and A. E. Terrano, Nucl. Phys. **B178**, 317 (1981).

[21] Z. Bern, L. Dixon and D. A. Kosower, Nucl. Phys. **B412**, 751 (1994).

[22] R. K. Ellis, W. T. Giele and E. Yehudai, private communication.

[23] D. B. Melrose, Il Nuovo Cimento **40A**, 181 (1965).

[24] W. van Neerven and J. A. M. Vermaseren, Phys. Lett. **B137**, 241 (1984).

[25] L. M. Brown and R. P. Feynman, Phys. Rev. **85**, 231 (1952).

[26] G. Passarino and M. Veltman, Nucl. Phys. **B160**, 151 (1979).

[27] Z. Bern, L. Dixon and D. A. Kosower, Phys. Lett. **B302**, 299 (1994), *ibid* **B318**, 649 (1993).

[28] J. A. M. Vermaseren, FORM *Users' Guide*, (1989).

[29] G. van Oldenborgh and J. A. M. Vermaseren, Z. Phys. **C46** 425 (1990).
G. van Oldenborgh, Ph.D. thesis, Universiteit van Amsterdam (1990).

[30] W.Beenakker, Ph.D. thesis, Rijksuniversiteit Leiden (1989).

[31] A. Signer, Ph.D. thesis, ETH Zürich (1995).

[32] R. G. Stuart, Comp. Phys. Comm. **56**, 367 (1988).

[33] G. t'Hooft and M. Veltman, Nucl. Phys. **B153**, 365 (1979).

[34] Z. Kunszt, A. Signer and Z. Trócsányi, Nucl. Phys. **B411**, 397 (1994).

[35] J. Ellis, M. K. Gaillard and G.G. Ross, Nucl. Phys. **B111**, 253 (1976).

[36] A. Ali, J. G. Körner, G. Kramer, Z. Kunszt, G. Shierholz, E. Pietarinen and J. Willrodt, Nucl. Phys. **B167**, 454 (1980),
D. Dankaert, P. de Causmaecker, R. Gastmans, W. Troost and T.T. Wu, Phys. Lett. **B114**, 203 (1982).

[37] R. K. Ellis, D. A. Ross and A. E. Terrano, Nucl. Phys. **B178**, 421 (1981).

[38] K. Hagiwara and D. Zeppenfeld, Nucl. Phys. **B313**, 560 (1989).

[39] F. A. Berends, W. T. Giele and H. Kuijf, Nucl. Phys. **B321**, 39 (1989).

[40] N. K. Falk, D. Graudenz and G. Kramer, Nucl. Phys. **B328**, 317 (1989).

[41] Z. Kunszt and P. Nason, *Z Physics at* LEP 1, CERN Yellow Report 89-08.

[42] G. Kramer and B. Lampe, Z. Phys. **C34**, 497 (1987),
G. Kramer and B. Lampe, Fortschr. Phys. **37**, 161 (1989)

[43] Z. Bern, L. Dixon, D. A. Kosower and S. Weinzierl, preprint hep-ph/9610370.

[44] L. Dixon and A. Signer, preprint hep-ph/9609460.

[45] ALEPH Collaboration, D. Decamp et al., Phys. Lett. **B284**, 151 (1992).

[46] DELPHI Collaboration, ICHEP94, Glasgow, 20-27 July 1994, Ref.0180.

[47] L3 Collaboration, L3 Note #1726.

[48] OPAL Collaboration, Z. Phys. **C65**, 367 (1995).

[49] ALEPH Collaboration, ICHEP94, Glasgow, 20-27 July 1994, Ref.0546.

[50] M. Schmelling, CERN-PPE/95-129, 15th International Conference on Physics in Collision, PHYSCOLL95, Cracow, Poland, June 1995.

[51] Z. Bern, L. Dixon and D. A. Kosower, preprint hep-ph/9606378.

[52] Z. Bern, L. Dixon and D. A. Kosower, private communication.

[53] G. Arfken, *Mathematical Methods for Physicists.* Third Edition, Academic Press, Inc. (1985).

[54] L. Lewin, *Dilogarithms and Associated Functions*, McDonald (1958).

[55] J. Collins, *Renormalization*, Cambridge Momographs on Mathematical Physics, Cambridge University Press (1992).